ISTANBUL TECHNICAL UNIVERSITY ★ GRADUATE SCHOOL OF SCIENCE ENGINEERING AND TECHNOLOGY

RADIAL BASIS FUNCTION SURROGATE MODEL-BASED OPTIMIZATION OF ROAD RESTRAINT SYSTEMS: THREE CASE STUDIES

Ph.D. THESIS

Sedat OZCANAN

Department of Civil Engineering

Transport Engineering Programme

AUGUST 2019

ISTANBUL TECHNICAL UNIVERSITY ★ GRADUATE SCHOOL OF SCIENCE ENGINEERING AND TECHNOLOGY

RADIAL BASIS FUNCTION SURROGATE MODEL-BASED OPTIMIZATION OF ROAD RESTRAINT SYSTEMS: THREE CASE STUDIES

Ph.D. THESIS

Sedat OZCANAN
(501122407)

Department of Civil Engineering

Transport Engineering Programme

Thesis Advisor: Prof. Dr. Ali Osman ATAHAN

AUGUST 2019

ISTANBUL TEKNİK ÜNİVERSİTESİ ★ FEN BİLİMLERİ ENSTİTÜSÜ

YOL GÜVENLİK ELEMANLARININ RADYAL TEMELLİ FONKSİYON TABANLI VEKİL MODEL İLE ENİYİLEMESİ: ÜÇ VAKA ÇALIŞMASI

DOKTORA TEZİ

Sedat ÖZCANAN
(501122407)

İnşaat Mühendisliği Anabilim Dalı

Ulaştırma Mühendisliği Programı

Tez Danışmanı: Prof. Dr. Ali Osman ATAHAN

AĞUSTOS 2019

Sedat Ozcanan, a Ph.D. student of ITU Graduate School of Science Engineering and Technology student ID 501122407 successfully defended the thesis/dissertation entitled “RADIAL BASIS FUNCTION SURROGATE MODEL-BASED OPTIMIZATION OF ROAD RESTRAINT SYSTEMS: THREE CASE STUDIES”, which he prepared after fulfilling the requirements specified in the associated legislations, before the jury whose signatures are below.

Thesis Advisor :	**Prof. Dr. Ali Osman ATAHAN** Istanbul Technical University	....
Jury Members :	**Prof. Dr. Hilmi B. CELIKOGLU** Istanbul Technical University	....
	Prof. Dr. M. Vefa AKPINAR Istanbul Technical University	....
	Prof. Dr. Şenol ATAOĞLU Karadeniz Technical University	....
	Prof. Dr. Hakan GÜLER Sakarya University	....

Date of Submission : 17 July 2019
Date of Defense : 08 August 2019

To my family,

FOREWORD

The completion of my Ph.D. dissertation has been a long journey. Through this journey, I was fortunate enough to know great people that I would like to thank and acknowledge. My deepest thanks and gratitude go to my advisor, Prof. Dr. Ali Osman Atahan, for supporting me during my work. Prof. Atahan is someone you will instantly love and never forget once you meet him. He is the funniest advisor and one of the smartest people I know. I hope that I could be as lively, enthusiastic, and energetic as Prof. Atahan. He has made himself available tirelessly to support me and my research. I was able to contact him and receive an immediate response at any hour of the day. His role in helping me complete this dissertation is immeasurable. I am also grateful for his efforts to ensure I am on the right track all the time.

I would like to express my sincere thanks to Prof. Dr. Hilmi Berk Celikoglu for his valuable guidance and consistent encouragement throughout the research process. I appreciate all his contributions of time and recommendations to make my Ph.D. experience productive and stimulating. I would like also to thank Prof. Dr. Abdullah Hilmi Lav for his help and support. He is really a great person that I enjoyed working with and learning from him. I also have to thank the members of my Ph.D. committee, Prof. Dr. Muhammet Vefa Akpinar for his advice, kindness and the time he gave to serve on my academic life. Also, many thanks to Prof. Dr. Senol Ataoglu.

I would like to thank my colleagues throughout this process who listened, supported and gave advice, as well as for being wonderful co-workers and friends, in particular, Hazal Yilmaz, Mehmet Ali Silgu, and Gozde Bakioglu. Thanks also to other colleagues that I had the pleasure of collaborating with on work not directly related to this thesis Prof. Dr. Kemal Selcuk Ogut, Dr. Nurbanu Caliskan, and Assoc. Prof. Dr. Pelin Alpkokin. Thanks also to members of the Transportation Engineering Division of Istanbul Technical University.

I would like to gratefully acknowledge financial support by the Scientific and Technological Research Council of Turkey, TUBITAK project number 213M516. Also, I would like to greatly acknowledge Dr. Murat BUYUK, Dr. Murat Ornek, Mr. Musab Erdem and Mr. Yakup Turedi for their contributions in the TUBITAK project number 213M516.

I would like to thank Kiper Engineering for their support in providing crash test reports and technical assistance.

And foremost, I would like to thank my parents, who supported me in all ways, did everything possible to encourage me and provided unconditional love and care. Special thanks to my sisters and my brothers, who all have been supportive and caring. I would not have made it this far without them. Thank you for everything!

July 2019

Sedat OZCANAN
(Civil Engineer-M.Sc)

TABLE OF CONTENTS

Page

ABBREVIATIONS

ASI	: Acceleration severity index
CBR	: California bearing ratio
DOE	: Design of experiment
EN1317	: European norm
FE	: Finite element
FEA	: Finite element analysis
FEM	: Finite element model
FFD	: Full factorial design
GA	: Genetic algorithm
GMSE	: General mean squared error
LHD	: Latin hypercube design
LS-DYNA	: Livermore software open code 3D finite element program
MAE	: Maximum absolute error
MASH	: Manual for assessing safety hardware
MOEA	: Multiobjective evolutionary algorithms
MOGA	: Multi-objective genetic algorithm
MOO	: Multi-objective optimization
NJ	: New Jersey
NSGA-II	: Non-dominated sorting genetic algorithm II
OWPE	: Optimal weighted point-wise ensemble
PED	: Post embedment depth
PRESS	: Prediction sum of square
$PRESS_{RMS}$	: Root mean square of PRESS
RBF	: Radial basis function
RBF-MQ	: Radial basis function-Multiquadric
RE	: Relative error
RMSE	: Root mean square error
$RMSE_{CV}$	: Root mean square cross-validation error
SSE	: Sum of squared errors
SBDO	: Simulation-based design optimization

SYMBOLS

c	: User-defined constant
d	: Euclidean distance
$\boldsymbol{f_i(x)}$	: *i*th objective function
$\boldsymbol{g_j(x)}$	: *i*th inequality constraint
$\boldsymbol{h_k(x)}$	: *i*th equality constraint
k	: Number of the omitted sample point
n	: Number of samples
N	: Sample size
w	: Working width
$\boldsymbol{x}$	: An n-dimensional vector
$\boldsymbol{x_{1,2}}$	: Variables
$\boldsymbol{x_i}$	: Vector of design variables at the *i*th sampling point
$\mathbf{x}^{L}$	: Lower bounds of x
$\mathbf{x}^{U}$	: Lower bounds of x
$\boldsymbol{y_{\mathrm{x}}}$	: True objective function
$\boldsymbol{\bar{y}_{\mathrm{x}}}$	: Approximate objective function
$\boldsymbol{\bar{y}_{\mathrm{i}}}$	: Surrogate estimation at *i*th training point by all sample
$\boldsymbol{\bar{y}_{\mathrm{i}}^{(-i)}}$	: Surrogate estimation at *i*th training point by except *i*th point
$\boldsymbol{\alpha}$	: Exit angle
$\boldsymbol{\beta_i}$	: Coefficient of the *i*th basis function
$\emptyset_{\boldsymbol{i}}$	: Basis function
$\boldsymbol{w_i(x)}$	: The weight of $\bar{y}_i$ at x

LIST OF TABLES

Page

LIST OF FIGURES

Page

RADIAL BASIS FUNCTION SURROGATE MODEL-BASED OPTIMIZATION OF ROAD RESTRAINT SYSTEMS: THREE CASE STUDIES

SUMMARY

The purpose of using roadside safety equipment is to protect vehicle occupants during an accident by reducing the severity of impact. Using poorly designed safety equipment can have serious consequences. While roadside safety elements are designed primarily for safety, cost-effectiveness cannot be overlooked. For guardrail designers it is essential to achieve a crashworthy and optimal system design. Therefore, one of the most critical parameters for an optimal road restraint system is the post embedment depth or the post-to-soil interaction. In addition, cross-sectional thickness of the system part also play an important role in guardrail safety and economic design. With all this, for roadside safety equipments, advantages provided by the material and ease of assembly/disassembly, the ease of repair provided by minimum deformation after a collision and sustainability are preferred reasons by authorities and practitioners. In the light of the above explanations, considering the factors affecting road safety systems, three cases were handled and their optimization is purposed in this thesis. The cases are determination of optimum embedment depths of C, H and S post types, cross-sectional optimization of H1W4 and H2W4 guardrail systems manufactured from S235JR, S275JR and S355JR grade steel materials, and achieve optimum safety design of the New Jersey (NJ) concrete barrier which is preferred system because of its advantages. The case studies are summarized as

Case 1:

This case aimed to assess the optimum post embedment depths of three different guardrail posts embedded in soil with varying density. Posts were subjected to dynamic impact loads in the field while a detailed finite element study was performed to construct accurate models for the post-soil interaction. It is well-known that experimental tests and simulations are costly and time consuming. Therefore, to reduce the computational cost of optimization, radial basis function-based metamodeling methodology was employed to create surrogate models that were used to replace the expensive three-dimensional finite element models. In order to establish the radial basis function model, samples were derived using the full factorial design. Afterwards, radial basis function-based metamodels were generated from the derived data and objective functions performed using finite element analysis. The accuracy of the metamodels were validated by “*k*-fold cross-validation”, then optimized using multi-objective genetic algorithm. After optimum embedment depths were obtained, finite element simulations of the results were compared with full scale crash test results. In comparison with the actual post embedment depths, optimal post embedment depths provided significant economic advantages without compromising safety and crashworthiness. It is concluded that the optimum post embedment depths provide an economic advantage of up to 17.89%, 36.75% and 43.09% for C, S, and H types of post, respectively, when compared to actual post embedment depths.

Case 2:

In the case two, it is aimed to optimize H1W4 and H2W4 performance level guardrails manufactured from S235JR, S275JR and S355JR grade steel materials in terms of safety and economy. For this purpose, surrogate model based optimization is utilized. In this context, the design variables are selected as post width (x1) and cross-sectional thickness of rail (x2), while objective functions are selected as working width (w) and vehicle exit angle (α). The design variables (x1, x2) are derived by full factorial design (FFD) method and crash test simulations are utilized to construct objective and constraint functions. Consequently, Radial Basis Function (RBF)-based metamodels are created with the help of the obtained data and later the accuracy of the models is validated. Finally, the RBF metamodels are optimized using the multi-objective genetic algorithm (MOGA). As a result of the simulation-based design optimization (SBDO), the optimum designs of H1W4 and H2W4 guardrail systems for different steel material grades are achieved. It is concluded that the final/optimal guardrail designs meet the EN1317 safety criteria as well as provide an economic advantage of up to 23% compared to existing guardrail designs.

Case 3:

In final case, along with the advantages provided by the material and ease of assembly/disassembly, the ease of repair provided by minimum deformation after a collision and its sustainability highlight the preference of concrete barriers for roadside safety. However, concrete barriers, as rigid systems, are highly risky in case of a collision. Because the top priority of the application purpose is safety, it is desirable to have designs which provide the necessary safety criteria in the relevant standards and which are highly safe in terms of environment, especially for drivers. In this case, the optimum safety design of the New Jersey (NJ) concrete barrier which reduces injury levels up to the acceleration severity index (ASI) and meets safety criteria for the EN1317/2 standard, is achieved by simulation-based design optimization (SBDO). For this purpose, the critical design points of the New Jersey type barrier have been determined. Then the critical design points were taken as variables and the safety criteria in EN1317 were taken as the objective function for multi-objective optimization (MOO). Once the variables and objective functions were determined, data was prepared with finite elements (FE) and the surrogate model was constructed using an optimal weighted pointwise of radial basis function (OWPE-RBF). Afterward, the multi-objective genetic algorithm (MOGA/NSGA-II) was employed to solve the MOO problem. The optimum safety design that was obtained was compared with the validated original design, i.e. full-size modeling in the finite element (FE) environment. As a result, both the critical design points of NJ type barriers and important determinations regarding the OWPE-RBF model were obtained. Above all, a design has been achieved with an ASI/injury level which is 22-23% safer by way of the proposed analytical model and the monitored path.

YOL GÜVENLİK ELEMANLARININ RADYAL TEMELLİ FONKSİYON TABANLI VEKİL MODEL İLE ENİYİLEMESİ: ÜÇ VAKA ÇALIŞMASI

ÖZET

Karayolu güvenliği; hem yolu kullananların can güvenliğinin, hem de yolun geçtiği çevrenin önem derecesine göre korunmasını amaçlamaktadır. Bu kapsamda varolan karayolu geometrik standartlarının yükseltilmesi, katılım denetimi ve hız kısıtı gibi önlemlerin yanında, yoldaki önem derecesi yüksek bölgelere yolkenar koruyucu yapıları yapılmaktadır. Otokorkuluk, çarpma yastığı, uç terminalleri ve benzeri yolkenar koruyucu yapıları (YKY), yol platformuna paralel olarak refüjde veya yolkenarında inşa edilen, araçların yoldan çıkmaları durumunda çarpma ihtimalleri bulunan suni engellerdir. YKY araçların yolkenarlarında bulunan doğal veya insan yapısı engellere çarpması, köprüden düşmesi, şarampole yuvarlanması gibi tehlikeli durumları önlemek ve dolayısıyla araç içerisindeki yolcuları korumak için kullanılır. Arasıra da olsa yayaları, bisikletlileri veya yol kenarında çalışan görevlileri araç trafiğine karşı koruma amaçlı da kullanılabilirler. YKY içerisinde en yaygın olarak kullanılanı otokorkuluklardır. Otokorkuluklar karayollarında kullanılan pasif güvenlik tertibatlarından biridir ve kendisine araç darbesi olana kadar yol güvenliğine herhangi bir katkıda bulunmazlar. Otokorkuluklar genel olarak çarpan araçları karayolu içerisinde, mümkünse güvenlik şeridinde tutmak, araçların hareket enerjisini yutmak ve onları yavaşlatarak durdurmak üzere tasarlanırlar.

Tasarımı amaçlanan mühendislik yapılarının tam boyutlu gerçek testleri hem pahalı hemde zaman almaktadır. Nümerik (sonlu elemanlar) modellemelerin ve sayısal algoritmaların gelişmesiyle beraber, mühendislik yapılarının tam ölçekli modellerinin, Ls-Dyna ve benzeri ticari sonlu elemanlar programları kullanılarak modellenmesi yaygınlaşmaktadır.

Nümerik benzetimler kullanılarak yapılan tasarımlar zaman ve verim açısından avantaj sağlamaktadır. Özellikle nümerik yöntemler analitik (matematik) yöntemlerle birleştirilerek yapılan benzetim tabanlı tasarım eniyileme çalışmalarıyla eniyi tasarımlar elde edilebilmektedir.

Benzetim tabanlı tasarım eniyilemesi yönteminde genel anlamda izlenen yol; öncelikle farklı kombinasyonlarda ve çeşitli benzetimler yapılarak sistemin davranışları belirlenir. Daha sonra elde edilen benzetim verilerine, uygun eniyileme yöntemi uygulanarak ideal tasarım elde edilir. Fakat çok sayıda benzetim yapmak yüksek maliyet ve zaman gerektirmektedir. Bundan dolayı genellikle sezgisel model/metamodel (surrogate model) tercih edilmektedir. Metamodel; uygulanan modelin, kendisinin çeşitli bileşenleri arasındaki ilişkilerin açıklanması ve tanımı için hizmet veren modelin modelidir. Esas modeli taklit eden model olarakta açıklanmaktadır. Metamodel çok sayıda benzetim yapmak yerine, benzetimi yapılacak modelleri taklit ederek, maliyet ve zamandan avantaj sağlayabilmektedir.

Otokorkuluklar genel olarak yatay doğrultuda ray ve dikey doğrultuda dikmelerden oluşur. Araç çarpması durumunda ray esneyerek darbe yüklerini dikmelere aktarır ve

dikmeler de yükü mesnetlendiği zemine iletir. Tasarımın istendiği gibi çalışabilmesinde dikmelerin zemine gömülme derinlikleri en önemli detaylardan birisidir. Bilindiği gibi karayollarında otokorkulukların çakıldığı zeminler genellikle büyük değişiklikler göstermesine rağmen otokorkuluk çakılma derinlikleri zeminlerin özelliklerine göre belirlenmemektedir. Uygulamada dikme gömülme derinliğinin her tip zeminde aynı olması mühendislik açısından kabul edilebilir bir durum değildir. Ayrıca otokorkulukları oluşturan ray ve dikme gibi ana parçaların kesit ve geometrik ölçüleri sistemin güvenlik performansını ve ekonomik tasarımı etkilemektedir. Tüm bunlarla beraber güvenlik, sağlamlık, malzeme ömrü ve montaj/demontaj avantajları otokorkuluk sistemlerinin tercih edilmesinde etkili faktörlerdir.

Yukarıdaki açıklamaların ışığında, karayolu güvenliği sistemlerini etkileyen faktörler göz önüne alındığında, üç vaka ele alınmış ve bu tezde eniyilemeleri amaçlanmıştır. Ele alınan bu vakalar/durumlar, C, H ve S tipi dikmelerin eniyi gömülme derinliklerinin belirlenmesi, S235JR, S275JR ve S355JR kalite çelik malzemelerden üretilen H1W4 ve H2W4 korkuluk sistemlerinin kesitsel eniyilemesi ve sağladığı avantajlar nedeniyle tercih edilen otokorkuluk sistemi olarak New Jersey (NJ) tipi beton bariyerin eniyi/en emniyetli tasarımının elde edilmesidir. Yapılan çalışmalar aşağıda özetlenmiştir.

Durum 1:

İlk durumda, üç farklı korkuluk dikmesinin değişenken yoğunlukta toprağa gömülü eniyi/faydalı derinliklerini bulmayı amaçladı. Dikmeler, sahada dinamik darbe yükleri ile test edilerek, dikme-toprak etkileşimi araştırılmış ve daha sonra detaylı sonlu elemanlar modelleri yapılmıştır. Deneysel testlerin ve benzetimlerin pahalı ve zaman alıcı olduğu iyi bilinmektedir. Bu nedenle, eniyileme hesaplama maliyetini düşürmek için, deneysel ve pahalı üç boyutlu sonlu eleman modellerini taklit edecek taşıyıcı/vekil modelleri oluşturmak için radyal temelli fonksiyon tabanlı metamodelleme metodolojisi kullanılmıştır. Radyal temelli fonksiyon modelini oluşturmak için, tam faktöryel tasarımı yardımıyla örneklemler türetilmiştir. Daha sonra, türetilmiş veriler sonlu elemanlar analizleri kullanılarak amaç fonksiyonları oluşturuldu. Türetilen değişkenler ve amaç/kısıt fonksiyonları yardımıyla radyal temelli fonksiyon tabanlı metamodeller üretildi. Metamodellerin doğruluğu "*k*-kat çapraz doğrulama" ile sınandı, daha sonra çok amaçlı genetik algoritma kullanılarak eniyileme yapıldı. Eniyi gömülme derinlikleri elde edildikten sonra, sonuçların sonlu eleman benzetimleri, tam ölçekli çarpışma testi sonuçlarıyla karşılaştırıldı. Eniyi gömülme derinlikleri gerçek gömülme derinlikleriyle karşılaştırıldığında, güvenlik ve çarpma dayanıklılığından ödün vermeden önemli ekonomik avantajlar sağlamıştır. Yapılan karşılaştırmadan, C, S ve H tipi dikmeler için sırasıyla % 17.89, % 36.75 ve % 43.09 gibi bir ekonomik avantaj sağlandığı sonucuna varılmıştır.

Durum 2:

İkinci durumda, S235JR, S275JR ve S355JR kalite çelik malzemelerden üretilen H1W4 ve H2W4 performans seviyesindeki korkulukların güvenlik ve ekonomik açısından optimize edilmesi amaçlanmaktadır. Bu amaçla, taşıyıcı/vekil model tabanlı eniyileme kullanılmıştır. Bu bağlamda, tasarım değişkenleri dikme genişliği (x1) ve rayın kesit kalınlığı (x2), objektif fonksiyonlar çalışma genişliği (w) ve araç çıkış açısı (α) olarak seçilmiştir. Tasarım değişkenleri (x1, x2), tam faktöryel tasarım (FFD) yöntemi ile türetilmiş, amaç ve kısıt fonksiyonlarını elde etmek için türetilen verilerin sonlu elemanlar benzetimleri kullanılmıştır. Sonuç olarak, radyal temelli fonksiyon (RBF) bazlı metamodeller, elde edilen veriler yardımıyla oluşturulmuş ve daha sonra modellerin doğruluğu sınanmıştır. Son olarak, RBF metamodelleri çok amaçlı genetik algoritma (MOGA) kullanılarak eniyilemesi yapılmıştır. Benzetime dayalı tasarım eniyilemesi (SBDO) sonucunda, farklı çelik malzemesi sınıfları için H1W4 ve H2W4 korkuluk sistemlerinin eniyi tasarımları elde edilmiştir. Eniyi otokorkuluk tasarımlarının EN1317 standartı güvenlik kriterlerini sağlamasının yanında, mevcut otokorkuluk tasarımlarına kıyasla % 23'e varan bir ekonomik avantaj sağladığı sonucuna varılmıştır.

Durum 3:

Son durumda, malzemenin sağladığı avantajlar ve montaj/sökme kolaylığı ile birlikte, bir çarpışmadan sonra en az hasarla sağlanan onarım kolaylığı ve sürdürülebilirliği, yol kenarı güvenliği için beton bariyerlerin tercihini arttırmaktadır. Bununla birlikte, rijit sistemler olarak beton bariyerler çarpışma durumunda oldukça risklidir. Bu sistemlerin uygulama amacının en büyük önceliği güvenlik olduğu için, ilgili standartlarda gerekli güvenlik kriterlerini sağlayan ve çevre açısından, özellikle sürücüler için oldukça güvenli olan tasarımlara sahip olmak istenmektedir. Bu çalışmada, New Jersey (NJ) beton bariyerinin, hızlanma şiddeti endeksine (ASI) bağlı yaralanma seviyesini azaltan ve EN1317/2 standardındaki güvenlik kriterlerini karşılayan eniyi/en emniyetli tasarımı, benzetim tabanlı tasarım eniyilemesi (SBDO) hedeflenmiştir. Bu amaçla, New Jersey tipi bariyerin kritik tasarım noktaları belirlenmiştir. Ardından kritik tasarım noktaları değişken olarak alınmış ve EN1317'deki güvenlik kriterleri çok amaçlı eniyileme (MOO) için amaç fonksiyonu olarak alınmıştır. Değişkenler ve objektif fonksiyonlar belirlendikten sonra, veriler sonlu elemanlar (FE) ile modellenerek taşıyıcı/vekil model, radyal baz fonksiyonunun eniyi ağırlıklı noktasal birliği (OWPE-RBF) şeklinde kurulmuştur. Daha sonra, MOO problemini çözmek için çok amaçlı genetik algoritma (MOGA/NSGA-II) kullanılmıştır. Elde edilen eniyi güvenlikli tasarım, doğrulanmış orijinal tasarımla, sonlu elemanlar (FE) ortamında tam boyutlu modelleme yapılarak kıyaslanmıştır. Sonuç olarak, NJ tipi bariyerlerin kritik tasarım noktaları ve OWPE-RBF modeliyle ilgili önemli tespitler elde edildi. Her şeyden önce, önerilen analitik model ve izlenen yol ile % 22-23 daha güvenli olan ASI-yaralanma seviyesine sahip bir tasarım elde edildi.

1. INTRODUCTION

The most widely used roadside safety elements are guardrails. Guardrails are one of the passive safety devices used on the roads and do not affect road safety until a vehicle crash occurs. Guardrails are generally designed to keep impacting vehicles on the road, if possible within the safety lane, by absorbing the motion energy of the vehicles and thus slowing them down [1].

Roadside safety aims to provide the utmost safety to vehicle occupants during an accident event. In this context, road restraint systems (RRS), such as longitudinal barriers are implemented in high-risk zones on highways. Longitudinal barriers generally consist of a rail in the horizontal direction and posts in the vertical direction. In the event of a vehicle impact, the rail deforms and transfers the impact loads to the posts while the posts transmit the load to the ground, where they are installed. Hence, Post Embedment Depth (PED) is considered an important aspect of the barrier design to work properly. From an engineering point of view, the PED should be determined based on soil properties. However, this is often neglected since not much data exists in the literature related to the determination of optimum PED based on soil properties for longitudinal barriers.

Together with the PED, the cross-section of the guardrail is another important factor that determines the safety performance and ergonomics of the guardrail. In particular, post and rail thickness are the most important guardrail elements in this sense. The factor to which the cross-section thickness depends on is the grade of steel material that used.

Finally, concrete barriers are the obstacles set in parallel to the moving road, which is used to prevent vehicles from leaving the road and/or to prevent errant vehicle from violating traffic safety during an accident. They are one of the most common types of roadside equipment commonly used to keep vehicle and pedestrian traffic out of working areas, protect workers, separate two-way traffic, and protect construction equipment in highway work areas. Their portability and versatility are advantageous in areas with less tolerance/margin. Typically, as parted barriers, concrete barriers can be end-to-end with a load-bearing connection. In addition, the partitioning of the barrier allows easy installation and relocation and re-positioning in the work area. Concrete barriers are available with semi-permanent applications to the ground with an auxiliary apparatus. Concrete barriers used for different application purposes, as mentioned above, must provide safety criteria in the relevant standards. The minimum safety criteria required for barrier design, especially for roadside safety, are specified in the MASH [2] and EN1317 [3] standards, which are taken as a reference worldwide. The barrier design process is a costly process that requires both numerical analysis and real crash testing from start to finish. In engineering designs, whose empirical and numerical tests are cost-effective and time-consuming, surrogate models have been developed to mimic real engineering models that greatly reduce the cost burden.

1.1 Simulation-Based Design Optimization (SBDO)

Simulation-based optimization integrates optimization techniques into simulation analysis. Because of the complexity of the simulation, the objective function may become difficult and expensive to evaluate.

Once a system is mathematically modeled, computer-based simulations provide information about its behavior. Parametric simulation methods can be used to improve the performance of a system. In this method, the input of each variable is varied with other parameters remaining constant and the effect on the design objective is observed. This is a time-consuming method and improves the performance partially. To obtain the optimal solution with minimum computation and time, the problem is solved iteratively wherein each iteration the solution moves closer to the optimum solution. Such methods are known as ‘numerical optimization’ or ‘simulation-based optimization’[4].

In the simulation experiment, the goal is to evaluate the effect of different values of input variables on a system. However, the interest is sometimes in finding the optimal value for input variables in terms of the system outcomes. One way could be running simulation experiments for all possible input variables. However, this approach is not always practical due to several possible situations and it just makes it intractable to run experiments for each scenario. For example, there might be too many possible values for input variables, or the simulation model might be too complicated and expensive to run for suboptimal input variable values. In these cases, the goal is to find optimal values for the input variables rather than trying all possible values. This process is called simulation optimization [5].

1.2 Multi-Objective Genetic Algorithm (MOGA/NSGA-II)

Multi-objective formulations are a realistic models for many complex engineering optimization problems. Customized genetic algorithms have been demonstrated to be particularly effective to determine excellent solutions to these problems. In many real-life problems, objectives under consideration conflict with each other, and optimizing a particular solution with respect to a single objective can result in unacceptable results with respect to the other objectives. A reasonable solution to a multi-objective problem is to investigate a set of solutions, each of which satisfies the objectives at an acceptable level without being dominated by any other solution. In this paper, an overview and tutorial is presented describing genetic algorithms developed specifically for these problems with multiple objectives. They differ from traditional genetic algorithms by using specialized fitness functions, introducing methods to promote solution diversity, and other approaches [6].

1.3 Purpose of Thesis

As mentioned above, the two important factors affecting the safety performance and ergonomic design of the guardrail are soil types, where the guardrails are embedded in, and the steel material types that used in the design. Together with these, acceleration severity index (ASI) based security of concrete barrier, which is most preferred road restraint systems, should be improved. Therefore, the purpose of the thesis is, firstly, to determine the optimum PED of standard longitudinal barriers based on the soil density properties of Turkish roadsides. To achieve this purpose, a series of experimental tests and computer simulations were utilized. Also, in order to reduce the number of finite element simulations and make the design process more economical and efficient, finite element simulation-based design optimization (SBDO) applications were also utilized. Hence, a metamodel of the target problem was created using multi-objective optimization and radial basis function (RBF) methods. Then, the objective function of the metamodels was optimized with a multi-objective genetic algorithm (MOGA) to achieve the desired PED for different guardrail posts. Secondly, after obtaining optimum PED, cross-sectional optimization of H1 and H2 guardrail systems, which are widely used in Turkey, manufactured by S235JR, S275JR, and S355JR steel materials is purposed. Based on the safety criteria described in the EN1317 standard, SBDO methodology was utilized. Within this framework, first, design variables and objective functions are defined for optimization. After calibration of the FE models, the derived design variables are modelled in the FE environment to form the objective functions. Later, RBF surrogate models are established with the aid of the obtained data. After validation of surrogate models, the MOGA was performed to get optimum results of guardrail systems. Finally, comparative simulation results of optimum models and consequences are presented. As the third, traffic accidents are one of the leading problems in transportation. Traffic accidents occur on the basis of road, weather conditions and driver perception negativity. Traffic accidents create great emotional and economic problems in human society due to physical pain, vital losses, and financial burdens. To reduce the number and mitigate the impacts of traffic crashes, numerous studies have been conducted to improve the understanding and prediction of traffic crashes [7]. However, it is known that a well-designed barrier helps to reduce the loss of life and property in accidents [8]. Barriers are a restraint system that are used to ensure road safety. They are classified as rigid, semi-rigid, and flexible. Concrete barriers are rigid, steel guardrails are semi-rigid, and steel rope guardrails are examples of flexible guardrail systems. Particularly rigid guardrail systems create serious safety problems for light vehicles. In the EN1317 [3] standard, ASI values of these systems generally become B/C level. In this case, the shape parameters, which affect the ASI-based safety/injury level, of the commonly used NJ-type concrete barrier, will be investigated. The NJ-type concrete barrier will be optimized in order to improve the ASI-based injury level by detecting the parameters. For this purpose, OWPE-RBF metamodel based optimization was used as an analytic method.

1.4 Hypothesis

The hypotheses were evaluated in this thesis given below:

- Using the surrogate model in design process of road restraint system can reduce computational cost and burden.

- Soil density and material grade depended optimization of road restraint systems enables more economical design.
- Safety related the ASI/Injury level of concrete barrier can enhanced by surrogate model.

The rest of the thesis is organized as follows: Chapter 2; explain and cover the literature studies about the surrogate models. Chapter 3; the research methodology used in the thesis is explained. Chapter 4; the RBF based metamodel optimization is given by explaining the case studies and highlighting the research objectives and the hypotheses. Chapter 5; the results obtained are evaluated in detail, and finally, Chapter 6 concludes the research findings and the recommendations, gives some contribution for futher studies.

2. LITERATURE REVIEW

2.1 Multiquadric-Radial Basis Function (RBF-MQ)

Full-scale crash testing is the widely accepted method used for the evaluation of road safety barriers. However, due to its excessive cost, limited data acquisition, and scheduling, it is not desirable to perform a series of crash tests. Thus, full-scale numerical simulations of crash tests are used to obtain ideas about the crash performance of designs and help improve them if necessary before going into full-scale crash testing [9]. For this purpose, LS-DYNA [10], a non-linear 3D multi-purpose finite element program is utilized. Full-scale crash tests are performed in accordance with standards. One of the widely used standards published by the American Association of State Highway and Transportation Officials is the Manual for Assessing Safety Hardware or MASH [2]. In Europe, on the other hand, the EN1317 [3] standard is utilized to evaluate the adequacy of roadside safety systems. This standard has been utilized since 2011 in Turkey.

Studies on the numerical modelling of longitudinal barriers began in the 1960s and particularly after 2000, there were significant improvements in full-scale crash testing simulations of RRS, such as concrete barriers, steel guardrails, cable barriers, and crash cushions or end terminals, etc. [11-32]. However, full-scale crash testing of engineered structures is both costly and time-consuming. With the development of accurate finite element models and algorithms, impact performance of RRS is more frequently assessed using LS-DYNA [10] and similar commercial finite element programs. In terms of time and efficiency, numerical simulations provide significant advantages. In particular, numerical methods can be combined with analytical methods to obtain optimum designs with simulation-based design optimization (SBDO) studies. There are many studies in the literature of this particular research area [33-44].

In general, SBDO method relies on evaluating various combinations to determine the response behavior of a particular system. Then, an optimization method is applied to the obtained simulation data to get an optimal design. However, many simulations are costly and require long running times. Instead of performing a lot of simulations, a metamodel, defined as a model of a simulated model, can provide cost and time advantages. Some studies related to this subject are as follows: Yin et al. [45] optimized the shape of MASH TL-3 concrete barriers using RBF-based metamodels and nonlinear finite element simulations. As a result, it was stated that the safety performance of the original concrete barrier was improved. In another study conducted by Yin et al. [46], the wheel snagging problem was targeted. To eliminate this situation, non-linear finite elements and metamodel-based design methods were successfully used to develop "η-shaped W-guardrail (η-WG)" optimization. The results presented were intended to improve the safety performance of longitudinal barriers. Hou et al. [47] focused on the optimization of New Jersey concrete barriers based on safety assessments. In the same study, the efficiency of RBF-MQ (multi-quadratic) and RBF-LP (linear polynomial) methods were also investigated and the RBF-MQ method was found to yield more effective results. In another study by Hou et al. [48] finite element simulations, RBF and multi-objective optimization were used to determine optimal post and rail thickness as well as post spacing for a steel longitudinal barrier. It was concluded that collision safety was improved in two different guardrail systems by removing the conditions that caused the tire snagging during a collision. Ozcanan and Atahan [49] aimed to optimize H1W4 and H2W4 performance level guardrails manufactured from S235JR, S275JR, and S355JR grade steel materials in terms of safety and cost-effectiveness. For this purpose, an RBF surrogate model-based optimization was utilized. It was concluded that the final guardrail designs met the safety criteria as well as providing an economic advantage of up to 23% compared to existing designs. In another study by Ozcanan and Atahan [50] was purposed to assess the optimum post embedment depths of three different guardrail posts embedded in soil with varying density. It was concluded that the optimum post embedment depths provide an economic advantage of up to 17.89%, 36.75% and 43.09% for C, S, and H types of post, respectively, when compared to actual post embedment depths. When these studies are examined, it can be seen that RBF-based surrogate modeling is preferred. Due to the fact that the RBF-based metamodels have the potential to be a significant tool in performance evaluation of RRS and improve analysis effectiveness by predicting results more accurately [51-52].

Radial basis functions (RBFs) are approximate mathematical models used as surrogates for fast changing and computationally expensive simulations. RBFs have many attractive features including: (i) their capability of accurately modeling arbitrary functions, (ii) their capability of handling scattered training points in multiple dimensions, and (iii) their relatively simple implementation compared to Kriging and neural networks [53-54]. Due to these potential capabilities, RBFs have been used in many engineering applications.

2.2 Optimal Weighted Pointwise Ensemble of Radial Basis Function (OWPE-RBF)

Experimental and computational simulation techniques play an important role in the design and optimization of complex engineering systems [55-58]. The techniques used for design and optimization require high cost and accuracy [59-60]. The costly and time-consuming optimization process is a major problem in terms of design sustainability. To overcome this problem, a surrogate model (also known as a metamodel), which is a complete substitute for experimental and computational simulation techniques, is used [61]. Metamodels are utilized to mimic computationally expensive simulation models or experiments by establishing the necessary relationship between limited data and system inputs and outputs. As polynomial response surface (PRS) [60, 62], kriging (KRG) [63-65], radial basis function (RBF) [66-68] and support vector regression (SVR) [69-70], many types of surrogate models have been applied successfully to lots of structures and for solving multidisciplinary design optimization problems.

The rapid development of various surrogate models, have provided flexibility in the choice of surrogate models for different problems, but has posed a challenge in selecting models for specific applications [71]. It is proven that a single surrogate model is not always the best model available for all engineering applications [72]. This is because real engineering problems usually have different linear or non-linear properties and each metamodel has its own advantages and disadvantages in terms of their structure [73-75]. For example, in a high-dimensional problem, the relationship between input and output may be linear, so a simple first-order PRS model may be sufficient and better to represent the problem [76]. On the other hand, for a non-linear relationship in a low-dimensional problem, an RBF model may be more appropriate for representing the problem [77]. Since it is difficult to predict behavior due to the complexity of practical engineering applications, it is extremely difficult to select the most appropriate metamodel before optimization. For this purpose, in order to benefit from the advantages of each surrogate model by the researchers, a hybrid/ensemble metamodel has been developed [72, 78]. Most of these developed hybrid/ensemble models are based on error correlation or variance of estimation. Furthermore, in these models, weight factors are constant throughout the entire design area. Although these models provide better accuracy than individual models for most problems, it has been observed that they do not always guarantee a better solution than the best selected individual model, and that potential gains for particularly high dimensional problems are reduced [79-81]. This is because globally constant weight coefficients of these models do not reflect the local accuracy of each surrogate model. Thus, these models may cause incorrect estimates in certain local areas. In order to overcome this deficiency, many researchers have tried to develop hybrid/ensemble metamodels capable of both global and local estimation accuracy. In these studies, adaptive hybrid surrogate models have generally been shown to perform better than hybrid models with constant weight [82-83]. Liu et al. [84] developed an optimal weighted pointwise ensemble (OWPE) to combine locally accurate predictions of RBF models with different basis functions. In this study, it was stated that the developed OWPE of RBF model made more accurate predictions than Acar [82], AHF [83], Goel [72] and Lee and Choi [85] hybrid/ensemble models.

3. RESEARCH METHODOLOGY

3.1 Radial Basis Function (RBF)-Based Metemodel

RBF is one of the multi-dimensional interpolation methods and has been widely used for approximating engineering system responses involving expensive numerical simulations [45]. These functions were developed for scattered multivariate data interpolation [86-87]. Theoretically, when $y(x)$ is the true objective function and the $\bar{y}(x)$ is the approximation, the basic form of RBF can be formulated as

$$\bar{y}_{RBF}(x) = \sum_{i=1}^{n} \beta_i \emptyset_i(\|x - x_i\|) = \beta^T \emptyset \tag{3.1}$$

where n is the number of samples, x is an n-dimensional vector of variables, x_i is the vector of design variables at the $\boldsymbol{i}$th sampling point, $\emptyset_{\boldsymbol{i}}$ is the basis function, $\|x - x_i\|$ is the Euclidean distance, and β_i is the coefficient of the ith basis function.

Some of the commonly used [45-48, 88-94] basis functions for constructing RBF are listed in Table 3.1. Where d is the Euclidean distance and c ($c > 0$) is a user-defined constant.

Table 3.1 : Some commonly used basis functions for RBF interpolation.

Name	Function
Multiquadric-MQ	$\emptyset(d) = \sqrt{c^2 + d^2}$
Inverse multiquadric-IMQ	$\emptyset(d) = 1/\sqrt{c^2 + d^2}$
Gaussian-GA	$\emptyset(d) = \exp(-cd^2)$
Cubic-CB	$\emptyset(d) = (c + d)^3$
Thin-plate spline-TPS	$\emptyset(d) = d^2 \ln(cd^2)$
Linear-LN	$\emptyset(d) = cd$

In the thesis, the multiquadric one is chosen which produces the most stable RBF of all [33].

The parameter c in the multiquadrics is a constant. The shape parameter c plays an important role in the accuracy of the RBF models. In thesis, it was chosen the multiquadric formulation of RBF because of its prediction accuracy and its commonly linear and possibly exponential rate of convergence with increased sampling points.

By substituting x and $\bar{y}_{RBF}(x)$ in Equation (3.1) with n vectors of the design variables and their corresponding true function values at the sampling points, we can obtain the following equations

$$y_1 = \sum_{i=1}^{n} \beta_i \emptyset_i(\|x_1 - x_i\|)$$

$$y_2 = \sum_{i=1}^{n} \beta_i \emptyset_i(\|x_2 - x_i\|)$$

$$\cdots \tag{3.2}$$

$$y_n = \sum_{i=1}^{n} \beta_i \emptyset_i(\|x_n - x_i\|)$$

The matrix form of Equation (3.2) is as follows

$$Y = \beta . \emptyset \tag{3.3}$$

where $Y = [y_1, y_2, \dots, y_m]^T$, yi (i = 1, 2,…,m) is the corresponding true function value, $\emptyset_{\boldsymbol{i,j}} = \emptyset(\|x_i - x_j\|)$ (i = 1, 2,…, m, j = 1, 2,…, m), and $\beta = [\beta_1, \beta_2, \dots, \beta_m]^T$. The coefficient vector β can be determined by

$$\emptyset^{-1} . Y = \beta \tag{3.4}$$

3.1.1 Optimal weighted pointwise ensemble (OWPE) of RBF-based metamodel

After building an RBF model for a computationally expensive black-box function, we should assess its prediction accuracy. Firstly, we want to measure the local accuracy of metamodels. Hence we can use the cross-validation error criterion that requires only the data at observed points. The generalized mean square cross-validation error (GMSE) is very similar to the prediction error sum of squares (PRESS) statistic. If there are N training points, then a metamodel is constructed N times, each time leaving out one of the training points. Then the difference between the exact response at the omitted point and that predicted by each variant metamodel is used to evaluate the global error as

$$GMSE = \frac{1}{N}\sum_{k=1}^{N}\left(y^k - \bar{y}^{(k)}\right)^2 \tag{3.5}$$

where y^k is the true response at $\boldsymbol{x}_k$ and $\bar{y}^{(k)}$ is the corresponding predicted value from the metamodel constructed using all except the kth design point. As evident by (3.5), the greater the number of training points the higher the cost of calculating the GMSE metric. This metric gives an average error in the estimated response at the selected training points. Therefore, depending on the number and distribution of training points, GMSE may not necessarily provide evidence of global error in the whole domain of input variables. Therefore, it was used only to construct an ensemble of metamodels to measure pointwise accuracy of the metamodel. The error metrics to calculate FE validation and global accuracy of the metamodel ensemble are given in the next section.

After calculation of pointwise error of the metamodel, OWPE of RBF is constructed using a weighted-sum formulation in which expressed as

$$\bar{y}_e(x) = \textstyle\sum_{j=1}^{k} w_j(x)\,\bar{y}_j(x)$$

$$\text{where} \quad \sum_{j=1}^{k} w_j(x) = 1 \tag{3.6}$$

In Equation (3.6), $\bar{y}_e$ is the constructed ensemble model, $\bar{y}_j$ is the jth component RBF model, $w_j(\boldsymbol{x})$ is the weight of $\bar{y}_j$ at $\boldsymbol{x}$, and k is the number of component RBF models built with different basis functions. It is found that the key of the proposed method is to assign proper pointwise weights to component RBF models over the design space so that this method can accurately identify and sufficiently highlight the locally accurate predictions of component RBF models. The construction of the OWPE method follows two main steps:

I. For obtaining the weights at observed points, we use the 0–1 weight strategy. This simple strategy can sufficiently highlight the locally accurate predictions of component RBF models.

II. For obtaining the weights at unobserved weights, one should construct optimal pointwise weight functions by solving an efficient one-dimensional min-GMSE auxiliary problem. These weight functions can adapt to the characteristics of component RBF models.

The second step is applied so that the ensemble metamodel can adapt to different problems. However, there is only one engineering design problem as case 3 in the thesis and *k*-fold cross-validation error metric was used for metamodel validation of the problem. Therefore, it is not necessary to apply the second step procedure, since the error metric uses its own samples/observed points for validation.

3.2 Metamodel Accuracy Metrics

Error quantification methods can also be classified into global and local error estimation methods [72]. The performance of the surrogate over the entire domain is evaluated by global error measures, while local or point-wise error measures provide the surrogate accuracy in different locations of the design domain.

The accuracy of an RBF model can be evaluated using the relative absolute error (RAE) and maximum absolute error (MAE) between the actual (y_i) and the predicted ($\bar{y}_i$) values at i^{th} test point. The maximum absolute error (MAE) and relative absolute error (RAE) are indicative of local deviations:

$$RAE_i = \left|\frac{y_i - \bar{y}_i}{y_i}\right| \tag{3.7}$$

$$MAE = \max|y_i - \bar{y}_i|, i = 1, 2 \dots n \tag{3.8}$$

To measure the accuracy of the resulting metamodels, we use the standard error measure: root-mean-squared error (RMSE). Small values of the RMSE are desired. An RMSE value of 0 indicates a perfect fit. The RMSE provides information about the accuracy of the actual surrogate. However, RMSE requires additional system evaluations at test points in the case of interpolating surrogates. The error measure is defined as

$$RMSE = \sqrt{\frac{1}{n}\sum_{i=1}^{n}(y_i - \bar{y}_i)^2} \tag{3.9}$$

where n is the number of validation points. The prediction sum of square (PRESS) is based on the leave-one-out cross-validation error:

$$PRESS = \frac{1}{N}\sum_{i=1}^{N}(\bar{y}_i - \bar{y}_i^{(-i)})^2 \tag{3.10}$$

where $\bar{y}_i$ and $\bar{y}_i^{(-i)}$ are the surrogate estimations at the i^{th} training point respectively predicted by the surrogate constructed using all sample points and the surrogate constructed using all sample points except the i^{th} point and N equals the sample size. In the thesis, it is also used the root mean square error of k-fold cross-validation ($RMSE_{CV}$) [95], i.e., root mean square of PRESS ($PRESS_{RMS}$), to measure the global accuracy of the surrogate over the entire design domain:

$$RMSE_{CV} = \sqrt{\frac{1}{k}\sum_{i=1}^{k}(\bar{y}_i - \bar{y}_i^{(-i)})^2} \tag{3.11}$$

where k is the number of omitted sample points. In the method, the variation of k from i to k searched; then for each k value, the average of the error measured on all possible combinations of k points used to provide a measure of the global accuracy of the surrogate. In the thesis, MAE, RAE, and RMSE are used for local error measurements and shape parameter (c) optimization, and k-fold cross-validation ($RMSE_{CV}$) is used for global error measurement.

3.3 Formulation of the Multi-objective Optimization

When optimization problems involve more than one objective function to be simultaneously optimized, then a multi-objective optimization (MOO) methodology is utilized [96]. An MOO problem can be mathematically formulated as

$$\begin{cases} min \;\; f_i(x), i = 1, \ldots, m_f \\ s.t. \;\; g_j(x) \le 0, \quad j = 1, \ldots, m_g \\ \qquad h_k(x) = 0, \quad k = 1, \ldots, m_h \\ \qquad x^L \le x \le x^U, \quad x = [x_1 \ldots, x_m] \end{cases} \tag{3.12}$$

where x is an n -dimensional vector of design variables, $f_i(x)$ is the ith objective function, $g_j(x)$ is the jth inequality constraint, and $h_k(x)$ is the kth equality constraint. The design ranges are given by x^L and x^U, denoting the lower and upper bounds of x , respectively.

3.4 Design of Experiments (DoE)

The DoE method, which is one of the steps in procedures of determining optimum conditions with fewer simulations, provides an effective way of creating representative design points. Widely used DoE methods that generate samples in the design space of SBDO studies, are full factorial design (FFD), Latin hypercube design (LHD), central composite design and Taguchi orthogonal array [45-48]. With each method having its advantage and disadvantage. The FFD and LHD are preferred as the DoE method to derive the sampling in the thesis.

3.4.1 Full factorial design (FFD)

Full factorial design (FFD) consists of two or more factors, each with discrete possible values or levels, and whose experimental units take on all possible combinations of these levels across all factors (variables). When the k number of levels is used for n variables, the total number of experiments will be mxn. If there are seven-levels (m) and three variables (n) used, the total number of experiments will be twenty-one.

FFD is a preferred method especially when there are few design variables [45-46]. This method is advantageous because it is a multidimensional method in that it allows the system to be evaluated economically by calculating the effect of the interaction between the factors and the linearity of the functions on the dependent variable. Thus, the initial samples of RBF metamodels are generated by FFD for case 1 and case 2.

3.4.2 Latin hypercube design (LHD)

In the context of statistical sampling, a square grid containing sample positions is a Latin square if (and only if) there is only one sample in each row and each column. A Latin hypercube is the generalization of this concept to an arbitrary number of dimensions, whereby each sample is the only one in each axis-aligned hyperplane containing it, as given in Figure 3.1. In this method; the variables are sampled using an equal sampling method. Then randomly combined clusters of these variables are used to calculate an objective function [45-48]. The implementation of the Latin hypercube design is easy and not too complicated. Hence, for sampling in case 3, the Latin hypercube design (LHD) is utilized.

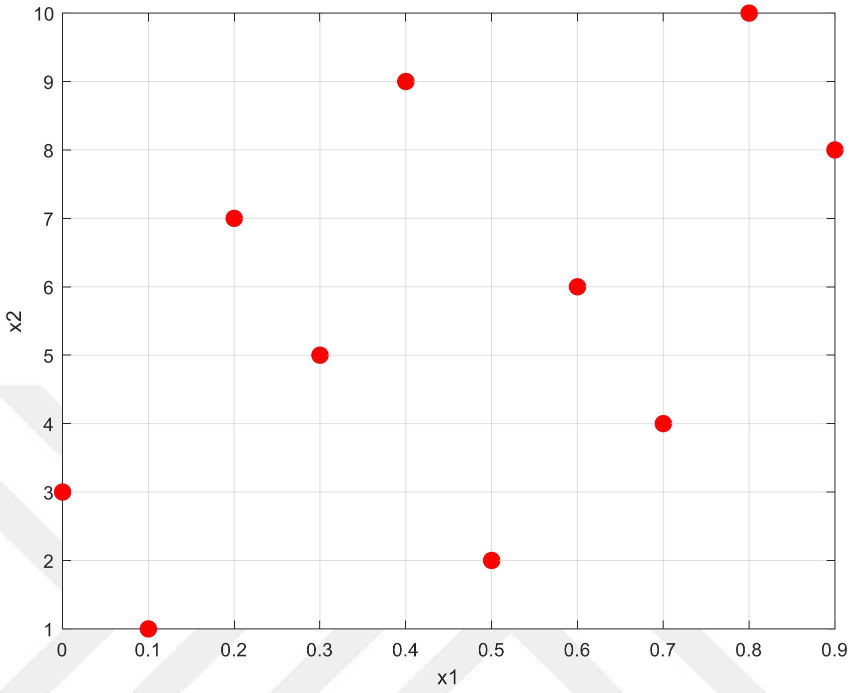

Figure 3.1 : Latin hypercube design sampling.

3.5 Procedure of Metamodel-Based Optimization

3.5.1 Case 1 and Case 2: RBF-MQ

The flowchart of the RBF-based metamodel is given in Figure 3.2. As it is understood from this diagram, first the initial parameters are defined and the interval values of the objective function and its variables are determined. Second, by utilizing the FFD DoE method, initial design samples are generated for the optimization variables. Next, design values are modelled in the LS-DYNA and then the values of constraint and objective functions are calculated. In the fourth step, the RBF-based metamodels are created according to Section 3.1, using the simulated constraint, objective functions, and design variables. In the next step, the accuracy of the RBF models is tested. If the RBF model is accurate enough, the process advanced to the next step. If not, the RBF model is extended by adding samples (fourth step). If the metamodel obtained is deemed acceptable, the next step involved optimization using MOGA (NSGA-II algorithm). Finally, when the optimal values were obtained, the optimization process is terminated.

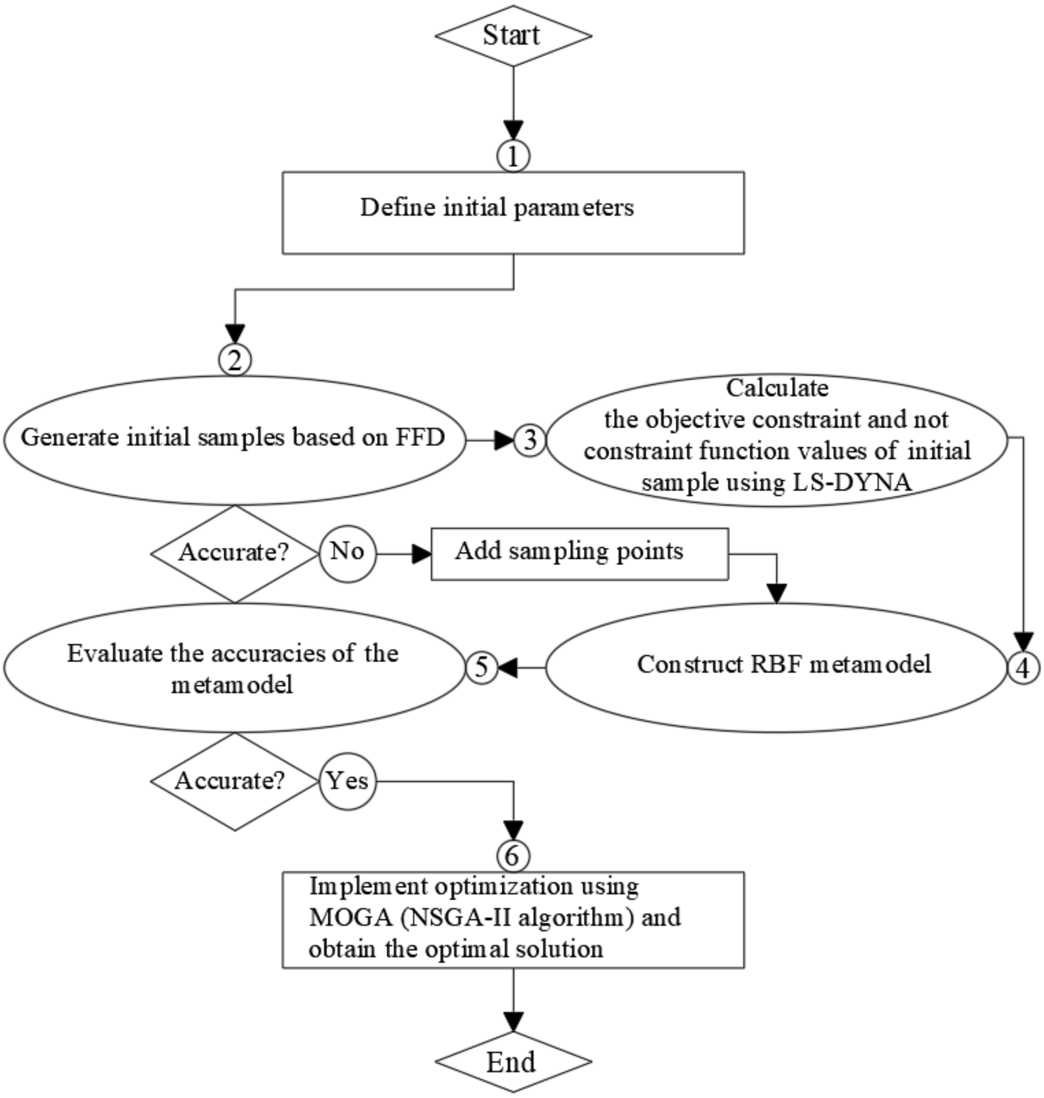

Figure 3.2 : Flowchart of RBF-based optimization method [49].

3.5.2 Case 3: OWPE-RBF

The flowchart of the OWPE-RBF-based metamodel is given in Figure 3.3. In the Step 1; firstly the initial parameters are defined and the interval values of the objective function and its variables are determined. Secondly, by utilizing the LHD DoE method, initial design samples are generated for the optimization variables. The Step 2; design values are modelled in the LS-DYNA and then the values of constraint and objective functions are calculated. In the Step3; the OWPE-RBF-based metamodels are created according to Section 3.1 and Section 3.1.1, using the simulated constraint, objective functions, and design variables. In Steps 3.1 and 3.2; k different metamodels are builded and then weights at points (x) are determined. The Step 4; metamodels are ensembled acording to the weights. The Step 5; the accuracy of the OWPE-RBF models is tested. If the RBF model is accurate enough, the process advanced to the next step. If not, the RBF model is extended by adding samples (third step). If the metamodel obtained is deemed acceptable, the next step involved optimization using MOGA (NSGA-II algorithm). Finally, when the optimal values are obtained, the optimization process is terminated.

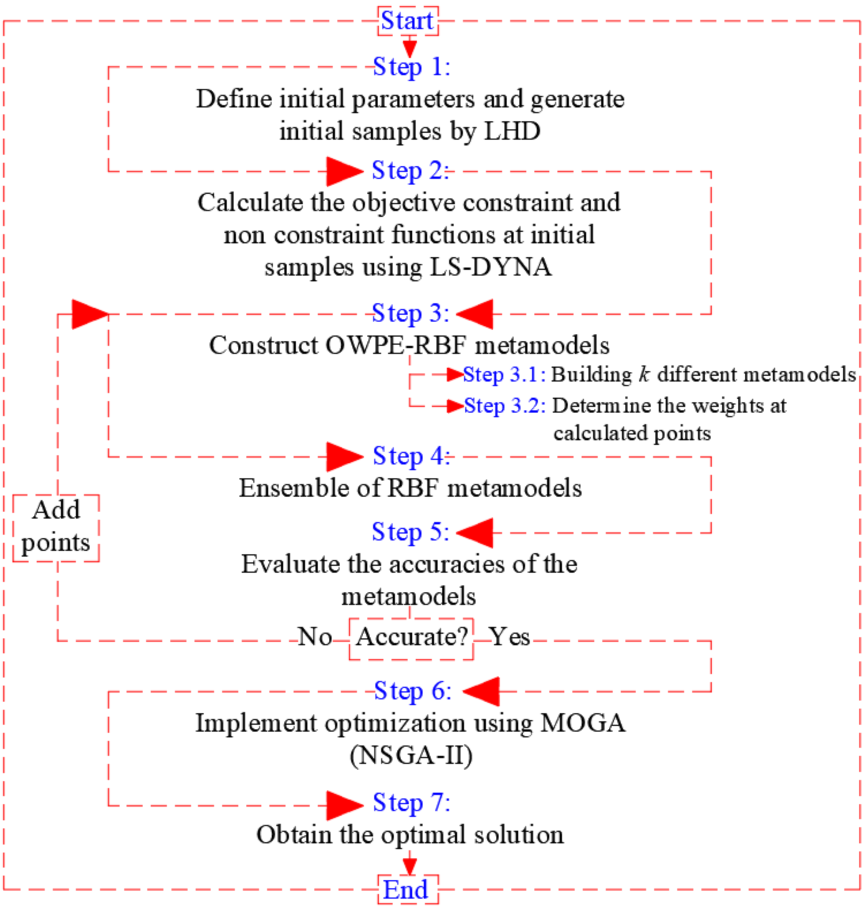

Figure 3.3 : Flowchart of OWPE-RBF-based optimization method.

4. METAMODELS AND MULTI-OBJECTIVE OPTIMIZATION

In this chapter, to highlight research objectives and hypotheses, three case of road restraint systems were chosen. Studies related the cases are given below.

4.1 Case 1: Soil Density Depended Optimization of Embedment Depth of C, H and S Post Type

4.1.1 Experimental setup and numerical models

The European crash test standard, EN1317 [3], is a performance based standard. In other words, in crash tests structural adequacy and impact characteristics of RRS are assessed without considering the characteristics of the individual parts. By using this standard, acceptability of RRS are determined and certification of suitability for use on highways is ensured. Although EN1317 provides detailed information about test procedures and acceptance criteria, little information is presented regarding soil properties, which has a significant effect on the behaviour of guardrails. It is considered that detailed studies, such as post-soil interaction, determination of post behaviour according to soil properties, are needed. For this reason, in this study 63 experimental impact tests were performed using three different guardrail posts (see Figure 4.1 and Table 4.1), with seven different embedment depths in dense, medium dense, and loose soils, as explained in Table 4.2.

Table 4.1 : Dimensional and material properties of posts used in this study [50].

Post Type	Guardrail Type	Length (mm)	Standard Cross-Sectional Dimensions (mm)	Wall Thickness (mm)	Material Type
C	H1, H2	1600	120x60x25	4.0	S355JR (St52)
S	H1, H2	1900	100x50x15	4.2	S235JR (St37)
H	H3, H4	2400	150x90x25	6.0	S235JR (St37)

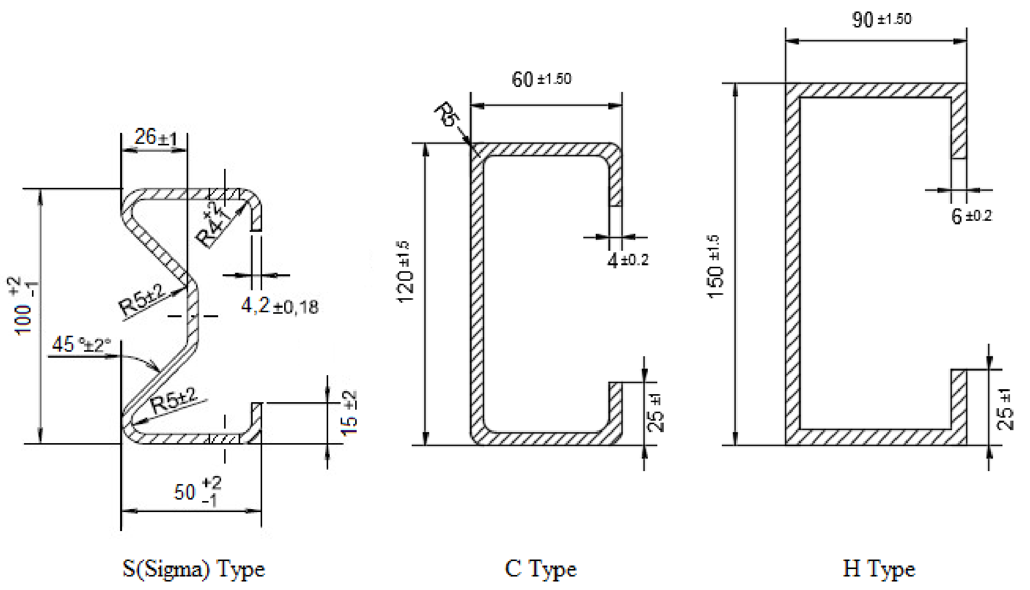

Figure 4.1 : Cross sectional shape of S, C, and H type posts [50].

Two important parameters used to determine the soil densities given in Table 4.2 are the California bearing ratio (CBR) and the internal friction angle (ϕ). The CBR is a penetration test for evaluation of the mechanical strength of natural ground subgrade and base courses beneath new road construction. The angle of internal friction for a given soil is the angle on the Mohr's Circle of the shear stress and normal effective stresses at which shear failure occurs. The internal friction angle provides valuable information about soil resistance. The soil density and the internal friction angle are important parameters that affect the post-soil interaction.

Table 4.2 : Mechanical properties of soil types used in this study [50].

Soil classes	Soil density (gr/cm^3)	Angle of internal friction (ϕ°)	California bearing ratio
Dense-D	2.00	48	95%
Medium-M	1.85	44	64%
Loose-L	1.70	36	36%

In the pendulum tests, a mass of 750 kg is raised to a height of 1.5 meters and released. When gravitational acceleration is taken as 9.81 m/s^2, the velocity of the pendulum mass just before impact is calculated as

$$V = (2gh)^{0.5} \tag{4.1}$$

where, V is impact speed, g is gravity acceleration, and h is fall height.

The energy that the pendulum just before impact is calculated as

$$E = 0.5mV^2 \tag{4.2}$$

where, E is kinetic energy, m is pendulum mass, and V is impact speed.

Figure 4.2 : The pendulum assembly used for applying impact tests in the project and the rigidly mounted accelerometer on the assembly (right), dynamic data collection mechanism used in the project (left), (1) data cable from the accelerometer, (2) 8-channel dynamic data collector, (3) data logger [50].

The velocity of the pendulum just before impact is calculated by Equation (4.1) as 5.43 m/s. After calculating the impact velocity, kinetic energy is calculated as 11.04 kJ using the standard kinetic energy equation given in Equation (4.2). Compared to the energy levels that vehicles apply to RRS in full scale crash tests, 11.04 kJ is considered a reasonable level to determine impact behavior of posts embedded in soil [97]. During the pendulum impact, it is expected that energy absorbed by the posts is proportional to the embedment depth and properties of the soil. In some impact tests, the 750 kg pendulum halted just after contacting the post, implying that all the energy is transferred to the post. In order to measure the effect of pendulum erecting during impact tests, an accelerometer sensor is used which can collect 3D acceleration data. The accelerometer assembly is fixed on the pendulum mass which is rigid as shown in Figure 4.2. This tool collects the acceleration-time data generated during the pulse at a frequency of 1/500 seconds and transfers it to an 8-channel dynamic data collector. In other words, 500 impulse data is collected during a pulse event which lasts 1 second. Table 4.3 shows the maximum deceleration values measured for pendulum tests performed in the field and the absorbed energies calculated using these values [97].

Table 4.3 : Absorbed energy and highest deceleration values obtained from 63 experimental pendulum tests [50].

Post type	Embedded depth (mm) (x_1)	Soil types (x_2)					
		D(Dense) = 2 gr/cm^3		M(Medium)=1.85 gr/cm^3		L(Loose) = 1.7 gr/cm^3	
		Energy (kJ)	Decel. (g)	Energy (kJ)	Decel. (g)	Energy (kJ)	Decel. (g)
C120x60x4 (C)	600	0.72	-2.88	0.66	-2.06	0.49	-1.08
	650	2.93	-4.05	2.11	-2.9	1.77	-2.45
	700	3.27	-4.52	2.35	-3.25	2.14	-2.96
	750	4.58	-6.33	3.29	-4.55	2.89	-3.99
	800	5.75	-11.95	4.14	-10.72	3.31	-7.93
	850	6.86	-18.48	4.94	-16.83	4.01	-13.54
	900	7.92	-25.85	6.13	-24.47	5.19	-18.87
C150x90x6 (H)	700	10.03	-34.81	9.56	-33.21	8.89	-31.65
	800	10.65	-35.05	10.12	-34.54	9.34	-32.68
	900	11.04	-35.26	10.74	-35.12	10.01	-33.84
	1000	11.04	-35.32	11.04	-35.51	10.71	-34.82
	1100	11.04	-35.45	11.04	-35.47	11.04	-35.21
	1200	11.04	-35.41	11.04	-35.61	11.04	-35.52
	1300	11.04	-35.56	11.04	-35.55	11.04	-35.49
S100x50x4.2 (S)	700	3.32	-4.59	3.07	-4.24	0.92	-1.27
	800	5.31	-7.34	5.11	-7.06	2.22	-3.07
	900	6.61	-9.14	6.39	-8.83	2.95	-4.08
	1000	7.51	-10.38	7.17	-9.91	3.61	-8.99
	1100	8.05	-18.13	7.77	-17.74	4.26	-15.89
	1200	8.44	-19.67	8.01	-18.07	6.03	-16.84
	1300	9.61	-25.28	8.31	-23.21	7.93	-21.75

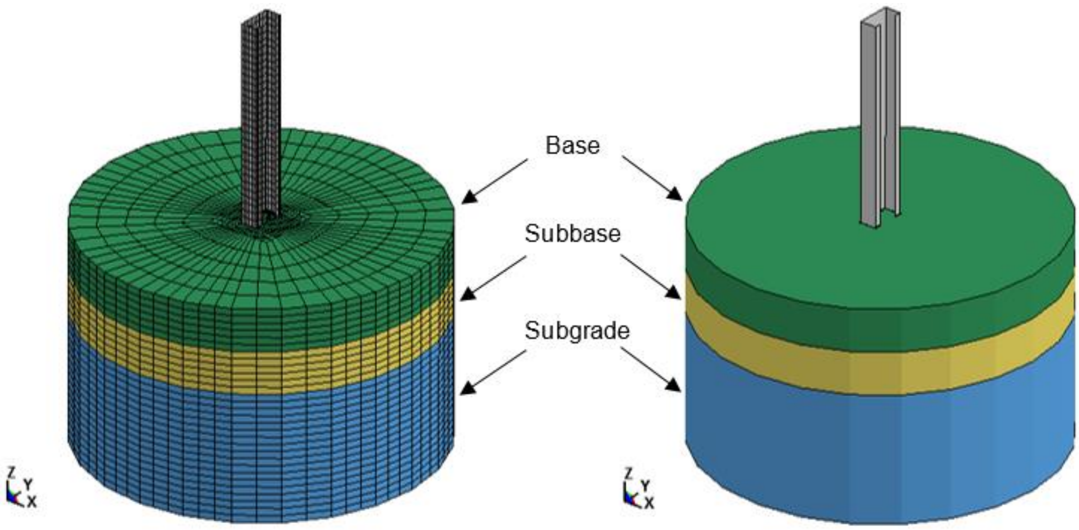

Figure 4.3 : FE model of soil layers and single embedded post [50].

Figure 4.3 shows the finite element model of a C-type post embedded in soil layers of base, subbase, and subgrade. For the material model of the posts, *MAT_PIECEWISE_LINEAR_PLASTICITY was selected and values, such as density, modulus of elasticity, Poisson's ratio, and yield strength were defined. In the soil model, the *MAT_DRUCKER_PRAGER material model, which is in compliance with the Mohr-Coulomb failure hypothesis, defined in LS-DYNA was used [98-99]. In this model, the bulk density, elastic shear modulus, Poisson's ratio, cohesion, and internal friction angle parameters were obtained from soil tests in the field and in the laboratory [97-98, 100]. The post and soil were modelled as shell and solid elements, respectively. The optimum mesh size of post was selected as 10 mm based on previous successful studies [16-17, 19-20, 22, 28, 30]. The critical area around posts were meshed at the same size as the post, with mesh sizes growing to 100 mm towards the outer edge of the soil model.

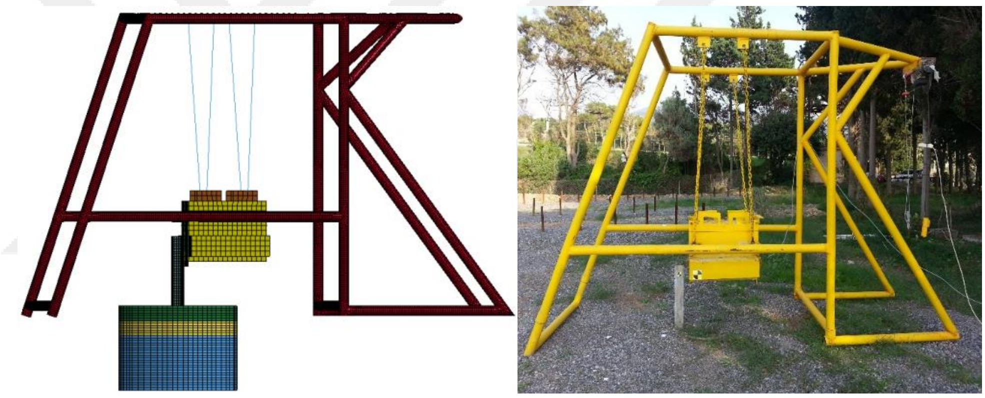

Figure 4.4 : Pendulum system and FEM used to perform impact tests in the study [50].

Table 4.4 : Comparison of FEA and experimental tests of DS700 [50].

Test	Experimental	FEA	RAE (%)
Deceleration (g)	-4.59	-4.38	4.58
Energy (kJ)	3.32	3.17	4.52

Figure 4.4 shows the impactor and the soil embedded post used in dynamic pendulum tests. All 63 of the impact tests were simulated using finite element simulation and performances were compared. Figure 4.5 shows a comparison for S (sigma) type post that is embedded 700 mm in dense (D) soil. Table 4.4 shows the maximum deceleration values measured in the experimental test and FE analysis, and the absorbed energies calculated using these values. As seen from the table, the error rates

are below 5%. In particular, as shown in Figure 4.6, the deceleration-time plots obtained from the DS700 (Dense soil, S type post embedded 700 mm) case test and its numerical analysis were found to be fairly close to each other. In all cases, test results, such as ground deformation, the motion of the post, and the behaviour of the pendulum were compared. It was determined that results obtained from numerical analysis agreed well with those obtained from experimental tests. Based on the results obtained, it can be concluded that the finite element models used in the study are accurate in modelling soil-post interaction [97].

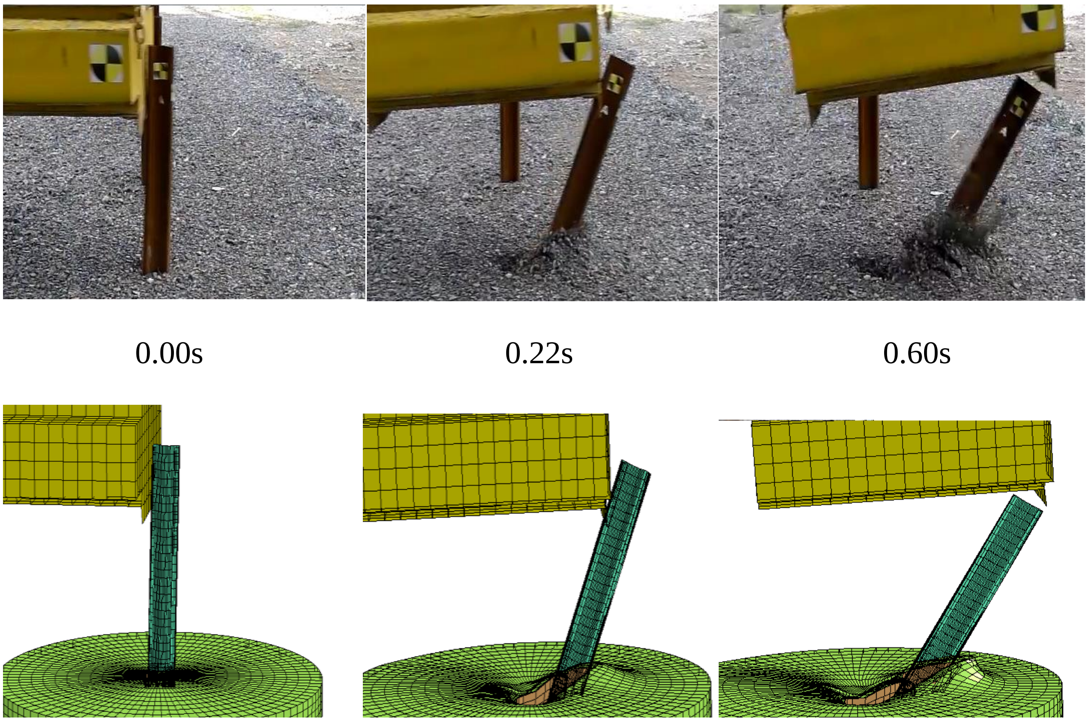

Figure 4.5 : Sequential pictures comparing LS-DYNA analysis and experimental test of DS700 [50].

The times for completion of the experimental and numerical analyses described above are presented in Table 4.5. As illustrated in this table, field tests as well as computer simulations require excessive times of 40 days and 22 days, respectively.

Table 4.5 : Experimental and FEA test time periods [50].

Test type	Number of test	Time period per test/run (hour)	Total time consuming (day)
Experimental	63	15 hours 14 minutes	40
FE analysis	63	8 hours 11 minutes (CPU times)	22

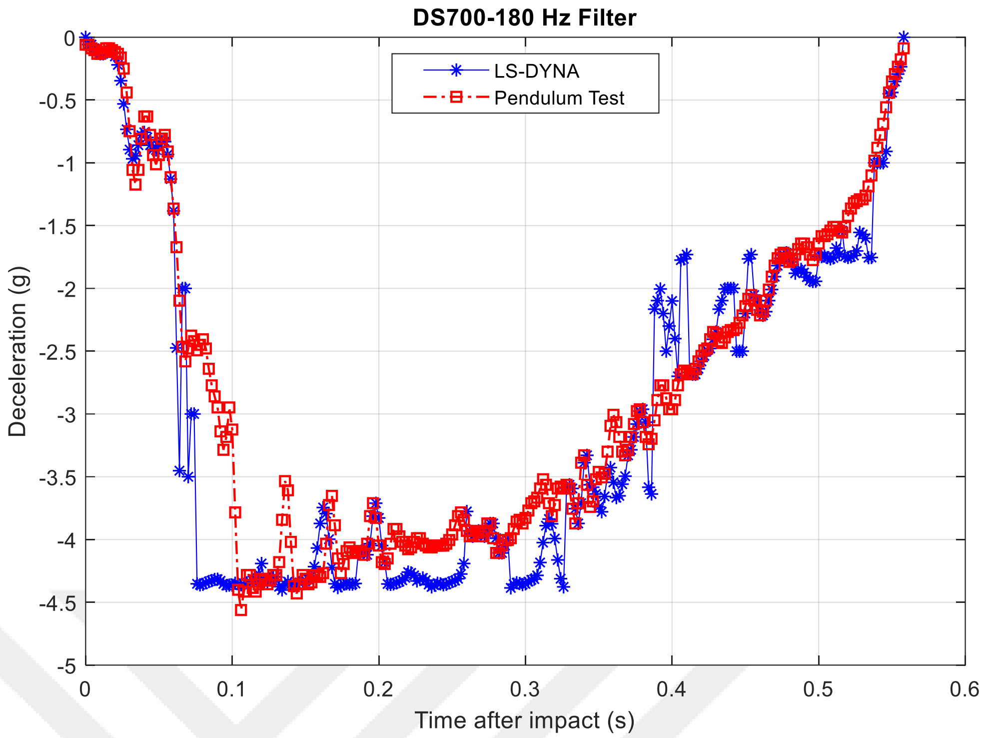

Figure 4.6 : Comparison of deceleration-time graphs obtained from LS-DYNA analysis and experimental test of DS700 [50].

4.1.2 Construction of RBF metamodel and accuracy test

An MOO problem was introduced based on the energy absorption capacities (*Energy*-kJ), the impact deceleration (*Decel*-g) values as the objective and constraint functions and the PED (*x1*) and soil types (*x2*) as the variables. First, the FFD method, using the MATLAB [101] "dFF=fullfact ([n k])" command, where *k* is number of levels and *n* is variables, was applied to generate the basic design values (*x1, x2*) for the optimization variables, given in Figure 4.7. Then, the values of *Energy* and *Decel* were computed using LS-DYNA, as given in Table 4.6. Next, using the data, surrogate models were constructed with the help of an RBF metamodeling technique. To implement the RBF surrogate model, the multiquadric radial basis function [102] was used, where the optimal shape parameter *c* was set to 0.1. Optimal shape parameter (*c*) was chosen by minimizing the error criteria as illustrated in Figure 4.8.

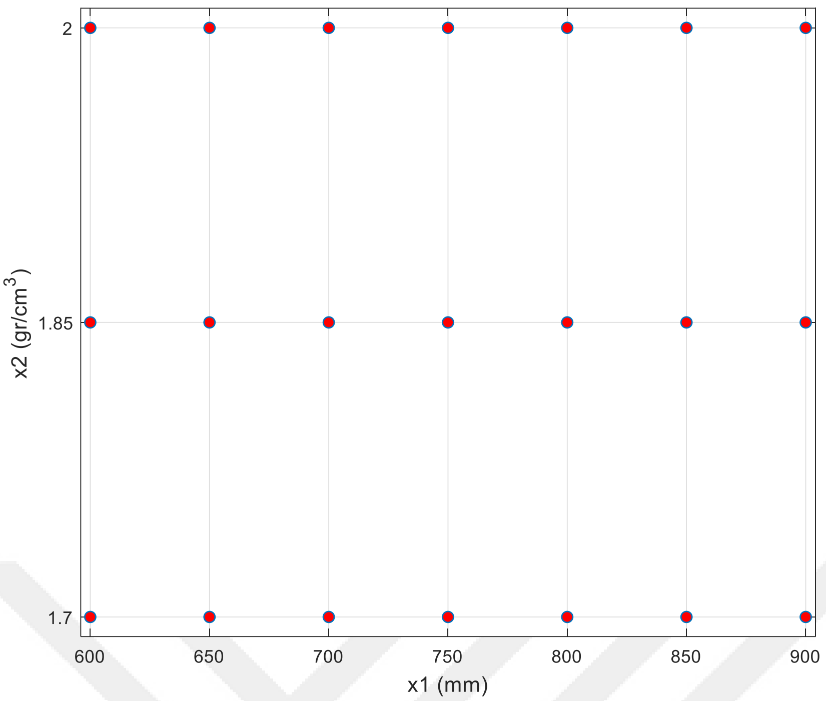

Figure 4.7 : Design values of C post by FFD [50].

Table 4.6 : Design sampling and objective function of C post [50].

Sample No	x_1 (mm)	x_2 (gr/cm^3)	Energy (kJ)	Decel (g)
1	600	1.70	0.49	1.08
2	600	1.85	0.66	2.06
3	600	2.00	0.72	2.88
4	650	1.70	1.77	2.45
5	650	1.85	2.11	2.90
6	650	2.00	2.93	4.05
7	700	1.70	2.14	2.96
8	700	1.85	2.35	3.25
9	700	2.00	3.27	4.52
10	750	1.70	2.89	3.99
11	750	1.85	3.29	4.55
12	750	2.00	4.58	6.33
13	800	1.70	3.31	7.93
14	800	1.85	4.14	10.72
15	800	2.00	5.75	11.95
16	850	1.70	4.01	13.54
17	850	1.85	4.94	16.83
18	850	2.00	6.86	18.48
19	900	1.70	5.19	18.87
20	900	1.85	6.13	24.47
21	900	2.00	7.92	25.85

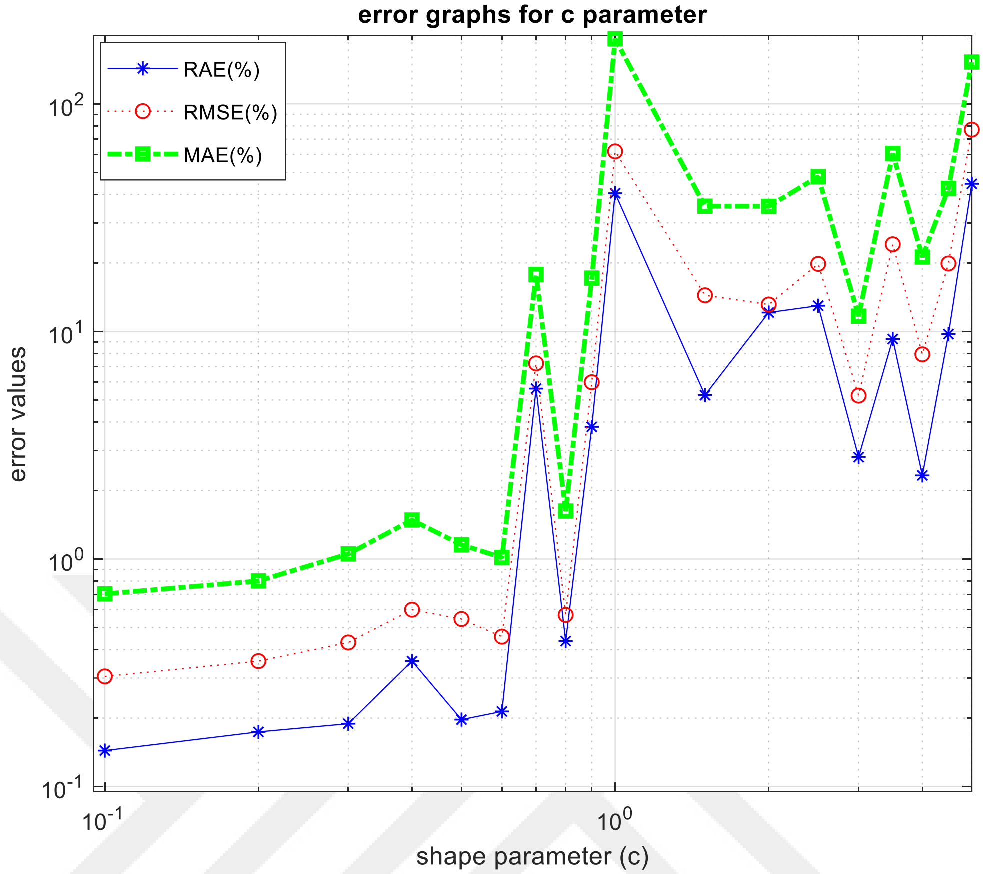

Figure 4.8 : Optimum shape parameter search for RBF-MQ metamodels [50].

Table 4.7 shows an RBF metamodel that mimics the original C post model. RBF-MQ-based metamodels were constructed by following the RBF procedure for all of the posts (C, H, and S).

Actual energy and deceleration measurements given in Table 4.6 and those ($\dot{Y}$) obtained from the RBF-MQ-based metamodel illustrated in Table 4.7 correspond well. To measure both the global and local fidelity of the RBF-MQ-based metamodels, k-fold cross validation was utilized. The variables were divided into k subsets, then, a surrogate model was constructed k times, each time leaving out one of the subsets from training, and using the omitted subset to compute the error measure of interest. Error values were calculated using Equation (3.11). Similar to the C post, the above procedure was also applied to the H and S posts in order to construct their metamodels. Results for the $RMSE_{CV}$ rates for all of the objective functions in the metamodels are given in Figure 4.9. Additionally, Figure 4.10 illustrates the average $RMSE_{CV}$ of the metamodels. Note that an $RMSE_{CV}$ value of 0 indicates a perfect fit. It can be concluded that the $RMSE_{CV}$ trained RBFs resulted in an almost perfect fit to the engineering design models.

Table 4.7 : RBF-MQ-based metamodel of C post [50].

Sample No	RBF model			
	Energy-kJ		Decel-g	
	β	Ẏ	β	Ẏ
1	1.09802	0.48	4.93394	1.08
2	-1.11897	0.66	-1.63227	2.06
3	0.05257	0.72	-3.24788	2.87
4	0.22425	1.78	0.12858	2.46
5	4.80908	2.10	7.00584	2.90
6	-5.04847	2.94	-7.14415	4.07
7	-0.97648	2.15	-1.34720	2.97
8	7.09600	2.34	9.79449	3.25
9	-6.11284	3.28	-8.43810	4.55
10	-0.61169	2.90	-0.76215	4.02
11	8.90195	3.28	12.18525	4.55
12	-8.29351	4.59	-11.39852	6.37
13	1.64711	3.33	16.95320	7.91
14	7.79876	4.13	-15.61263	10.73
15	-9.44380	5.75	-1.31952	11.91
16	1.52815	4.04	19.42349	13.53
17	9.89934	4.93	-16.39716	16.85
18	-11.42640	6.87	-3.03106	18.44
19	1.95575	5.22	36.94970	18.82
20	8.49909	6.12	-42.18954	24.49
21	-10.45334	7.92	5.22242	25.72

As illustrated in Figure 4.9, the accuracy of all objectives are different. Each objective function in an engineering problem defines a different behavior of the problem. Thus, these behaviors become different as given in the surface plot of the metamodels in Figure 4.11. Since the objective functions of the metamodel mimic engineering behaviors, each of the 2 objective functions used in this study within the metamodel is expected to have different accuracy and behavior.

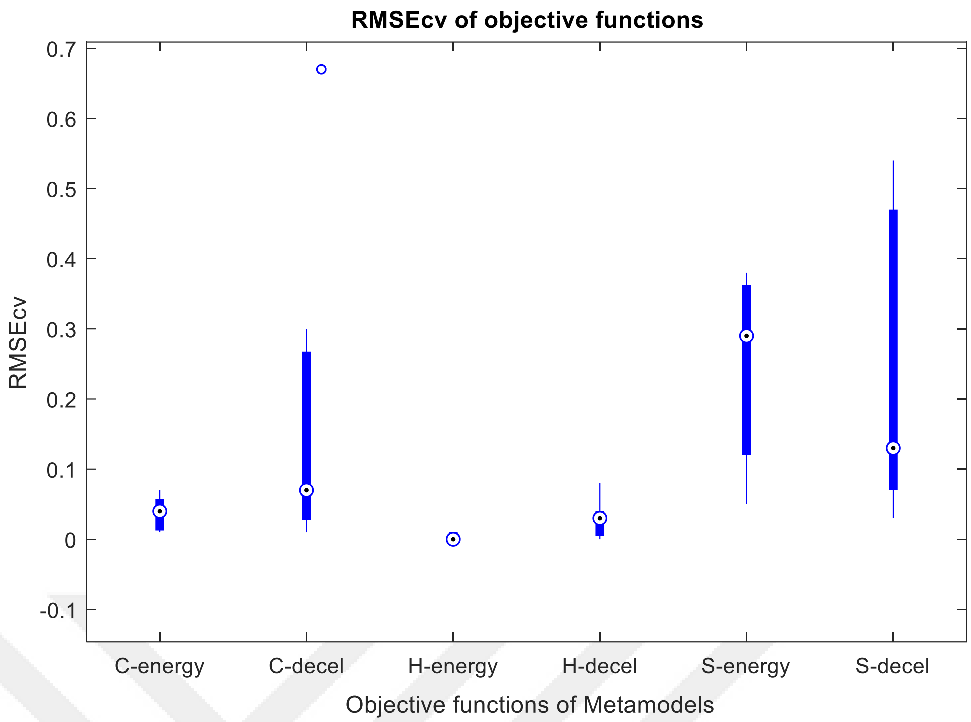

Figure 4.9 : $RMSE_{CV}$ of RBFs objective functions [50].

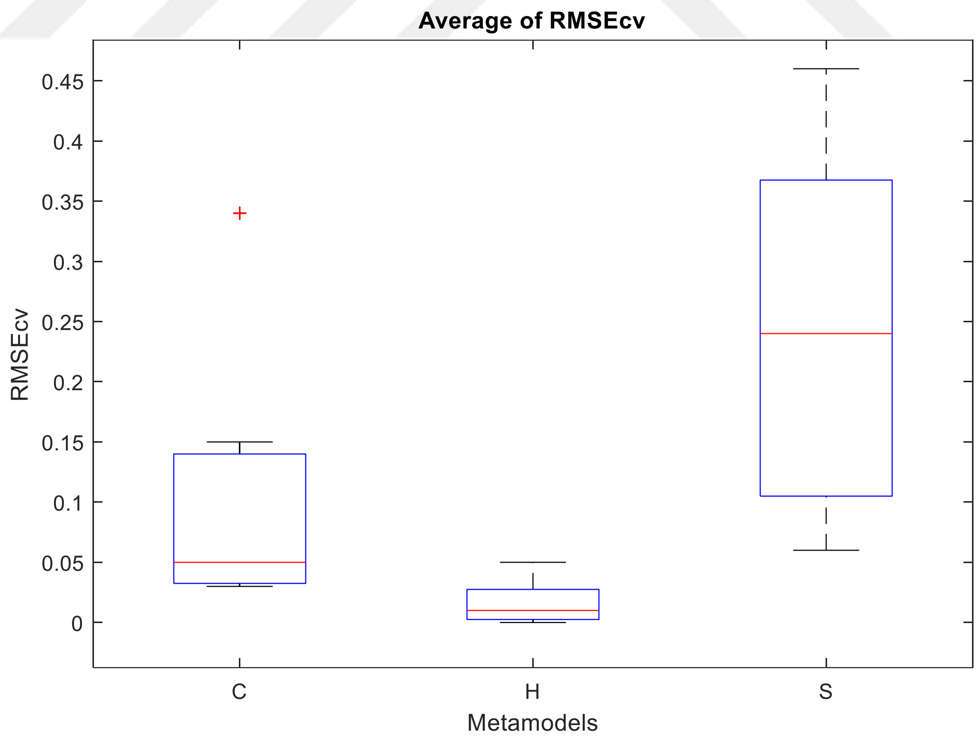

Figure 4.10 : Average $RMSE_{CV}$ of RBFs metamodels [50].

In this case, the *k*-fold cross-validation errors at all training points were used as global and local error measures. The metamodel error values of $RMSE_{CV}$ are provided in this study. For an engineering design model, it is important to balance the accuracy of model predictions with the computational complexity of the model used. Model prediction errors that lie within a specified range may be acceptable. Based on prior experience or practical design requirements, the designer may know what levels of errors are acceptable for a particular problem. Most studies [45-48] state that a 2% error might be desirable; a 2–10% error is acceptable; and higher than 10% error is unacceptable. It can be seen from the Figures 4.9 and 4.10 that the $RMSE_{CV}$ of RBFs are less than 0.3%, which demonstrated that the prediction results of the surrogates were accurate enough for engineering design.

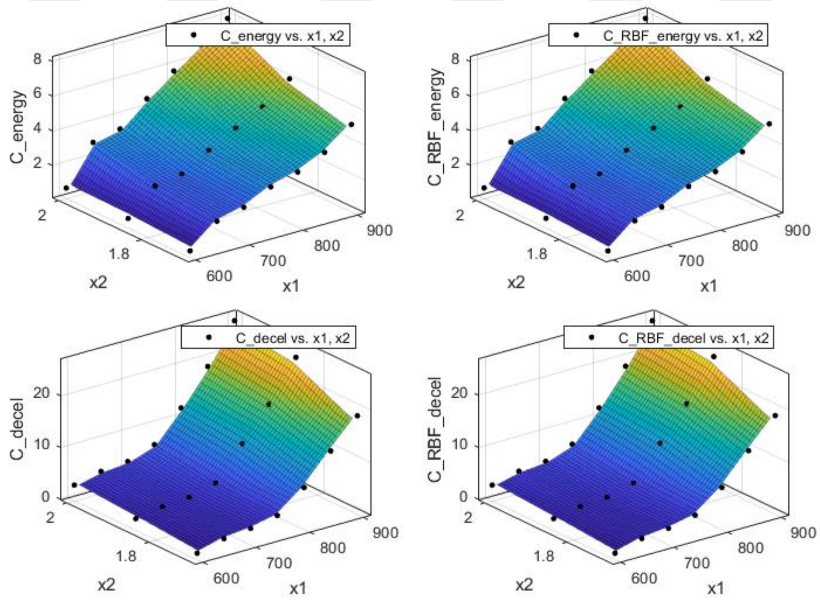

Figure 4.11 : Surface plot of C, H, and S metamodels [50].

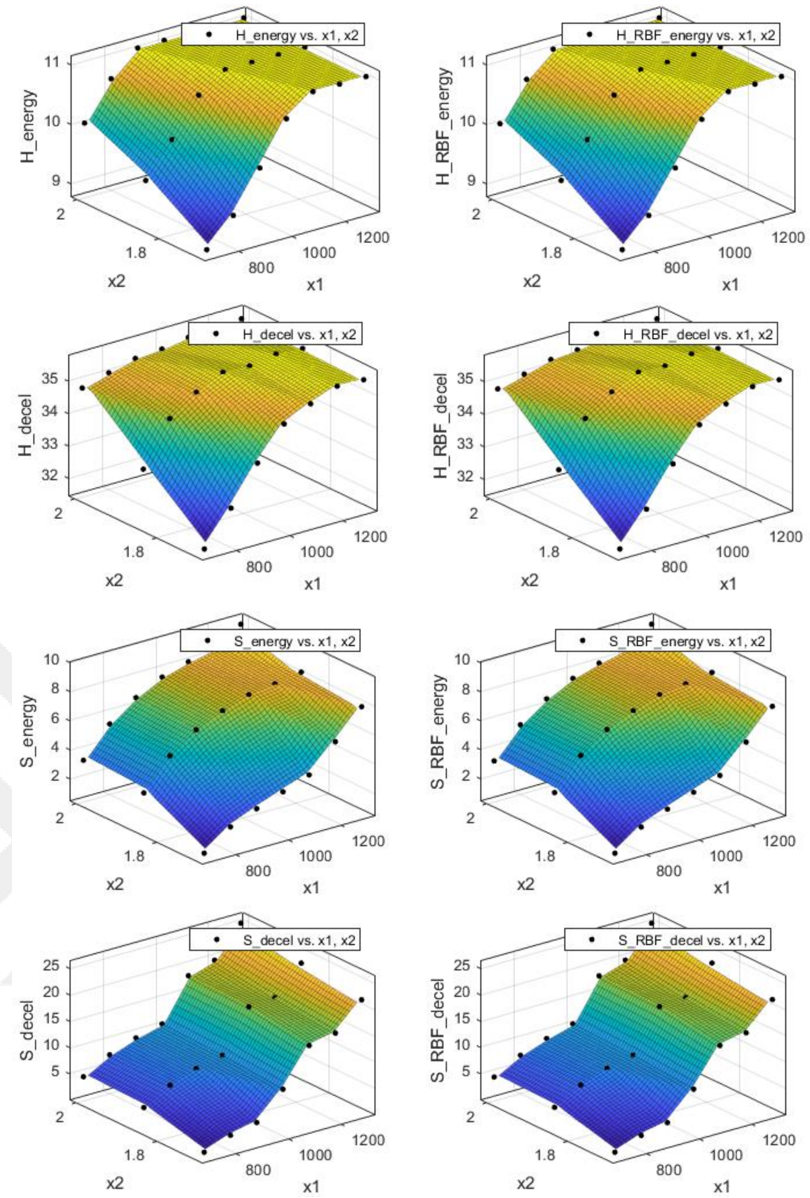

Figure 4.11 (continued): Surface plot of C, H, and S metamodels [50].

4.1.3 Multiobjective optimization formulation and optimal values

Criteria, such as the impact deceleration, the displacement and the energy absorption capacity of a system are utilized to evaluate the classification and performance of the RRS. The factors for determining these criteria are the strength of the soil and the PED that provide interaction with the soil. Since steel longitudinal barriers are semi-rigid systems, it is required that the energy absorption capacities and impact decelerations are high and low, respectively. It is known that the rigidity of the system increases when the strength of the soil and the PED increases. Therefore, the soil types and PED factors should be well analyzed for an effective and efficient RRS performance design.

In this case, determination of optimum embedding depths of C, H, and S type guardrail posts in three types of soil (dense, medium dense, loose) conditions were aimed. Because of this, as detailed in the previous section, energy absorption capacity (*Energy*) and impact deceleration (*Decel.*) values at optimization were taken as objective functions, and PED (*x1*) with soil density (*x2*) as variables. The range of the PED-*x1* was set from 600 mm to 950 mm for a C post and 700 mm to 1300 mm for H and S posts. On the other hand, the range of the soil density-*x2* was set from 1.7 gr/cm^3 to 2 gr/cm^3. As mentioned before, the impact performance of longitudinal barriers RRS depends on energy absorption capacity and impact deceleration. The minimum value for the *Energy* in Equation (4.3), determined as 5 kJ (see Table 4.3), which is the minimum effective energy value for the C and S posts [97], is accepted as the constraint.

$$\begin{cases} \text{Min. } [\text{Energy}(x1, x2), \text{Decel}(x1, x2)] \\ \quad \text{s.t. } 600 \text{ mm} \le x1 \le 900 \text{ mm} * \\ \quad\quad 700 \text{ mm} \le x1 \le 1300 \text{ mm} ** \\ \quad\quad 1.7 \text{ gr/cm}^3 \le x2 \le 2.0 \text{ gr/cm}^3 \\ \quad\quad \text{Energy}(x1, x2) \ge 5.00 \text{ kJ} \\ \quad\quad \text{for D} - \text{soil } x2 \le 2.00 \text{ gr/cm}^3 \\ \quad\quad \text{for M} - \text{soil } x2 \le 1.85 \text{ gr/cm}^3 \\ \quad\quad \text{for L} - \text{soil } x2 \le 1.70 \text{ gr/cm}^3 \end{cases} \tag{4.3}$$

* For C post

** For H and S posts

where, *Energy* is the energy absorption capacity of the post, *Decel* is the impact deceleration, *x1* is the PED, and *x2* is the density of soil. The optimization problem was solved with MATLAB code, using the gamultiobj command which is a variant of NSGA-II [103]. NSGA-II is a well-known, fast sorting and elite multi objective genetic algorithm. NSGA-II, in most problems, is able to find a much better spread of solutions and better convergence near the true Pareto-optimal front compared to other elitist MOEAs that pay special attention to creating a diverse Pareto-optimal front [103]. The NSGA-II was shown to be an effective method [103-104] and was employed in this study to solve the MOO problem given in Equation (4.3). As shown in Table 4.8, the MOGA (NSGA-II) toolbox in MATLAB was used for optimization and the MOGA (NSGA-II) parameters are presented. The 'crossoverarithmetic' creates children that are the weighted arithmetic mean of two parents. Children are always feasible with respect to linear constraints and bounds. The 'mutationadaptfeasible' is a default mutation function when there are constraints, randomly generating directions that are adaptive with respect to the last successful or unsuccessful generation. The mutation chooses a direction and step length that satisfies bounds and linear constraints. The 'MaxStallGenerations' is used to set number of generation. To investigate the effect of number of iterations (or generations) on the accuracy of optimization results, the solutions were obtained at five different iterations for DC, as shown in Figure 4.12. It can be seen from the figure that the convergence direction is from initial solution to optimal solution and there is no significant difference among the solutions when the number of iterations is more than 50. Thus, in this study, the maximum number of iterations was set to 200 and used as the convergence criterion for solving the MOO problem. Similarly, optimal results were obtained for all combinations of C, H and S posts in dense, medium and loose soil, as given in Table 4.9. Due to the high accuracy error rate obtained for the RBF models, the optimum values determined in the thesis are deemed feasible.

Table 4.8 : Parameters of MOGA (NSGA-II) algorithm [50].

Parameters	Value/Function
Number of points on the Pareto front	18
Population size	100
Number of iterations	'MaxStallGenerations'(200)
Crossover option	'crossoverarithmetic'
Mutation option	'mutationadaptfeasible'

Table 4.9 : Optimal values of C, H and S posts within soil types [50].

Type of Soil&Post	Optimal values			
	x_1 (mm)	x_2 (gr/cm^3)	Energy (kJ)	Decel (g)
DH	700	2.00	10.08	-34.21
DC	780	2.00	5.00	-12.97
DS	759	2.00	5.00	-7.04
MH	700	1.85	9.81	-33.67
MC	828	1.85	5.00	-14.66
MS	915	1.85	5.00	-9.21
LH	700	1.70	9.54	-33.13
LC	877	1.70	5.00	-16.35
LS	1071	1.70	5.00	-12.87

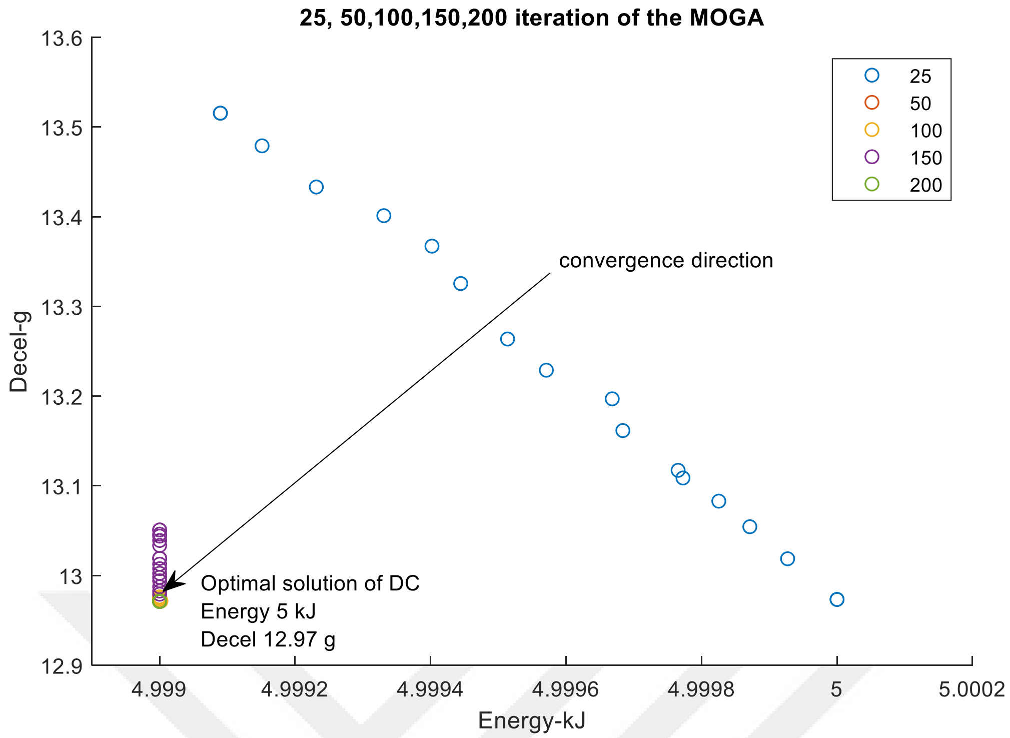

Figure 4.12 : Pareto front convergence plot of C post in dense soil (DC) [50].

4.1.4 Modelling and testing of optimal values

At this stage of the study, full scale crash test assessments were carried out in order to test the efficiency of the optimum PEDs. In these tests, the barrier systems, which are presently in use, consisting of post, rail, and offset block elements were modelled. The accuracy of full-scale crash simulations were validated against real crash test results. Available crash tests correspond to the DS1200, DC950 and DH1230 cases. As can be understood from the codes, all three crash tests were carried out under dense soil conditions. Note that full scale crash tests were carried out in accordance with EN1317 crash test conditions explained in Table 4.10.

Table 4.10 : EN1317 test acceptance criteria for H1 and H2 level guardrail systems [50].

RRS Level	Test Code	Impact speed (km/h)	Impact angle (°)	Vehicle mass (kg)	Type of vehicle
H1	TB11	100	20	900	Car
	TB42	70	15	10000	Truck
H2	TB11	100	20	900	Car
	TB51	70	20	13000	Bus

Safety assessment criteria in EN1317 standard is used to evaluate the effectiveness of optimal PEDs. Figure 4.13 illustrates safety assessment criteria defined in the EN1317 part 2. TB11, TB42, TB51 crash tests related to H1 and H2 level systems widely used in Turkey and their evaluation criteria are presented in Table 4.11.

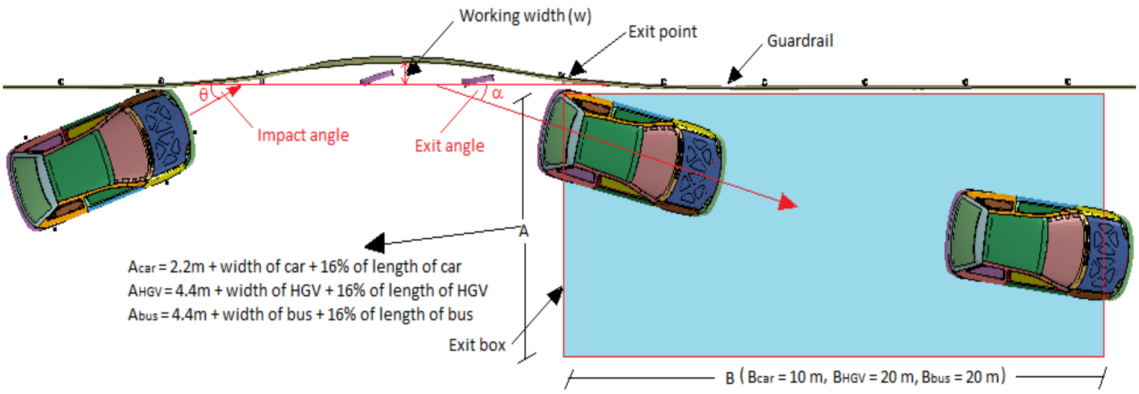

Figure 4.13 : Illustration of crash test details in EN1317 part 2 [50].

Table 4.11 : EN1317 test evaluation criteria for H1 and H2 level RRS constructed with optimal PEDs [50].

RRS Level	Test	Working width (W) (m)	Exit box (width(A) x length(B)) (m)*	Exit angle (α) (°)**
H1	TB11	---	4.4x10	≤19
	TB42	≤1.3	8.22x20	≤17
H2	TB11	---	4.4x10	≤19
	TB51	≤1.3	8.95x20	≤19

*Calculated based on EN1317 part 2
**Calculated based on exit box length

Table 4.12 : Quantitative comparison between crash tests and FE analysis for TB11, TB42 and TB51 tests [50].

Test	FE models		Full scale crash tests		RAE of w (%)	RAE of α (%)
	Working width (w) (m)	Exit angle (α) (°)	Working width (w) (m)	Exit angle (α) (°)		
TB11	426	10.5	447	11	4.76	4.55
TB42	1036	12	994	12	4.20	0
TB51	815	4	846	4	3.66	0

Numerical analyses of the longitudinal barriers corresponding to the real crash tests were performed using the LS-DYNA program. Figures 4.14-4.16 compare qualitative results obtained from full scale crash testing and FEA. Additionally, quantitative comparison between crash tests and FE analysis given in Table 4.12. As can be seen from the table, the maximum RAE between the real tests and the FEA results are smaller than 5%, which is deemed acceptable. After validation of the numerical models a total of 18 additional FE simulations were performed for all optimum PEDs. Qualitative comparisons obtained from these analyses are presented in the Appendix. As evident from these figures, results obtained both from the numerical analysis and the real crash tests correspond well. Based on the quantitative results presented in Table 4.13, it can be concluded that optimum PEDs used in the simulations provide acceptable crash test performances.

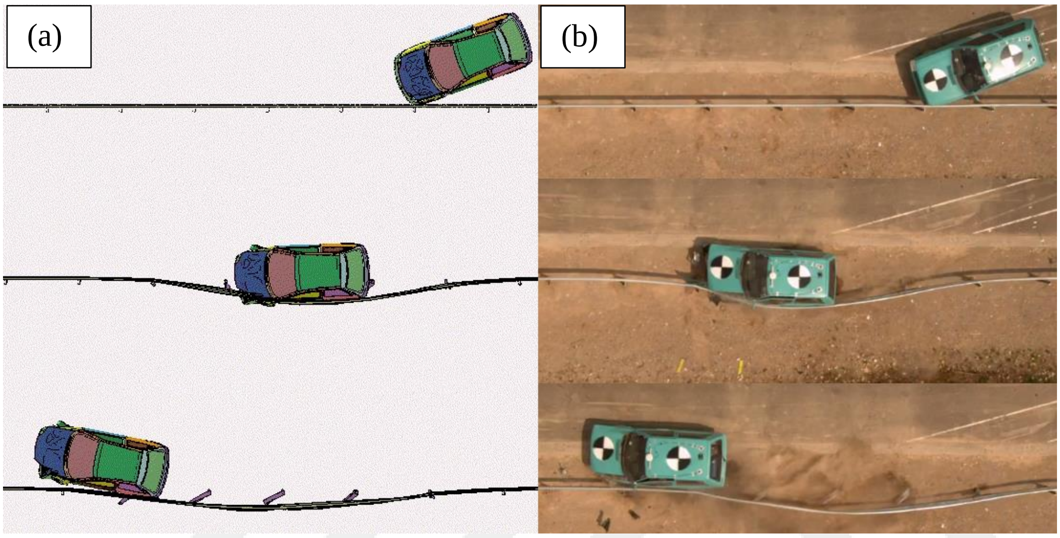

Figure 4.14 : Qualitative comparison for TB11 test (a) FE model (b) Crash test [50].

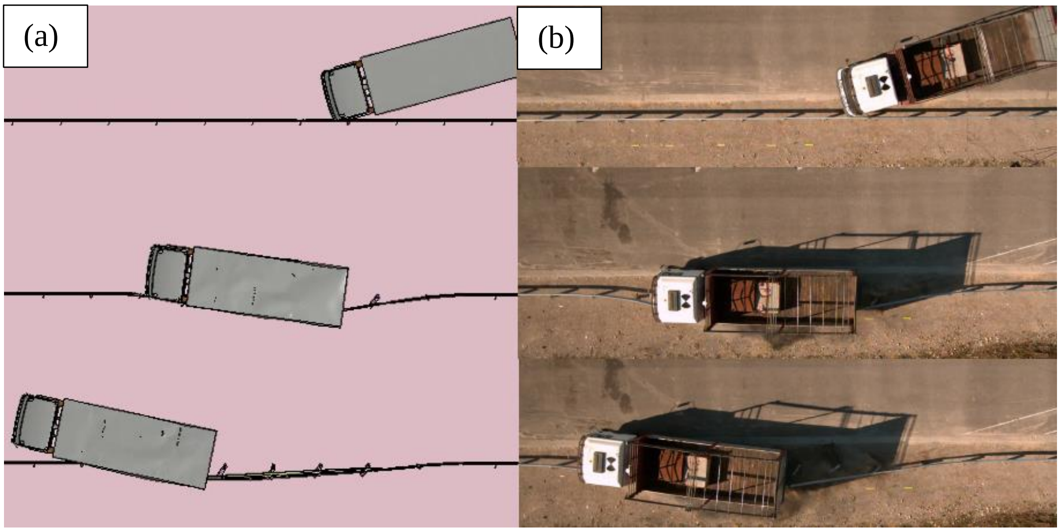

Figure 4.15 : Qualitative comparison for TB42 test (a) FE model (b) Crash test [50].

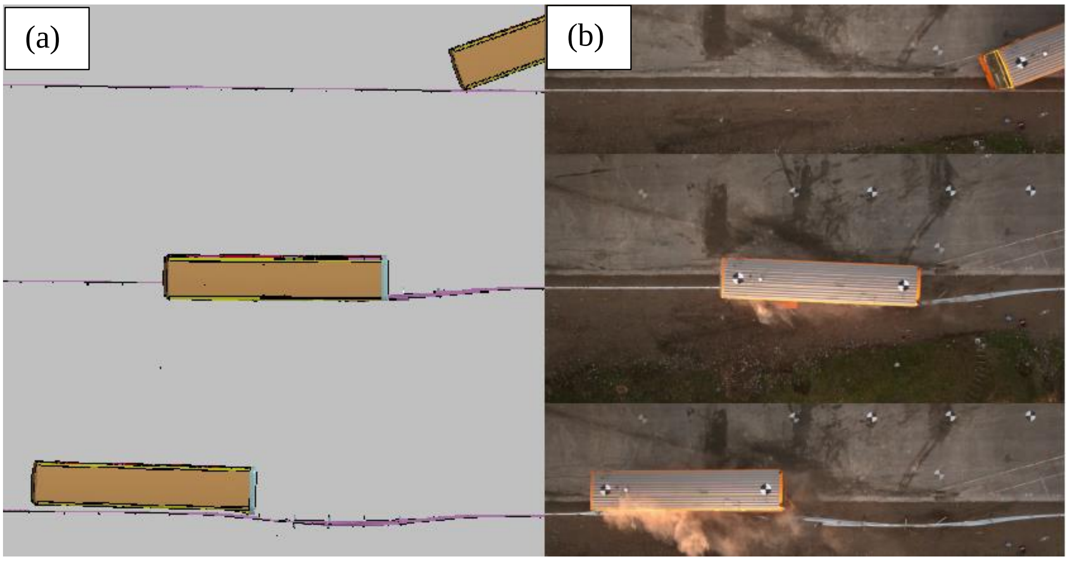

Figure 4.16 : Qualitative comparison for TB51 test (a) FE model (b) Crash test [50].

Table 4.13 : Numerical analysis results obtained from simulations [50].

Soil&Post type	Optimal values			TB11		TB42		TB51	
	x_1 (mm)	x_2 (gr/cm^3)	System type	W (mm)	α (°)	W (mm)	α (°)	W (mm)	α (°)
DH	700	2.00	H2	286	8			1019	4
DC	780	2.00	H1	564	11	1146	12		
DS	759	2.00	H2	347	9			1086	4
MH	700	1.85	H2	291	8			1091	4
MC	828	1.85	H1	572	11	1144	12		
MS	915	1.85	H2	356	9			1094	4
LH	700	1.70	H2	309	9			1172	5
LC	877	1.70	H1	576	11	1132	12		
LS	1071	1.70	H2	358	9			1103	4

4.2 Case 2: S235JR, S275JR and S355JR Material-Based Cross-sectional Optimization of H1W4 and H2W4 Performance Level Guardrails

4.2.1 The Details and FE models of H1-H2 guardrail systems

H1W4 and H2W4 represent two most widely used barrier systems in Turkey. These two systems could be constructed using different steel grades, such as S235JR, S275JR and S355JR and their combinations. In the design of roadside safety systems, even though it gives particular importance to the safety, the cost effectiveness cannot be overlooked. The main components that form the two guardrail systems are the rail and post. The geometry and cross-sectional properties of these parts play an important role in both, a safe and economical design. In addition, the post geometric width-x_1 and the rail sectional thickness-x_2 are two major factors affecting the performance of the guardrail systems. Therefore, the x_1 and the x_2 were chosen as design variables for optimization of the guardrail systems.

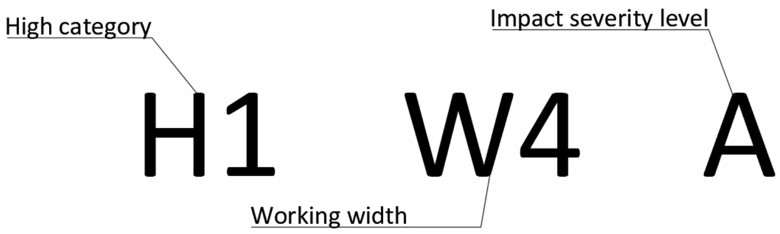

Figure 4.17 : Symbol meanings of H1W4A system [49].

Figure 4.17 shows the meanings of the symbols which are forming the name of a guardrail system that is classified according to EN 1317 standards. Commonly used materials and technical specifications of H1W4A and H2W4A systems are given in Table 4.14. As can be seen, the same size of C type post are used for both H1 and H2 systems, but rail types are different. In addition, the sectional thickness of the post is fixed whereas the sectional thickness of rails vary depending upon the material grade.

Table 4.14 : Technical details of guardrail systems used in this study [49].

Guardrail system type	Rail	Post	Material	Rail thickness (mm)	Post thickness (mm)
H1W4A	W	C120X60X20	S235JR	3.0	4.0
			S235JR /275JR *	3.0	4.0
			S275JR	3.0	4.0
			S275JR /355JR **	3.0	4.0
			S355JR	2.5	4.0
H2W4A	3N		S235JR	3.0	4.0
			S235JR /275JR *	3.0	4.0
			S275JR	3.0	4.0
			S275JR /355JR **	3.0	4.0
			S355JR	2.5	4.0

*Rail's material is S235JR and post's material is S275JR
**Rail's material is S275JR and post's material is S355JR

In Figures 4.18 and 4.19, both geometric details and FE models of the H1W4 and H2W4 systems are given. As can be seen from the figures, the geometric width of the post is an effective factor on the buckling strength. Similarly, the rail sectional thickness is effective on strength and rupture of the rail during a collision. This is why these variables were chosen as optimization design variables.

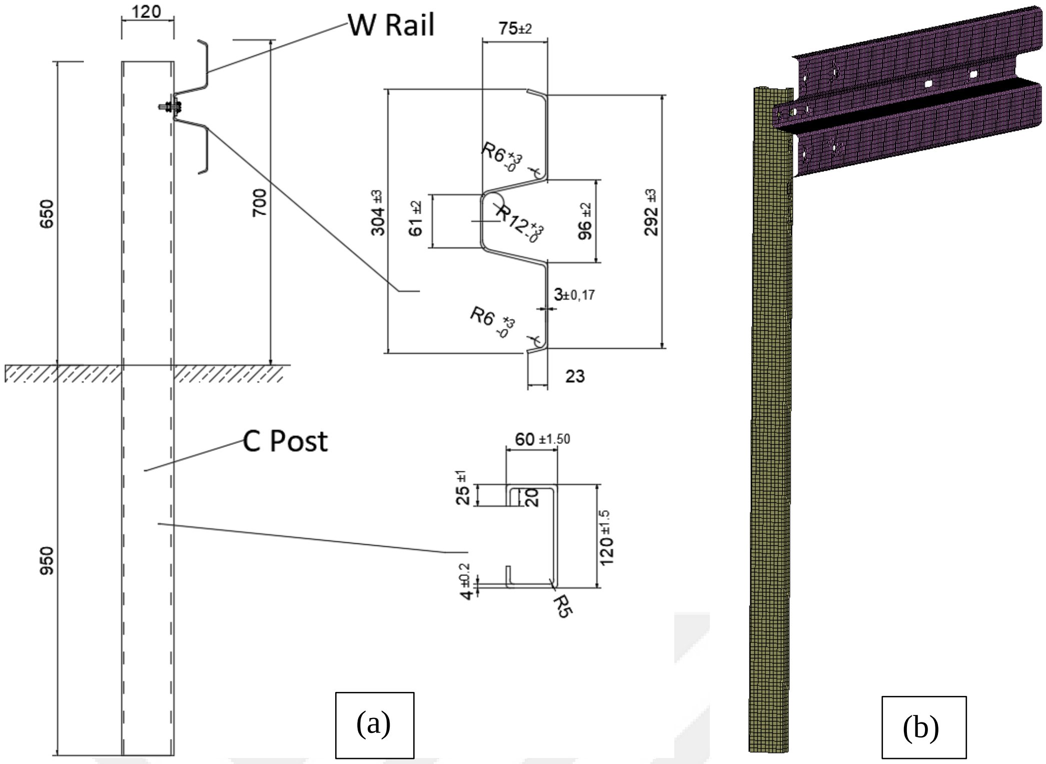

Figure 4.18 : (a) H1W4 guardrail system details and (b) FE model of the design [49].

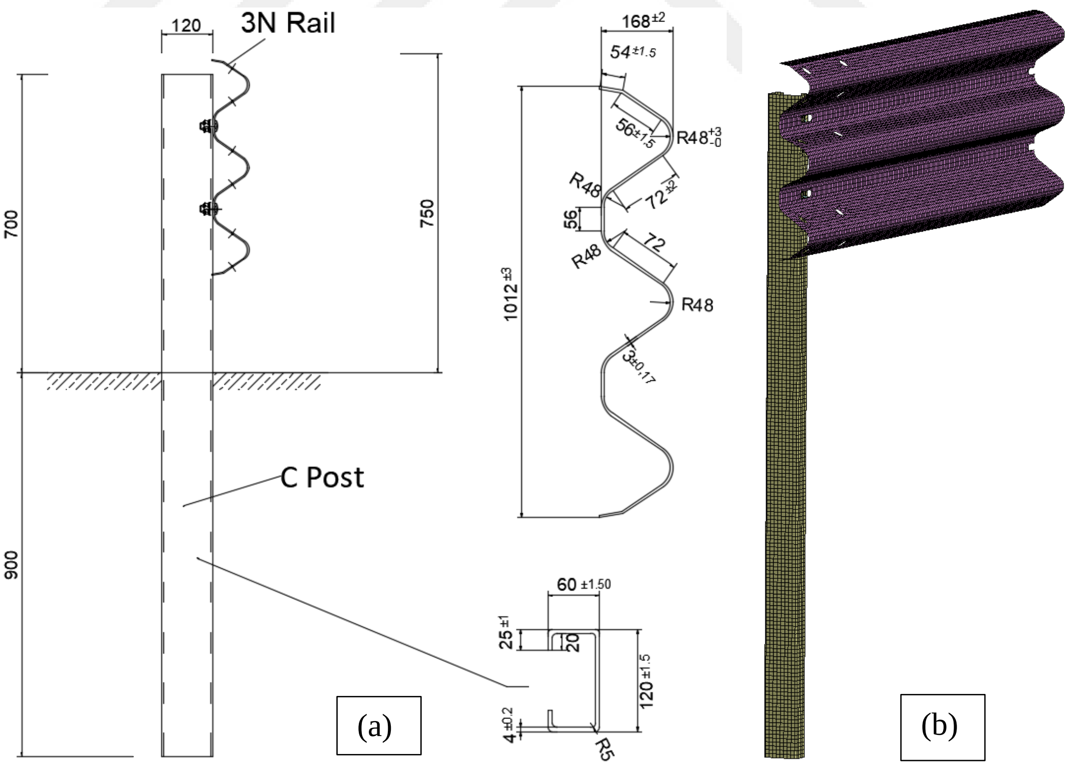

Figure 4.19 : (a) H2W4 guardrail system details and (b) FE model of the design [49].

4.2.2 Safety and crash test criteria of guardrail systems design

The evaluation of the road safety designs in Turkey is performed in accordance with the EN1317 standards. Therefore, safety criteria and crash tests specified in EN1317 are taken as reference to perform the optimization. The test acceptance criteria that are specified in EN1317 for H1 and H2 systems, are given in Table 4.15. Figure 4.20 shows the FE models of the vehicles used in the TB11, TB42 and TB51 tests. Details on vehicle crash test descriptions and containment levels are given in EN1317 part 2 [3].

Table 4.15 : EN1317 test acceptance criteria for H1 and H2 guardrail systems (CEN 2014) [49].

System type	Test	Impact speed (km/h)	Impact angle (Θ) (°)	Total mass (kg)	Type of vehicle
H1	TB11	100	20	900	Car
	TB42	70	15	10000	Rigid HGV*
H2	TB11	100	20	900	Car
	TB51	70	20	13000	Bus

*Heavy Goods Vehicle

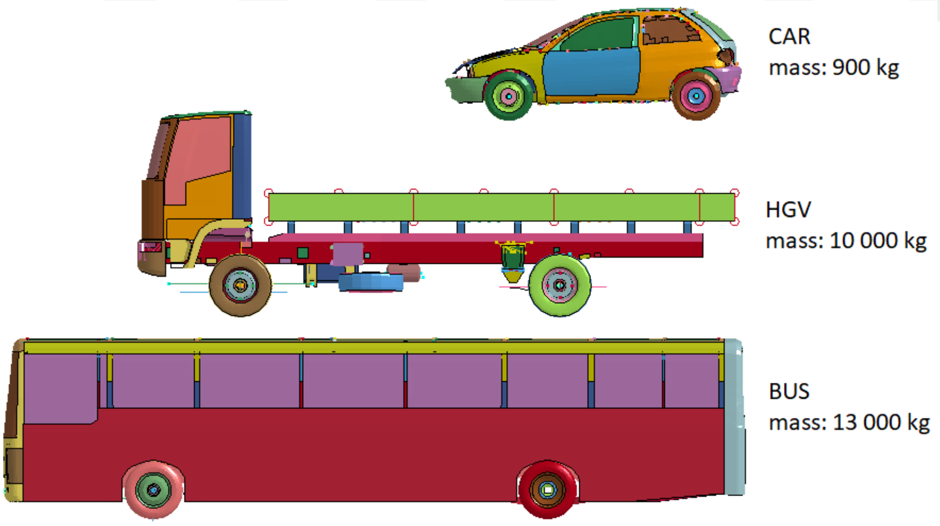

Figure 4.20 : The FE models of vehicles used in TB11, TB42 and TB51 tests (FEMA 2002) [49].

Table 4.16 gives the evaluation criteria for TB11, TB42 and TB51 tests used in the classification of H1 and H2 barrier systems. The optimization of the guardrail systems is based on these criteria. In the table, two important criteria, which are the guardrail working width (w) and vehicle exit angle (α), are used as the objective and constraint functions for optimization, respectively. Figure 4.21 shows the test case according to EN1317 standards. As can be seen from the figure, the working width (w) is the greatest displacement of the guardrail during an impact. After a vehicle has impacted into the guardrail, it leaves the guardrail from an exit point. An exit box can be designed as a rectangular shaped box, calculated from the beginning of the vehicle exit point, the width (A) and length (B) of the impacting vehicle. One of the evaluation criteria of a crash test according to EN1317 is that a vehicle must remain inside the short edge of the exit box when exiting the barrier. The aim here is to prevent vehicles entering the traffic after an accident. Hence, calculation of the exit angle of a vehicle is of importance in terms of test acceptance.

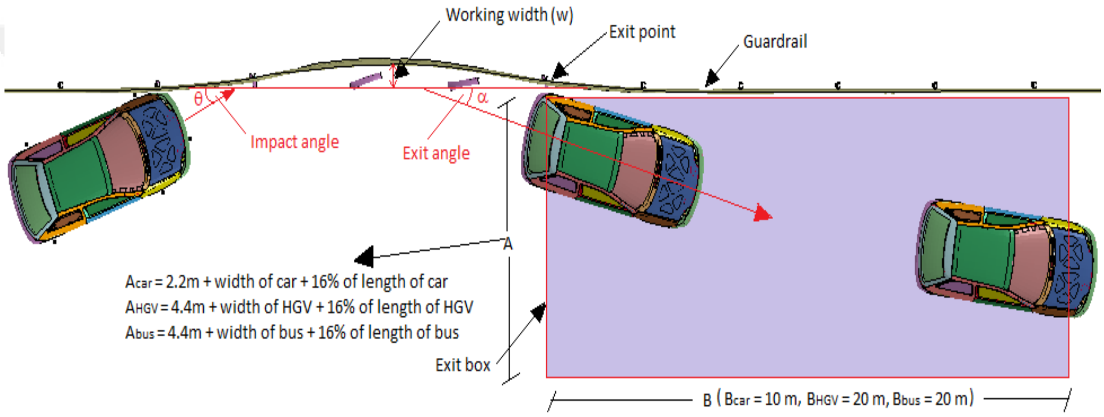

Figure 4.21 : Illustration of crash test condition of EN1317 and exit box calculation [49].

In Turkey the maximum acceptable lateral displacement or working width is 1.3 m or W4 level. Also, for the test conditions of TB11, TB42 and TB51, the maximum exit angle (α) is no more than 19° in reference to guardrail.

Table 4.16 : EN1317 test evaluation criteria for H1 and H2 guardrail systems [49].

System Type	Test	Working width (W) (m)	Exit box (width(A) x length(B)) (m)*	Exit angle (α) (°)**
H1W4A	TB11	≤1.3	4.4x10	≤19
	TB42	≤1.3	8.22x20	≤17
H2W4A	TB11	≤1.3	4.4x10	≤19
	TB51	≤1.3	8.95x20	≤19

*Calculated based on EN1317/2
**Calculated based on exit box length

4.2.3 Validation of the FE models

In the section above, the tests to be performed for H1 and H2 systems are given in Table 4.15. Full scale crash test data, for TB11, TB42 and TB51 tests, used in this study is taken from previous crash test reports [106]. Based on these tests, full-scale finite element models of H1 and H2 systems were created using LS-DYNA software. The validity of these models created in the FE environment was compared against the actual crash test data. As shown in Figures 4.22-4.24, results obtained from the FE models and the real crash tests show good agreement. The values of the guardrail working width (w) and the vehicle exit angle (α) for the TB11, TB42 and TB51 crash tests and the corresponding FE models for H1 and H2 systems are given in Table 4.17. The maximum relative absolute errors (RAE) between the real tests and the FE result are found to be smaller than 5%, which is acceptable.

Table 4.17 : Comparison of data obtained from real tests and FE models [49].

Test	FE models		Real crash tests		RAE of w (%)	RAE of α (%)
	Working width (w) (m)	Exit angle (α) (°)	Working width (w) (m)	Exit angle (α) (°)		
TB11	426	10.5	447	11	4.76	4.55
TB42	1036	7.7	994	8	4.20	4.38
TB51	815	3	846	3	3.66	3.45

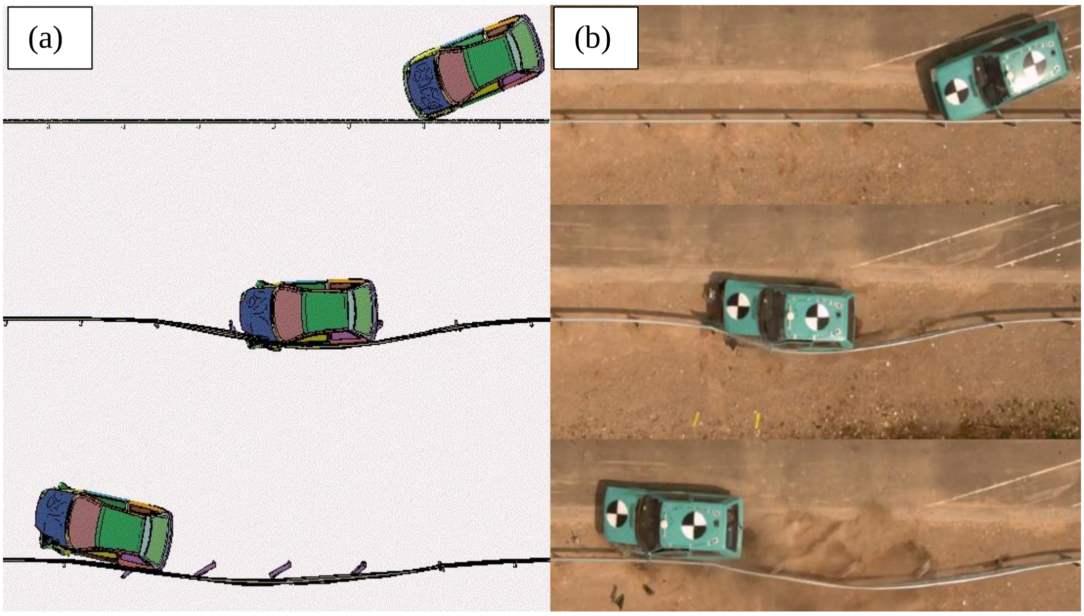

Figure 4.22 : (a) FE model of TB11 (b) Real test of TB11 [49].

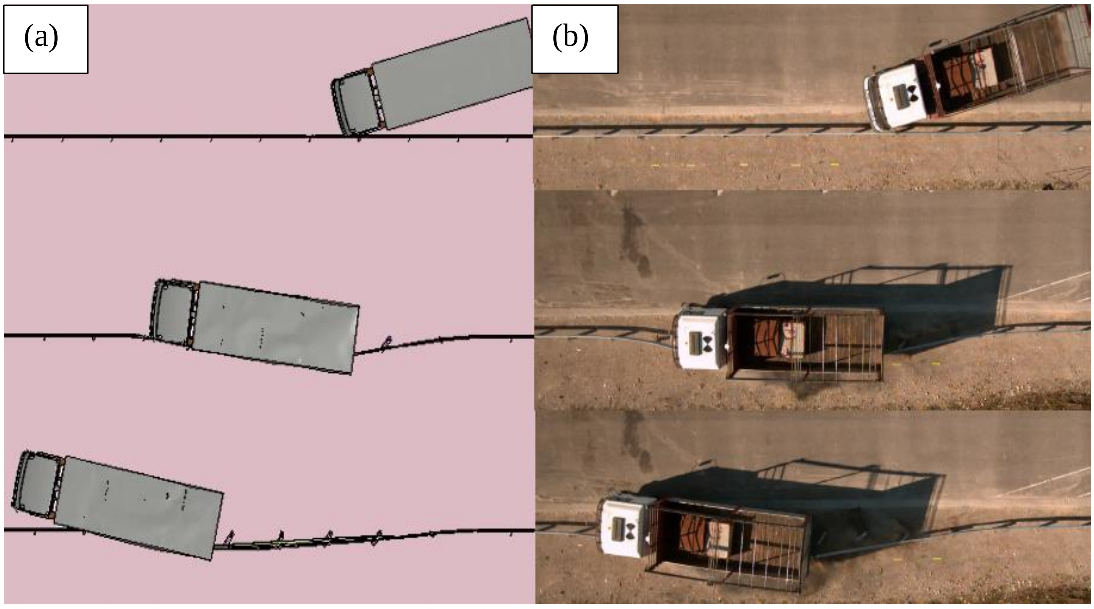

Figure 4.23 : (a) FE model of TB42 (b) Real test of TB42 [49].

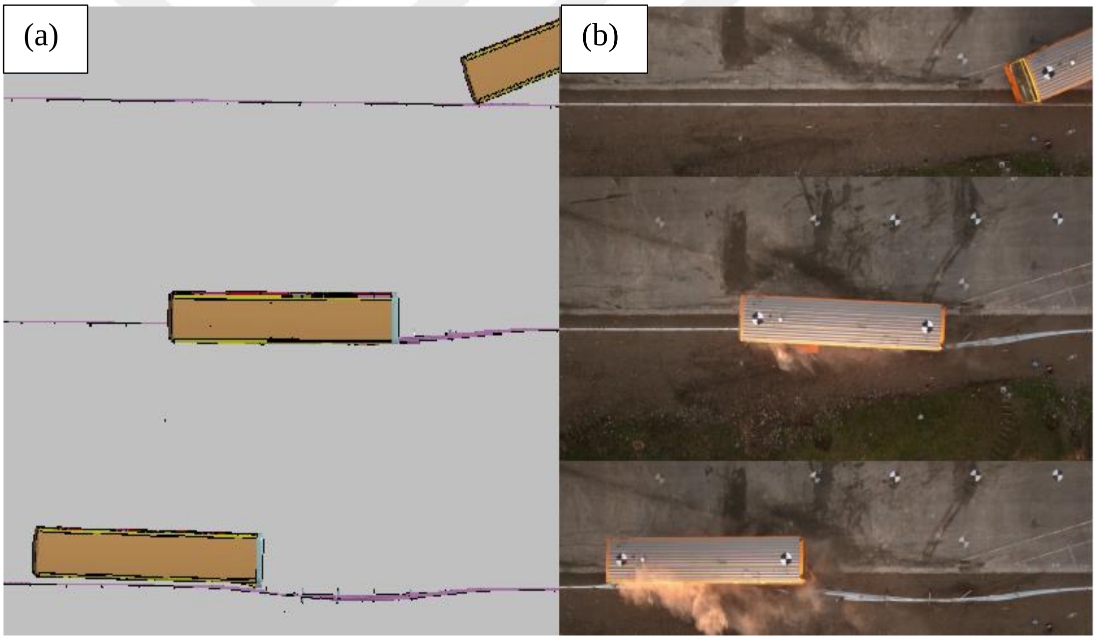

Figure 4.24 : (a) FE model of TB51 (b) Real test of TB51 [49].

4.2.4 Construction of RBF-based metamodels and validation

As mentioned above, two important factors that affect the performance of the guardrail are geometric width of the post and sectional thickness of the rail. Therefore, they are considered as design variables for SBDO. These variables are denoted as the geometric width of the C type post - x1 and the cross-sectional thickness of the rail - x2 for the H1W4 and H2W4 guardrail systems. The ranges of x1 and x2 are set as 100–125 mm and 2.5–3.0 mm, respectively. Since lower values than the minimum values for these variables are not accepted in practice, the minimum constraint values are taken in this way. Figure 4.25 shows the 36 sampling points which are derived by the FFD. Samples of the H1 and H2 guardrail systems formed by S235JR, S275JR and S355JR steel grades are derived using this method.

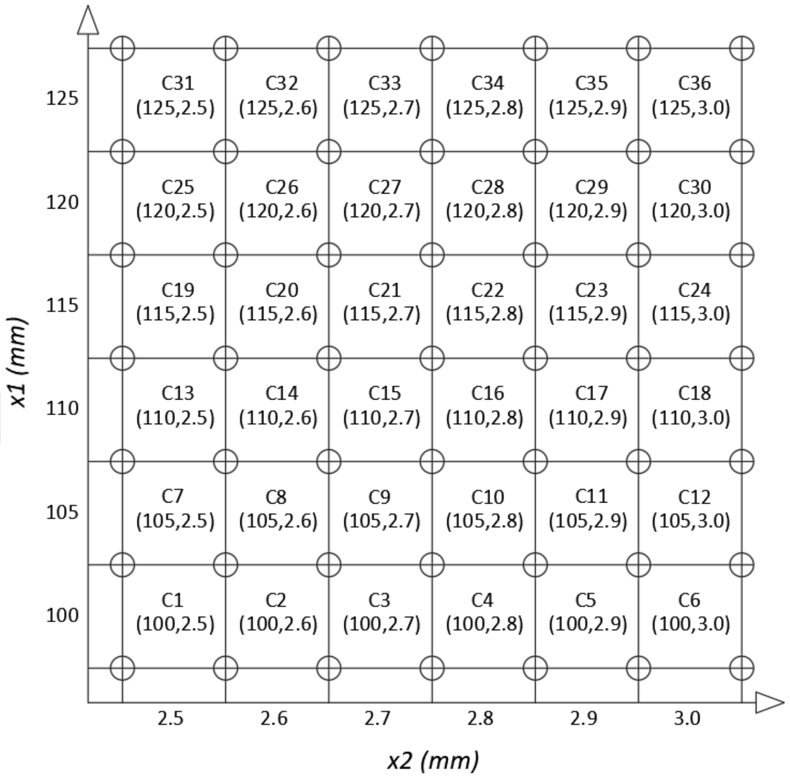

Figure 4.25 : Illustration of the 36 cases investigated in this study [49].

As the objective and constraint functions, the guardrail working width (w) and vehicle exit angle (α) are selected from the test acceptance criteria in EN1317. Table 4.18 shows the values of the guardrail working width (w) and vehicle exit angle (α) obtained from 36 cases and their corresponding responses from the FE simulations for the H1W4 system constructed by the S235JR grade steel. By using the values provided in Table 4.18, the RBF-based surrogate model for H1W4A/S235JR is established by the RBF method. To implement the RBF surrogate model, the multiquadric radial basis function [102] is used, where the optimal shape parameter is set to c = 0.9. Optimal shape parameter (c) is chosen by minimizing some error criteria as illustrated in Figure 4.26.

For the H1 and H2 systems consisting of S235JR, S275JR and S355JR grade steel and their combinations (Table 4.14), the initial samples are derived by FFD as shown in Figure 4.25. In total 10 RBF-based metamodels of H1 and H2 systems are created by following the procedure described above. To avoid overloading of the paper, the sample tables for only one model (H1W4A/S235JR) are given here. However, in the following sections, the results for all models are tabulated and summarized.

Table 4.18 : The FE simulation results of design samples of H1W4/S235JR [49].

	H1W4A					
	x_1 (mm)	x_2 (mm)	w^{TB11} (mm)	w^{TB42} (mm)	α^{TB11} (°)	α^{TB42} (°)
S235JR (St-37)	100	2,50	700	1627	13,2	14,6
	100	2,60	667	1550	12,9	14,5
	100	2,70	634	1473	12,7	14,4
	100	2,80	601	1396	12,5	14,3
	100	2,90	568	1319	12,3	14,1
	100	3,00	534	1242	12,1	14,0
	105	2,50	660	1565	12,9	14,5
	105	2,60	629	1494	12,7	14,4
	105	2,70	599	1422	12,5	14,2
	105	2,80	569	1351	12,3	14,1
	105	2,90	539	1280	12,0	14,0
	105	3,00	509	1208	11,8	13,9
	110	2,50	620	1504	12,7	14,4
	110	2,60	593	1438	12,5	14,2
	110	2,70	566	1372	12,2	14,1
	110	2,80	538	1306	12,0	14,0
	110	2,90	511	1240	11,8	13,9
	110	3,00	484	1174	11,5	13,8
	115	2,50	612	1486	12,5	14,3
	115	2,60	586	1422	12,3	14,1
	115	2,70	559	1357	12,0	14,0
	115	2,80	533	1293	11,8	13,9
	115	2,90	507	1229	11,5	13,8
	115	3,00	480	1165	11,2	13,6
	120	2,50	606	1470	12,3	14,1
	120	2,60	580	1407	12,0	14,0
	120	2,70	554	1344	11,8	13,9
	120	2,80	528	1281	11,5	13,8
	120	2,90	502	1218	11,2	13,6
	120	3,00	476	1156	11,0	13,5
	125	2,50	600	1457	12,1	14,0
	125	2,60	575	1395	11,8	13,9
	125	2,70	549	1333	11,5	13,8
	125	2,80	523	1270	11,2	13,6
	125	2,90	498	1208	11,0	13,5
	125	3,00	472	1146	10,7	13,3

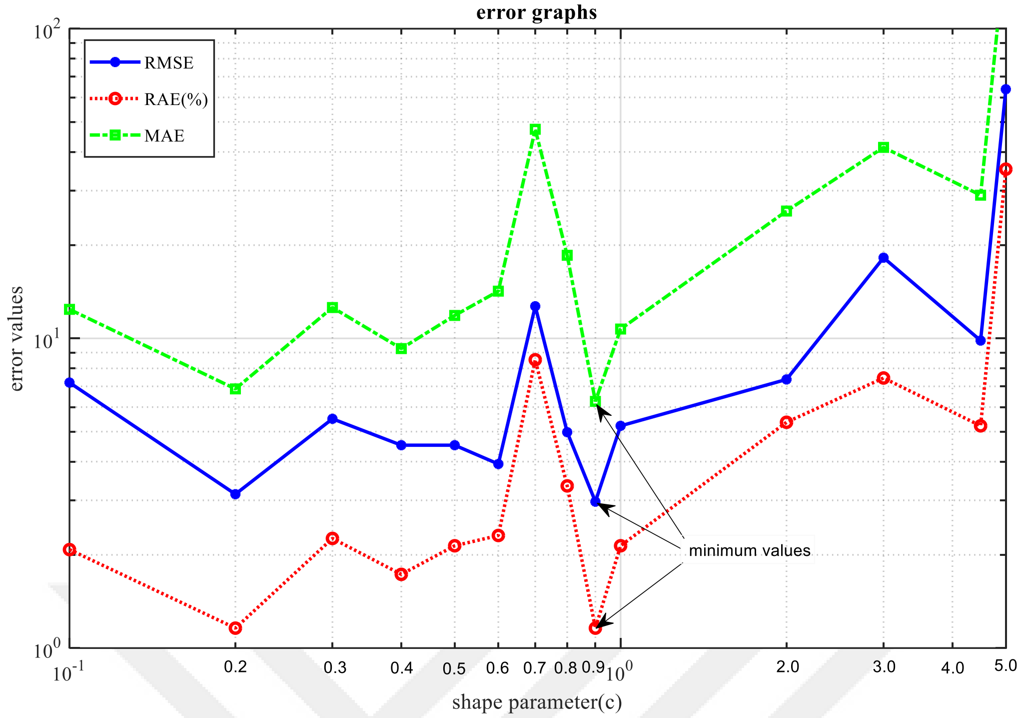

Figure 4.26 : The impact of shape parameter (c) on the behavior and fidelity of the RBF-multiquadric surrogate model [49].

4.2.5 Accuracy of the Surrogate Models

In the metamodel based optimization method, the accuracy of the metamodel affects the accuracy of the optimum result because the objective function values are calculated using the metamodel. Before using RBF metamodels in optimization, the fidelity of surrogate models for H1W4 and H2W4 systems are evaluated in two ways: (i) using additional samples that are randomly generated within the design space and (ii) *k*-fold cross-validation.

4.2.5.1 Validating the metamodel by validation samples

The validation samples are derived to validate the metamodels. For this purpose, the metamodels are trained with the help of the samples until the desired error rate is obtained for the metamodel estimates. The optimization are applied when the requested error rate is obtained. For the H1W4/S235JR case, the values of w and α at the 6 validation points are obtained using FE simulations and RBF prediction, as given in Table 4.19. As shown in Figure 4.27, the average relative absolute errors (RAE) are calculated by using these test data for the 10 surrogates in total. The average RAE (%) rate is around 16%, in other words, surrogate prediction accuracy is around 84%. That error level of surrogate accuracy is not satisfactory to use in optimization. Hence to improve accuracy of metamodels, additional data should be used. As known, using additional data in different locations of the design domain enhances the prediction of surrogates. Therefore, to improve the fidelity of the RBF metamodels, first 6 validation samples are added to the initial 36 design samples. A total of 42 design samples are used to create new updated RBF metamodels.

Table 4.19 : First validation samples of H1W4A/S235JR [49].

S.no	Variables		RBF-MQ prediction				FEA result			
	x_1 (mm)	x_2 (mm)	w^{TB11} (mm)	w^{TB42} (mm)	α^{TB11} (°)	α^{TB42} (°)	w^{TB11} (mm)	w^{TB42} (mm)	α^{TB11} (°)	α^{TB42} (°)
1	119	2.7	406	1012	22.3	11.5	555	1347	11.8	13.9
2	102	2.5	493	1227	30.5	19.0	685	1603	13.1	14.5
3	114	3.0	336	881	15.6	13.0	481	1167	11.3	13.6
4	111	2.8	288	826	12.4	13.9	538	1304	11.9	14.0
5	107	2.6	462	1208	33.6	25.8	615	1472	12.6	14.3
6	123	2.9	432	943	20.2	10.1	499	1212	11.1	13.5

The updated metamodels are validated using 4 additional samples on which the FE simulation is performed to obtain the values for the evaluation criteria as shown in Table 4.20. By using these samples, MAEs (%) of the objective functions in surrogates are calculated as shown in Figure 4.28. As illustrated in the figure, the accuracy of all objectives are different. Each objective function in engineering problem defines the behavior of a different part. Thus, these behaviors become different. Since the objective functions of the metamodel mimic engineering behaviors, each of the 4 objective functions used in this study within the metamodel is expected to have different accuracy. The accuracy and behavior of the objectives can also be seen in Figure 4.28 and Figure 4.29.

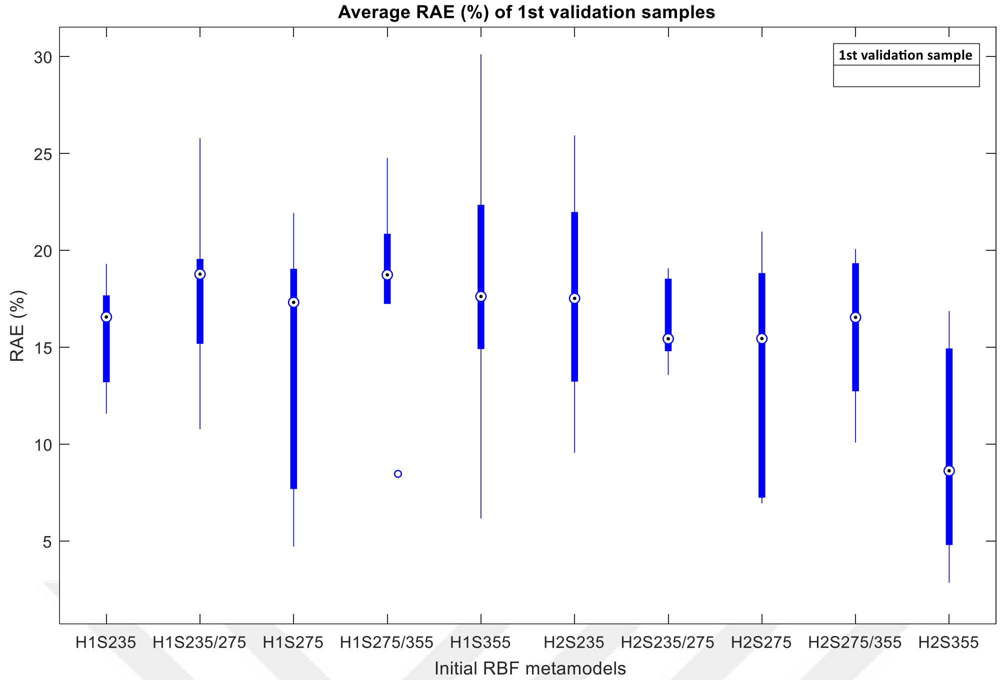

Figure 4.27 : Average RAE (%) of 1st validation samples of initial RBF metamodels [49].

The average RAE (%) of the 2nd validation samples tested on updated RBF metamodels are demonstrated in Figure 4.30. The figure shows that there is a significant improvement in the surrogates' accuracy. The general mean of average RAE (%) of the 1st and 2nd validation samples are given in Figure 4.31. As shown in this figure, the mean dropped from around 16% to 2-3%. In other words the prediction rate of RBF metamodels is enhanced by the 2nd set of validation samples from 86% to 97-98% which is deemed satisfactory.

Table 4.20 : Second validation samples of H1W4A/S235JR [49].

S.no	Variables		RBF-MQ prediction				FEA result			
	x_1 (mm)	x_2 (mm)	w^{TB11} (mm)	w^{TB42} (mm)	α^{TB11} (°)	α^{TB42} (°)	w^{TB11} (mm)	w^{TB42} (mm)	α^{TB11} (°)	α^{TB42} (°)
1	113	2.5	609	1466	11.5	14.0	616	1401	11.5	13.7
2	106	2.9	548	1309	12.2	14.0	541	1299	13.1	13,5
3	123	2.7	536	1300	11.4	13.6	557	1258	10.6	13.3
4	101	2.8	616	1436	12.4	14.1	596	1354	11.6	13.7

In general, for complex engineering design problems, the RAE (%) of metamodels should be less than 2-10% [45-48]. For this reason, in this study, it is thought that a 2-3% rate of average RAE can be acceptable for engineering design.

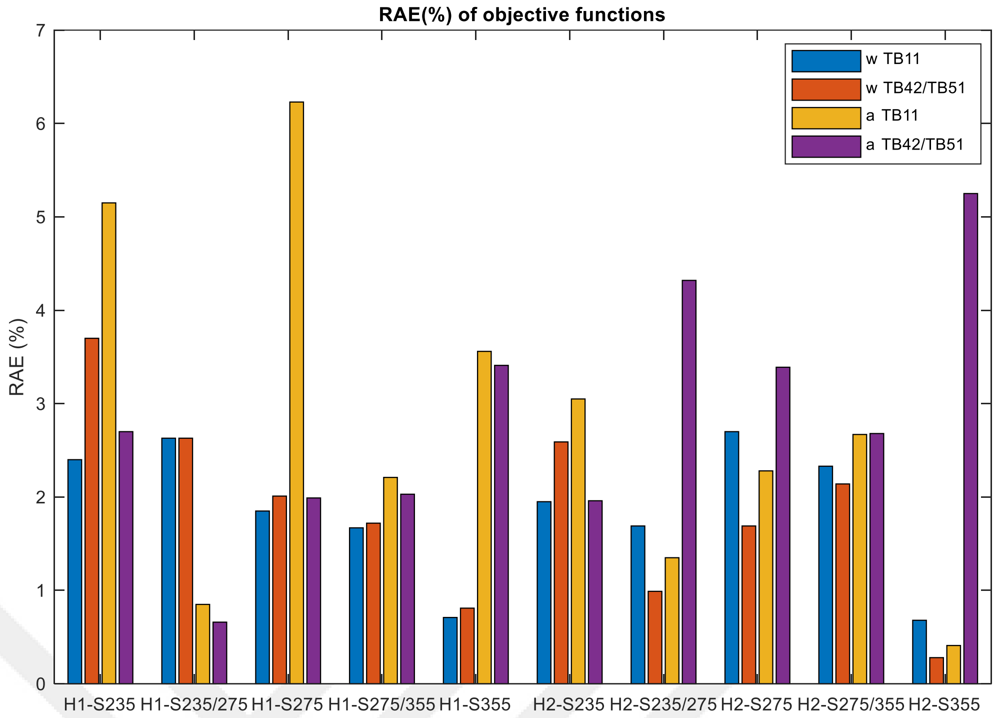

Figure 4.28 : RAE (%) of 2nd validation samples of objective functions in updated RBF metamodels [49].

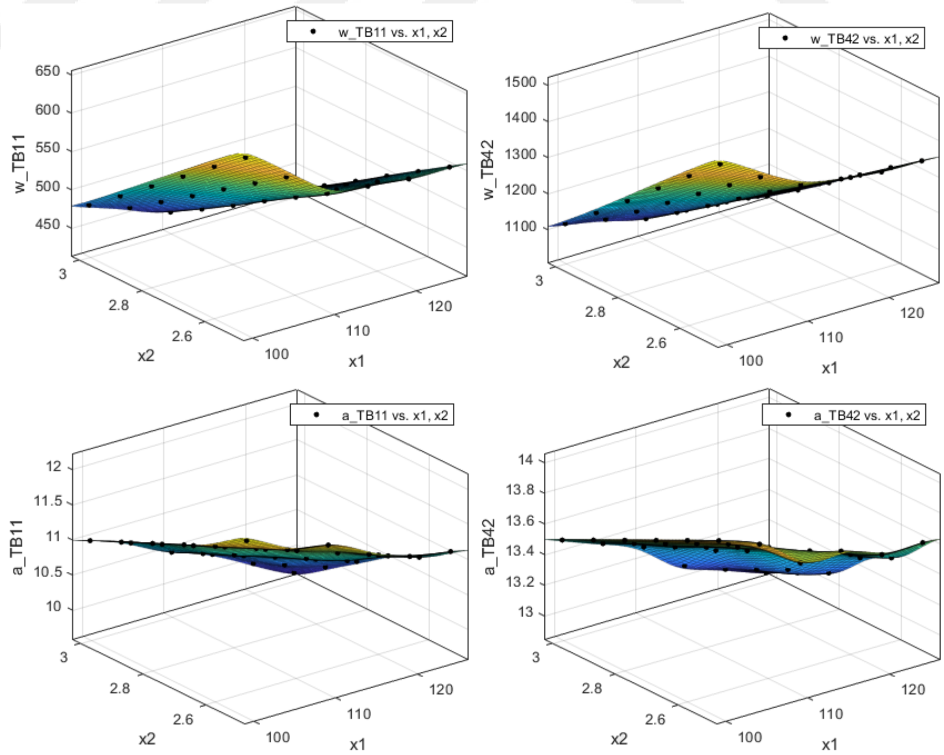

Figure 4.29 : Metamodel surface plots of objective functions in H1W4-S235JR [49].

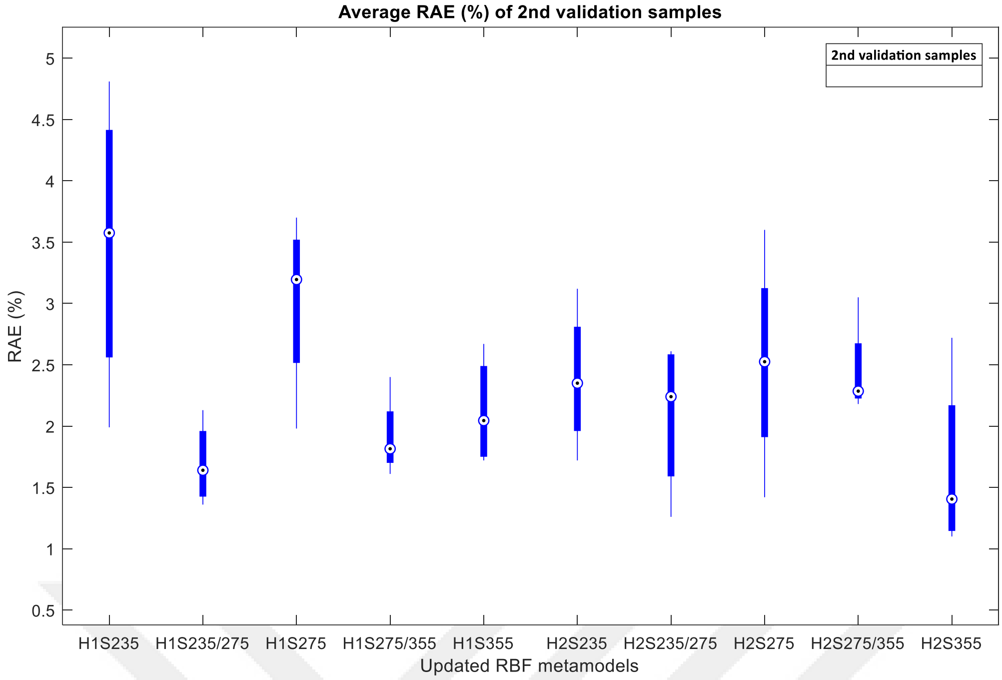

Figure 4.30 : Average RAE (%) of 2nd validation samples of updated RBF metamodels [49].

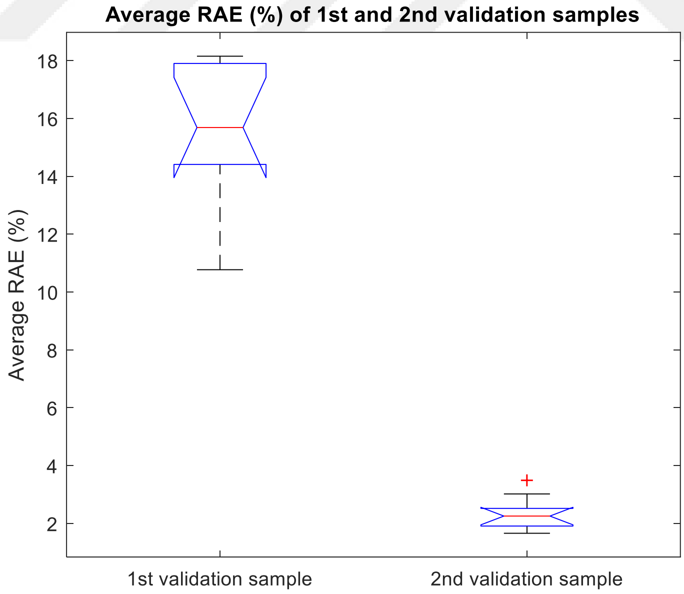

Figure 4.31 : Mean of average RAE (%) of 1st and 2nd validation samples [49].

4.2.5.2 *k*-fold cross-validation

The accuracy of the constructed surrogate models is evaluated by using root mean square *k*-fold cross-validation error metric, $RMSE_{CV}$. To calculate the $RMSE_{CV}$, first the surrogate model samples are divided in 9 fold (where 9 is the number of training points), while leaving out one of the training points as the validation data each time. Then, an error value is obtained using Equation (10). Prediction errors of objective functions in H1 and H2 systems are given in Figure 4.32. Similar to MAE (%) local error measurements, the $RMSE_{CV}$ values of all objective functions are different from each other. Figure 4.33 shows the average $RMSE_{CV}$ of all metamodels. An $RMSE_{CV}$ value of 0 indicates a perfect fit. We can say that the $RMSE_{CV}$ trained RBFs result in an almost perfect fit to the engineering design model.

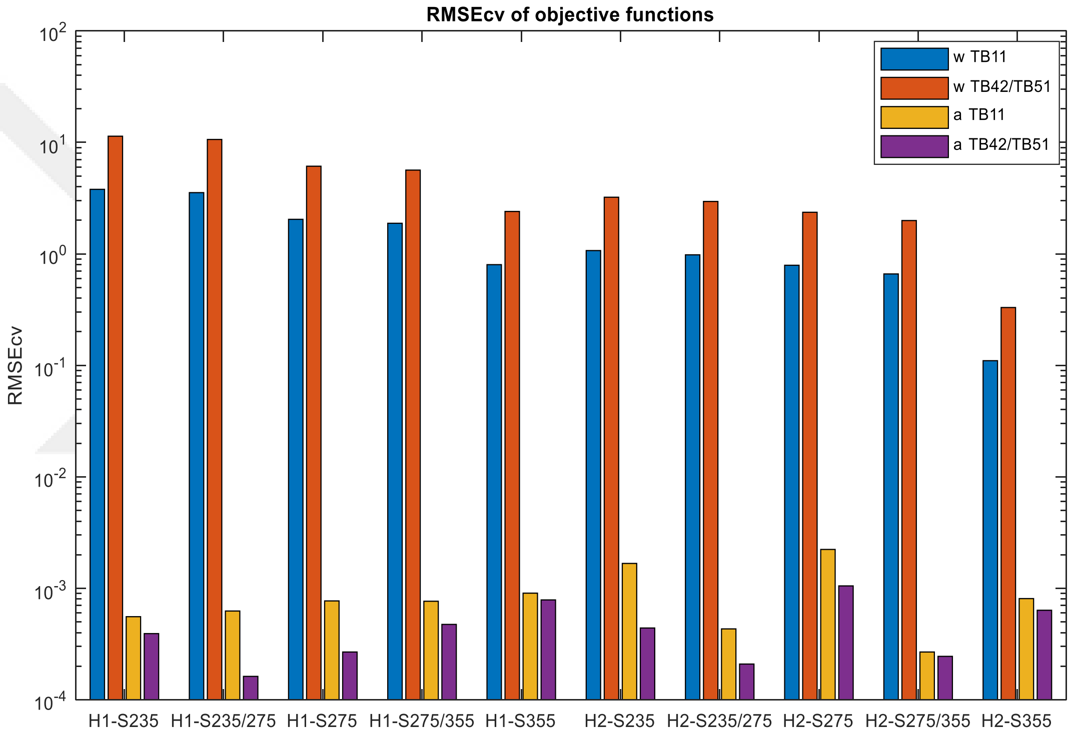

Figure 4.32 : $RMSE_{CV}$ of objective functions in initial RBF metamodels [49].

Both global and local error measure metrics are used to assess the accuracy of surrogate models. In this paper, the *k*-fold cross-validation errors at all training points are used as local error measures. The metamodel error values of $RMSE_{CV}$ and RAE (%) are provided in Table 4.21. As can be seen from Figure 4.34, when compared with errors estimated on test points in the local neighborhood of updated RBFs, the *k*-fold cross-validation error is found to be reasonably accurate in capturing local errors. Metamodel surface plots of w of true, initial and updated RBFs can be seen in Figure 4.35. When compared with true models, initial RBF trained by $RMSE_{CV}$ seems to fit better than updated RBF trained by validation points. As generally known, the main purpose of simulation-based design is to install metamodels that can mimic the behavior of computationally expensive simulations. Thus, instead of additional systems evaluation by validation points, using *k*-fold cross-validation reduces computational burden.

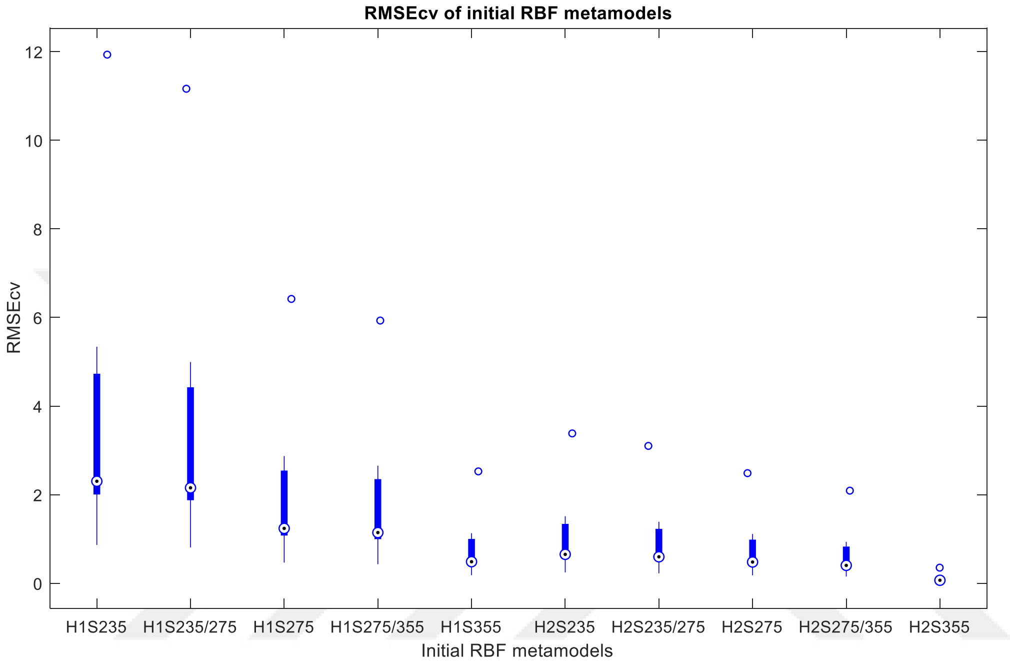

Figure 4.33 : Average RMSE$_{CV}$ of initial RBF metamodels [49].

Table 4.21 : Average RAE (%) of updated RBF and RMSE$_{CV}$ of initial RBF metamodels [49].

System type	Material	RMSEcv	RAE (%)
H1W4	S235	3,786	3,486
	S235/275*	3,541	1,693
	S275	2,036	3,019
	S275/355**	1,881	1,907
	S355	0,801	2,121
H2W4	S235	1,073	2,388
	S235/275*	0,984	2,086
	S275	0,789	2,516
	S275/355**	0,663	2,452
	S355	0,112	1,655

*Rail's material is S235 and post's material is S275
**Rail's material is S275 and post's material is S355

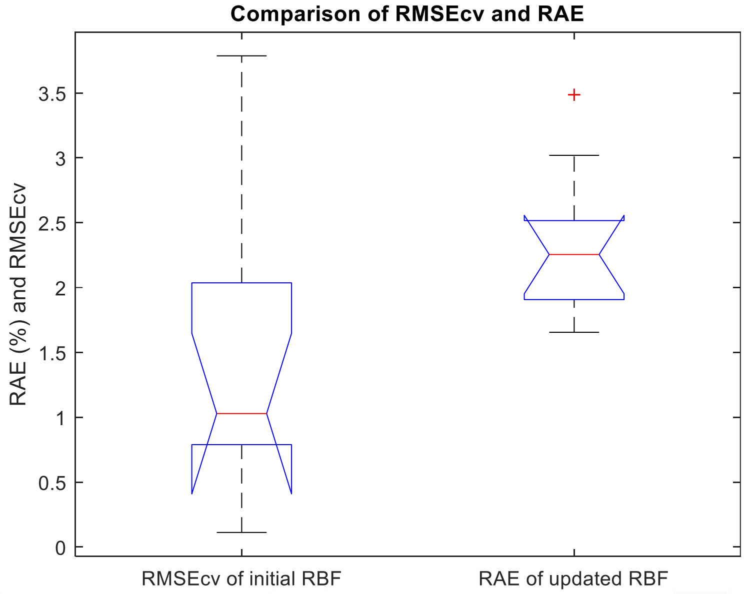

Figure 4.34 : Comparison of $RMSE_{CV}$ of initial RBF and RAE (%) of updated RBF metamodels [49].

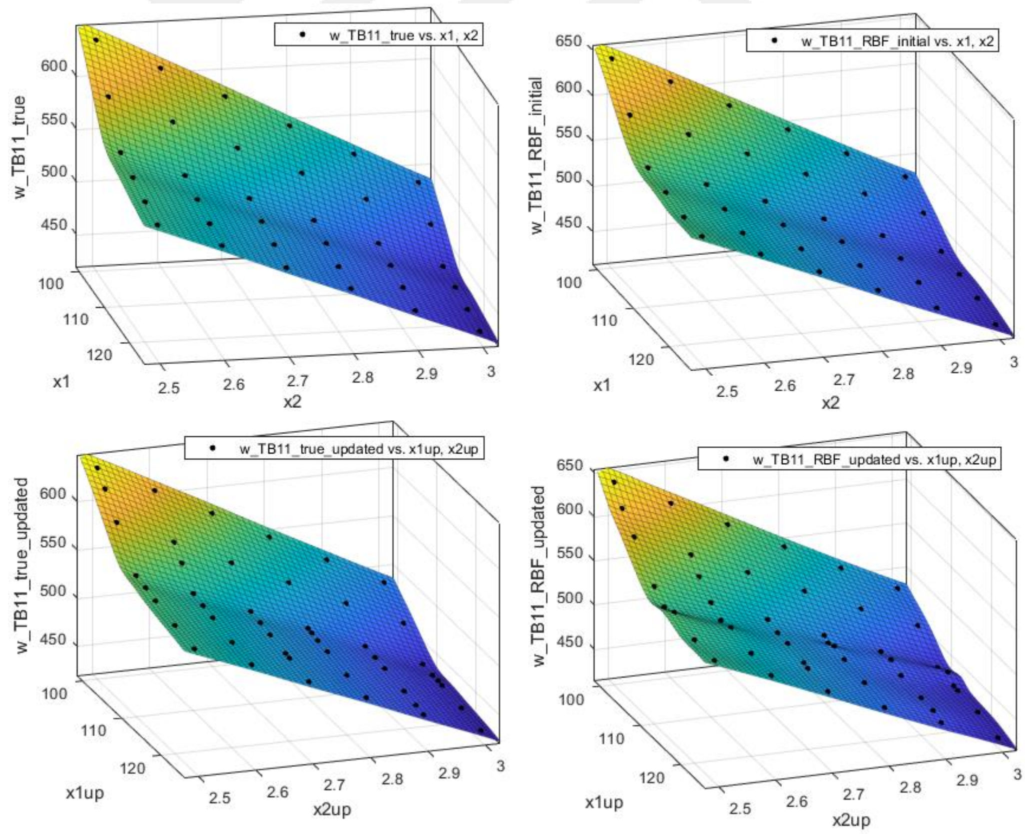

Figure 4.35 : Metamodel surface plots of w of true, initial and updated H1W4-S235JR [49].

4.2.6 MOO formulation and optimal values

As previously mentioned, the geometric and cross-sectional size of post and rail play an important role in both, a safe and economical design. Therefore, the post geometric width (x_1) and the rail sectional thickness (x_2) are chosen as design variables in this study. The ranges of x_1 and x_2 are set as 100–125 mm and 2.5–3.0 mm, respectively. From the test acceptance and safety criteria in EN1317, the guardrail working width (w) and vehicle exit angle (α) are regarded as objective and constraint functions. The limit for w is set to be 1300 mm which is the maximum working width of W4 in EN1317. For α, first, the exit boxes of TB11, TB42 and TB51 are drawn in the light of the specified points in EN1317 standard. Next, the limits of the α are calculated according to the exit box given in Table 4.16. The α values of TB42 are 17 and 19 for TB11 and TB51, respectively. The α value difference in TB42 is that the vehicle impact angle is different from TB11 and TB51. Since this study aims at the safest and most economical guardrail system, the optimum size/cross-sections, that provide the safety criteria at the maximum limit values, are investigated. Therefore, the optimization solution that maximizes the two objective functions yields the most economical geometry and cross-sectional measurements. By using the optimization methodology given in Formula (4.4), the problem of optimizing the safest and most economical designs of H1W4 and H2W4 systems is formulated as follows:

$$\begin{cases} \text{Min.} & [-\mathrm{w}(\mathrm{x1},\mathrm{x2}), -\alpha(\mathrm{x1},\mathrm{x2})] \\ \text{s.t.} & 100\ \text{mm} \le \mathrm{x1} \le 125\ \text{mm} \\ & 2.5\ \text{mm} \le \mathrm{x2} \le 3.0\ \text{mm} \\ & \mathrm{w}_{\mathrm{TB11,TB42,TB51}} \le 1300\ \text{mm} \\ & \alpha_{\mathrm{TB42}} \le 17^\circ \\ & \alpha_{\mathrm{TB11,TB51}} \le 19^\circ \end{cases} \tag{4.4}$$

The MOGA (NSGA-II) toolbox in Matlab (2017b) [101] is used for optimization with the MOGA (NSGA-II) parameters as given Table 4.22. The 'crossoverarithmetic' creates children that are the weighted arithmetic mean of two parents. Children are always feasible with respect to linear constraints and bounds. The 'mutationadaptfeasible' is a default mutation function when there are constraints, it randomly generates directions that are adaptive with respect to the last successful or unsuccessful generation. The mutation chooses a direction and step length that satisfies bounds and linear constraints. The 'MaxStallGenerations' is used to set the number of generations. To investigate the effect of number of iterations (or generations) on the accuracy of optimization results, the solutions are obtained at eight different iterations, as shown in Figure 4.36. It can be seen from the figure that there is no significant difference among the solutions when the number of iterations is more than 100. Thus, in this study, the maximum number of iterations is set to 400 and used as the convergence criterion for solving the MOO problem.

Table 4.22 : Parameters of MOGA (NSGA-II) algorithm [49].

Parameters	Value/Function
Number of points on the Pareto front	25
Population size	100
Number of iterations	'MaxStallGenerations'(400)
Crossover option	'crossoverarithmetic'
Mutation option	'mutationadaptfeasible'

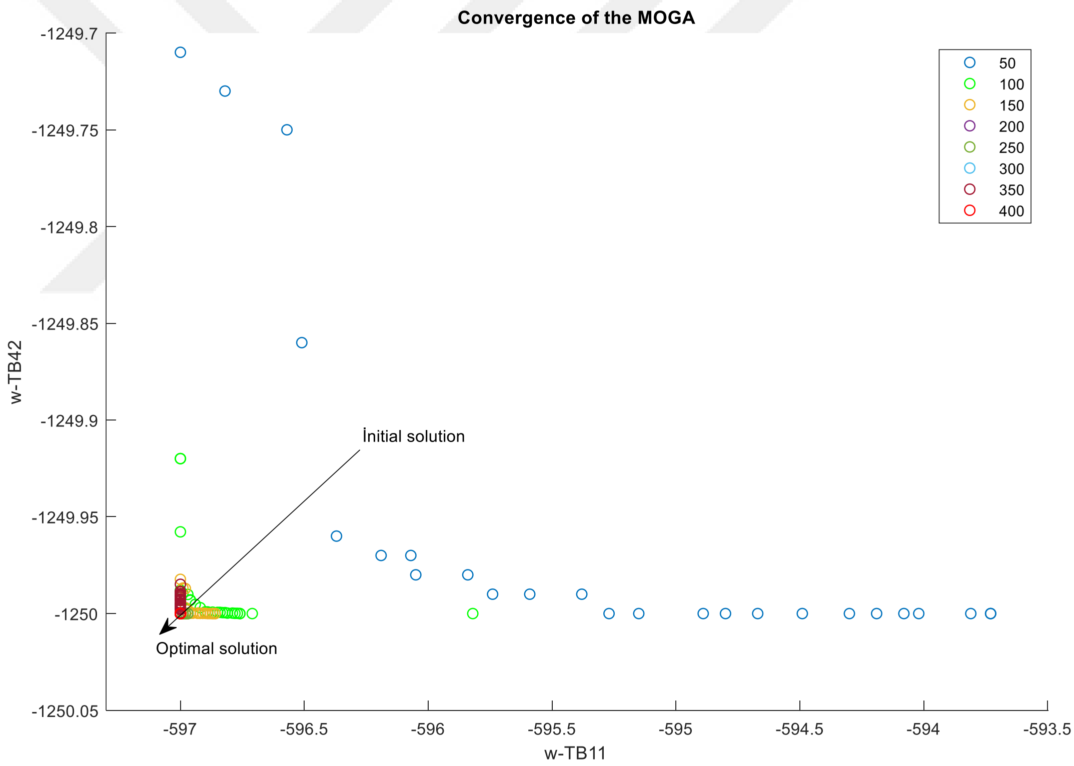

Figure 4.36 : MOGA convergence plots of H1W4-S235JR [49].

The optimization procedure that is given above was implemented to both, initial and updated RBF, to optimize the H1W4 and H2W4 guardrail systems which are composed by S235JR, S275JR and S355JR grade steel and their combination. The optimum design variables (x_1, x_2) corresponding to the optimal solutions of initial and updated RBF metamodels are given in Table 4.23. As can be understood from the table, the optimization results of both, initial and updated RBF, metamodels are nearly the same. It can be said that, additional data validation is meaningless or no more affects the multidisciplinary optimization with linear constraints. That is probably due to the DoE method of deriving the design space or put linear constraint in design domain. Consequently, as mentioned before, updated RBF metamodels are obtained using additional data. When using the additional data, the predicted responses using the metamodel are compared to the true responses at untried locations, which are obtained using additional runs of the full scale guardrail models. Thus, they cause extra computational burden and take long time. But when using existing data by *k*-fold cross-validation, prediction accuracy of the metamodel is determined without requiring additional (likely computationally expensive) simulations or analyses. In this approach, we take advantage of the data used to fit the metamodel for validation purposes. In terms of practicality, the *k*-fold cross-validation strategy provides a reasonable indicator of metamodel fidelity without the use of additional computationally expensive analyses.

Table 4.23 : Optimal design variables of initial and updated RBF metamodels [49].

System type	Material type	RBF	x_1 (mm)	x_2 (mm)	w^{TB11} (mm)	$w^{TB42/51}$ (mm)	α^{TB11} (°)	$\alpha^{TB42/51}$ (°)
H1W4	S235JR	initial	104,61	2,79	-576,42	-1300,00	-11,69	-13,84
		updated	104,79	2,78	-576,11	-1300,00	-11,64	-13,80
	S235JR / 275JR*	initial	102,55	2,71	-550,64	-1300,00	-11,45	-13,78
		updated	102,09	2,71	-550,02	-1300,00	-11,48	-13,74
	S275JR	initial	100,38	2,56	-562,86	-1300,00	-11,12	-13,55
		updated	100,90	2,55	-561,33	-1300,00	-11,15	-13,55
	S275JR/ 355JR**	initial	100,00	2,50	-474,70	-1061,50	-10,11	-13,13
		updated	100,18	2,53	-472,17	-1050,00	-10,01	-13,01
	S355JR	initial	100,00	2,50	-436,20	-1020,82	-9,63	-12,88
		updated	100,00	2,50	-436,09	-1020,40	-9,41	-12,87
H2W4	S235JR	initial	100,00	2,50	-396,93	1149,00	-18,45	-9,21
		updated	100,00	2,50	-396,86	1148,97	-18,35	-9,17
	S235JR/ 275JR*	initial	100,00	2,50	-381,55	-1108,17	-17,97	-9,21
		updated	100,00	2,50	-380,27	-1105,29	-17,94	-9,17
	S275JR	initial	100,00	2,50	-364,53	-1036,54	-17,96	-12,95
		updated	100,00	2,50	-362,53	-1032,45	-17,86	-12,94
	S275JR/ 355JR**	initial	100,00	2,50	-362,00	-915,43	-16,92	-12,42
		updated	100,00	2,50	-360,48	-915,64	-16,90	-12,45
	S355JR	initial	100,00	2,50	-347,59	-908,73	-16,47	-12,13
		updated	100,00	2,50	-346,18	-908,84	-16,33	-12,07

*Rail's material is S235JR and post's material is S275JR
**Rail's material is S275JR and post's material is S355JR

4.2.7 Modeling of optimal values and comparison with real crash tests

The optimum design variables (x_1, x_2) are modeled in the FE environment as full scale guardrail systems. The numerical values from the FE simulation of the systems and the optimum values from the RBF-based metamodels, are given in Table 4.24. The results of the working width (w) and exit angle (α) obtained from the FEAs remain within the limit/constraint values determined for the SBDO. This indicates that the optimum values agree well with the safety criteria described in EN1317.

Table 4.24 : Comparison of results obtained by RBF and FEA [49].

Design type	System type	Material	x_1 (mm)	x_2 (mm)	w^{TB11} (mm)	$w^{TB42/TB51}$ (mm)	α^{TB11} (°)	$\alpha^{TB42/TB51}$ (°)
RBF metamodeling optimum	H1W4	S235JR	105	2.8	576	1300	11.7	13.8
		S235JR/275JR*	103	2.8	551	1300	11.4	13.8
		S275JR	101	2.6	563	1300	11.1	13.6
		S275JR/355JR**	100	2.5	475	1061	10.1	13.1
		S355JR	100	2.5	436	1021	9.6	12.9
	H2W4	S235JR	100	2.5	397	1149	18.4	9.2
		S235JR/275JR*	100	2.5	382	1108	18.0	9.2
		S275JR	100	2.5	365	1037	18.0	12.9
		S275JR/355JR**	100	2.5	362	915	16.9	12.4
		S355JR	100	2.5	348	909	16.5	12.1
FEA of Optimal Variables	H1W4	S235JR	105	2.8	586	1293	11.5	13.6
		S235JR/275JR*	103	2.8	519	1231	11.2	13.6
		S275JR	101	2.6	564	1286	11.0	13.5
		S275JR/355JR**	100	2.5	495	1056	10.2	13.1
		S355JR	100	2.5	447	1014	9.8	13.0
	H2W4	S235JR	100	2.5	397	1149	18.0	9.1
		S235JR/275JR*	100	2.5	388	1106	17.8	9.0
		S275JR	100	2.5	372	1038	17.5	12.8
		S275JR/355JR**	100	2.5	362	915	17.0	12.5
		S355JR	100	2.5	351	909	16.7	12.2

*Rail's material is S235JR and post's material is S275JR
**Rail's material is S275JR and post's material is S355JR

In addition, as shown in Table 4.25, RBF metamodel based optimization results are compared with those obtained from the FEA study. For an engineering design model, it is important to balance the accuracy of model predictions with the computational complexity of the model used. Model prediction errors that lie within a specified range may be acceptable. Based on prior experience or practical design requirements, the designer may know what levels of errors are acceptable for a particular problem. Like many studies [45-48], 2% relative error might be desirable; 2–10% error is acceptable;

and higher than 10% error is unacceptable. It can be seen from the table that the mean value of RAE (%) between the metamodel predictions and the validated FEA simulation results are less than 0.95%, which demonstrates that the optimization result is accurate and can be accepted in engineering design. As explained above, the average $RMSE_{CV}$ and RAE values of RBFs fidelity are found as 2-3(%) and 1-2(%), respectively. As a result of this high accuracy rate obtained for the RBF models, the results of the optimization and the engineering design models (FEA) are consistent. All this supports that the optimum values obtained in this study are feasible.

Table 4.25 : RAE (%) of FEA of optimal variables and RBF metamodeling optimum [49].

System type	Material	x_1 (mm)	x_2 (mm)	RAE (%) w^{TB11} (mm)	$w^{TB42/TB51}$ (mm)	α^{TB11} (°)	$\alpha^{TB42/TB51}$ (°)	Average of all
H1W4	S235JR	105	2,8	1,64	0,54	1,64	1,76	1,39
	S235JR/275JR*	103	2,8	6,10	5,61	2,22	1,35	3,82
	S275JR	101	2,6	0,20	1,09	1,07	0,39	0,69
	S275JR/355JR**	100	2,5	4,10	0,52	0,93	0,25	1,45
	S355JR	100	2,5	2,42	0,67	1,78	0,90	1,44
H2W4	S235JR	100	2,5	0,02	0,00	2,47	1,24	0,93
	S235JR/275JR*	100	2,5	1,66	0,20	0,93	2,37	1,29
	S275JR	100	2,5	2,01	0,14	2,61	1,14	1,48
	S275JR/355JR**	100	2,5	0,00	0,05	0,47	0,68	0,30
	S355JR	100	2,5	0,97	0,03	1,38	0,56	0,73
							Mean of all RBFs	0,95

*Rail's material is S235JR and post's material is S275JR

**Rail's material is S275JR and post's material is S355JR

4.3 Case 3: ASI-Based Safety Enhanced of NJ Concrete Barrier

4.3.1 Validation of the FE model

Before being used in ASI-based barrier optimization, FE models were validated by comparing the full-scale crash test results belonging to KİPER Co. Ltd. [107-108]. In crash tests, 900 kg passenger cars and 38000 kg trucks were used for TB11 and TB81 tests, respectively. Table 4.26 shows the EN1317 test acceptance criteria, and Figure 4.37 shows the vehicles used in the tests. The geometrical details and the FE model of the NJ-type concrete barrier that optimized are shown in Figure 4.38.

Table 4.26 : EN1317 test acceptance criteria for H4b barrier.

System Type	Test	Impact speed (km/h)	Impact angle (°)	Total mass (kg)	Type of Vehicle
H4b	TB11	100	20	900	Car
	TB81	65	20	38000	Articulated HGV*

*Heavy Goods Vehicle

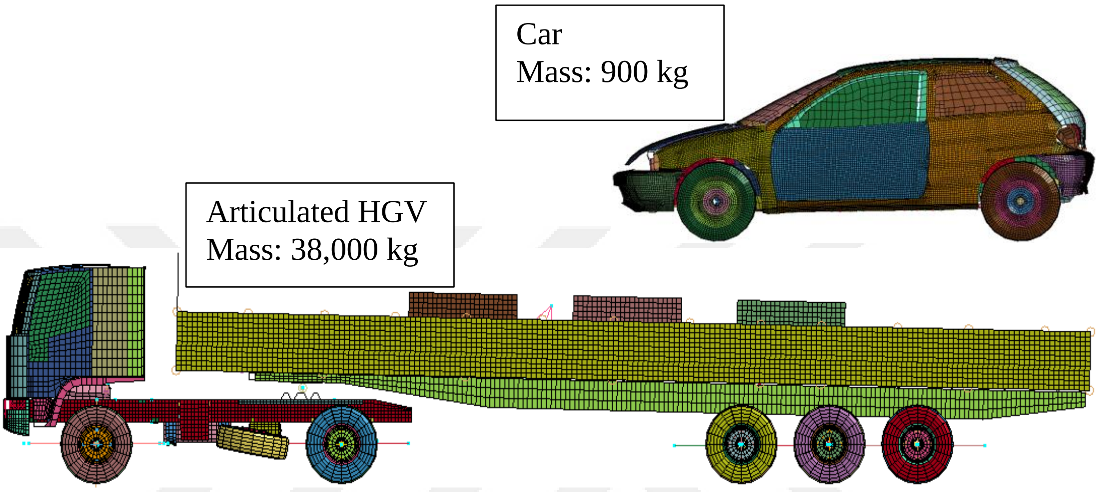

Figure 4.37 : The FE models of vehicles used in TB11 and TB81 tests (FEMA 2002).

In Table 4.27, EN1317 safety criteria to be used as an objective function in NJ-type concrete barrier optimization are given. The exit angle (EA) and the exit box are determined according to the EN1317 standard. The exit box dimensions and details are given in Figure 4.39 in light of the criteria given in the standard. The maximum safe exit angles (EA) were calculated as 19° for the passenger car and 22° for the truck. Since the angle of rotation (RollA) is directly related to the rollover of the vehicle, it is an important parameter in determining the barrier performance and the degree of safety. Although the larger values were taken, the maximum rotation angle was taken as 20° in order to remain on the safe side. The acceleration severity index (ASI) value is the index value taken from the KIPER real crash test result [107]. In light of these evaluation criteria, FE models were validated by comparison with the real crash tests.

Table 4.27 : EN1317 test evaluation criteria for H4b barrier.

System Type	Test	Exit box (width(A) x lenght(B)) (m)*	Exit angle (EA) (°)**	Roll angle (RollA) (°)	ASI
H4b	TB11	4.3x10	≤19	≤20	≤1.42(B)
	TB81	9.5x20	≤22	≤20	-

*Calculated based on EN1317/2
**Calculated based on exit box length

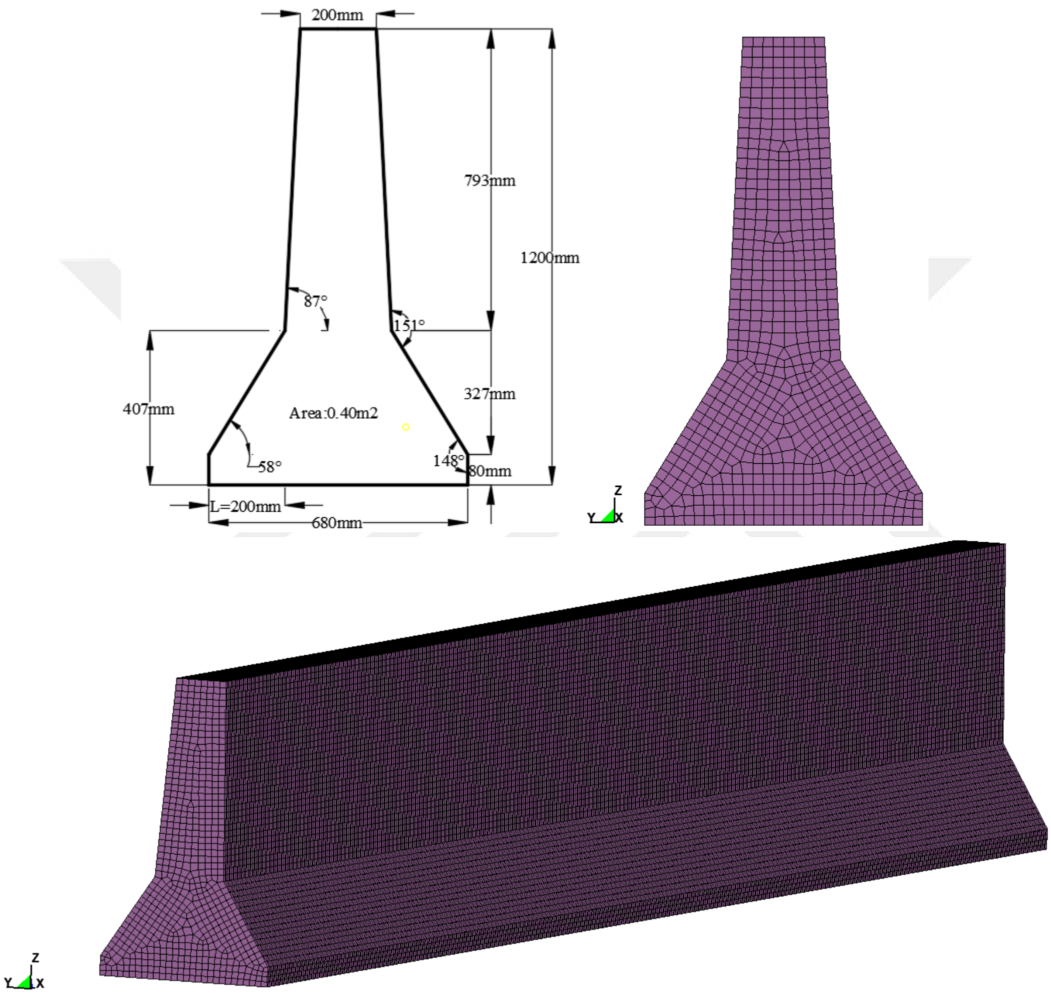

Figure 4.38 : The cross-sectional sizes of KİPER H4b concrete barrier and FE model of design.

Figures 4.40 and 4.41 show the comparison of real crash tests with the FEA results obtained by modeling the 900 and 38000 kg vehicles in the LS-DYNA [10] environment as TB11 and TB81 tests, respectively. Front views of vehicle responses are seen. From qualitative comparisons, it was observed that the FEA results produced similar and compatible vehicle responses with the actual crash test results. In Table 4.28, a quantitative comparison was fulfilled and the relative error margin was calculated as 0-5% among the quantitative values obtained. It can be seen from the margin of error that the FE simulation results are in good agreement with the test data. In addition, the ASI graph from KİPER TB11 test report [107] and that obtained from the FE model of the TB11 test are given in Figures 4.42 and 4.43, respectively. Compatible results can be read from the graphs. Based on these comparisons, the FE models were deemed suitable for assessing the safety-based optimization and performance of the NJ-type concrete barrier.

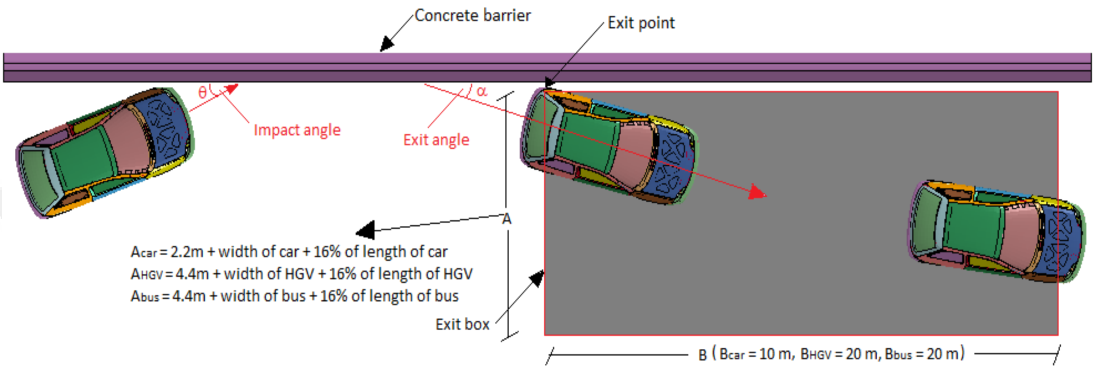

Figure 4.39 : Illustration of crash test details in EN1317 part 2.

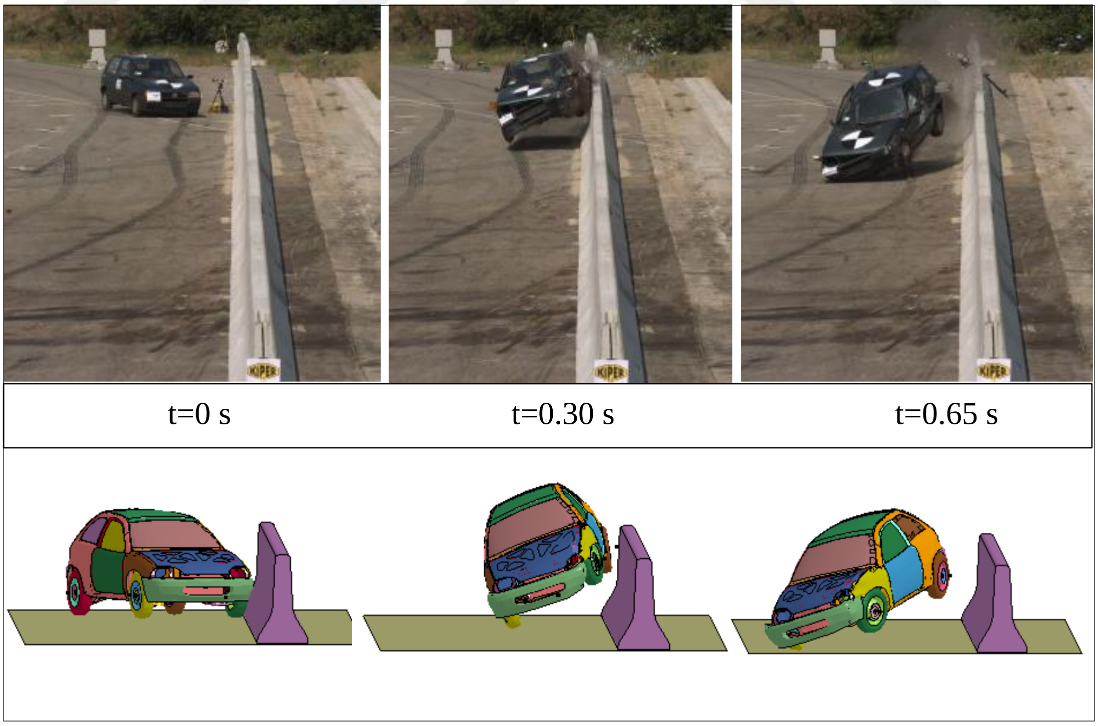

Figure 4.40 : Qualitative comparison for FE model and real TB11 crash test on Kiper Barrier [107].

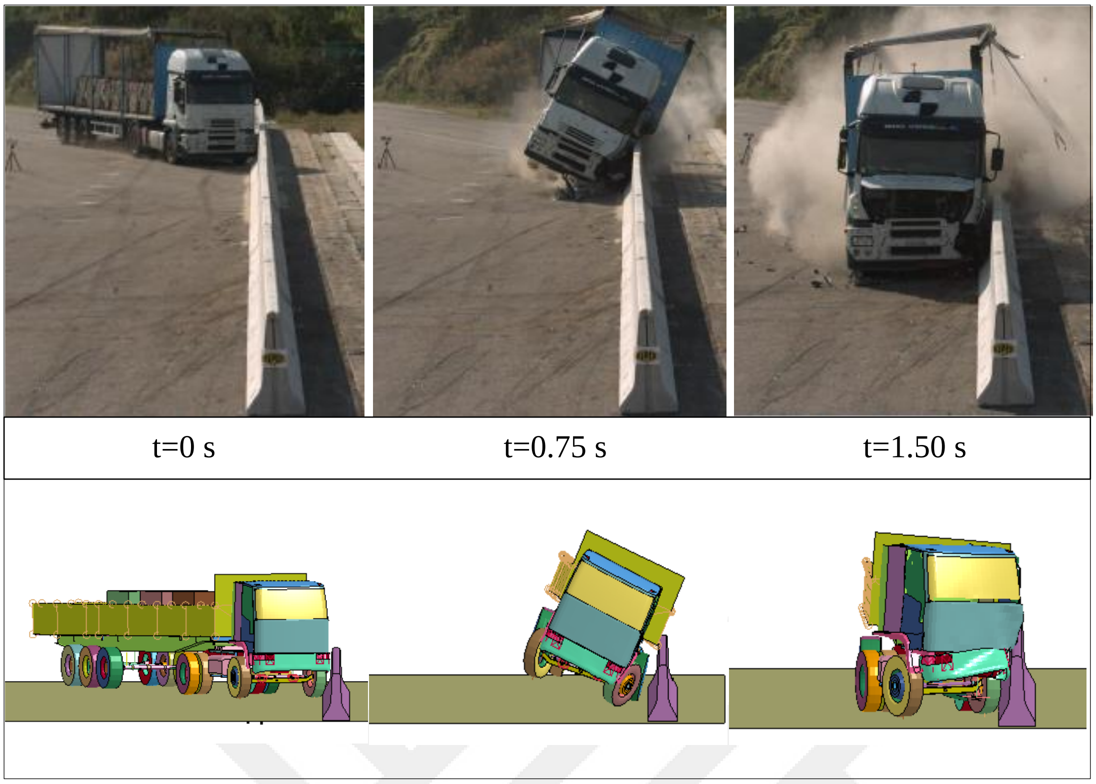

Figure 4.41 : Qualitative comparison for FE model and real TB81 crash test on Kiper Barrier [108].

Table 4.28 : Quantitative comparison between crash tests and FE analysis.

Evaluation Criteria	Real crash test		FE analysis		RAE (%)	RAE (%)
	TB11	TB81	TB11	TB81	of TB11	of TB81
EA	12.5	0.0	12.0	0.0	4.0	0.0
RollA	10.0	39.0	10.5	38.0	5.0	2.6
ASI	1.42	-	1.39	-	2.1	-

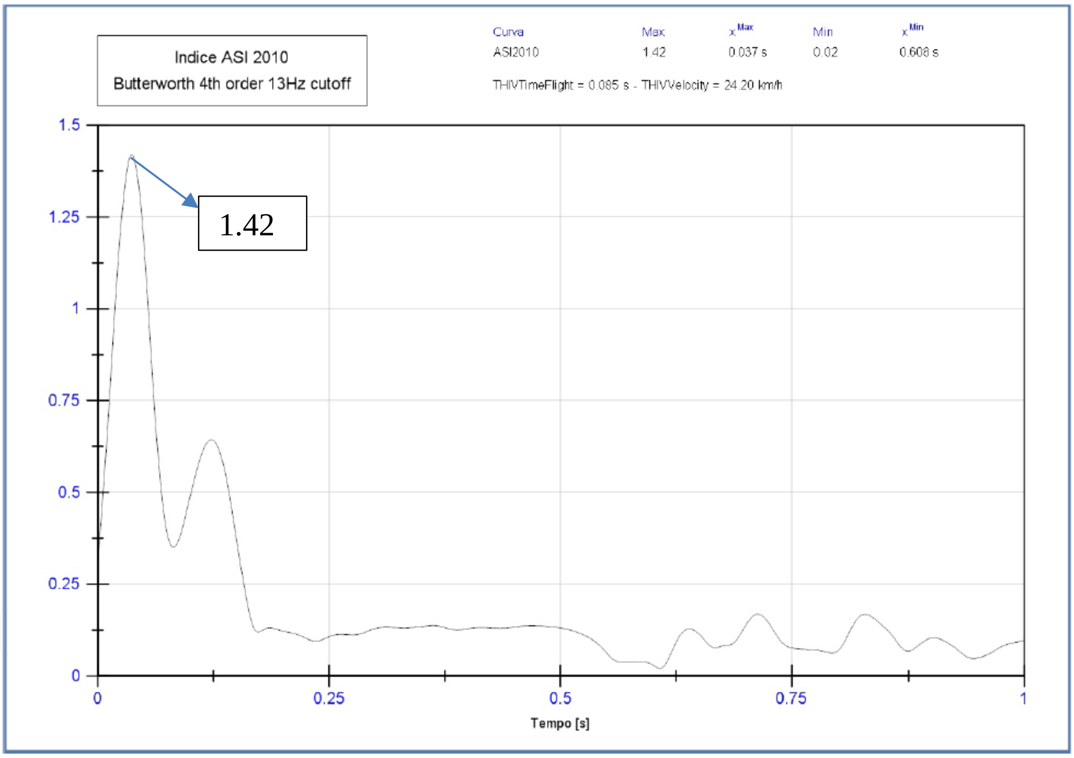

Figure 4.42 : ASI graph from TB11 test report [107].

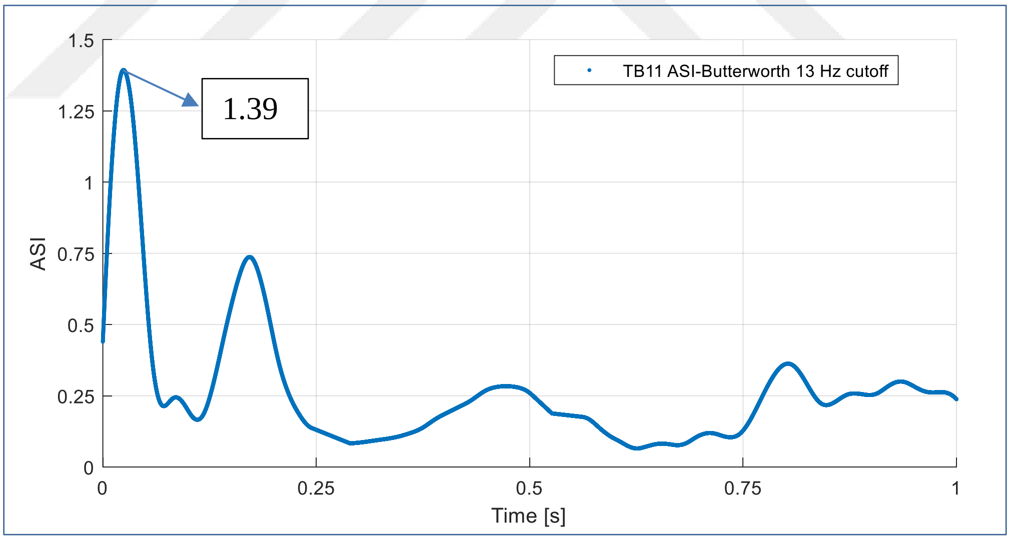

Figure 4.43 : ASI graph from FEA of TB11.

4.3.2 Critical design point of NJ Concrete barrier

As known, guardrails are named according to the degree of safety and performance levels. As passive safety elements that ensure road safety, guardrails are required to ensure maximum safety for the driver. But this is not possible as the systems become rigid. The safety level of the concrete barrier, as a rigid system, is particularly low. For the NJ-type barrier, it is aimed to investigate the critical design parameters that affect the safety degree and to achieve high-security degree barrier optimization with the help of these parameters. The NJ-type concrete barrier that was optimized is given in Figure 4.44. As can be seen, the points to be used for design are indicated on the figure. These points are the rounding of the corner points on the barrier, x1 edge, x2 angle, x3 angle, and x4 barrier surface friction coefficient. Depending on the ASI values, the effect margins of the points on the risk of injury and the design were investigated. The aim of investigating these points is to determine which parameters are effective on ASI and the critical points for the NJ-type concrete barrier design.

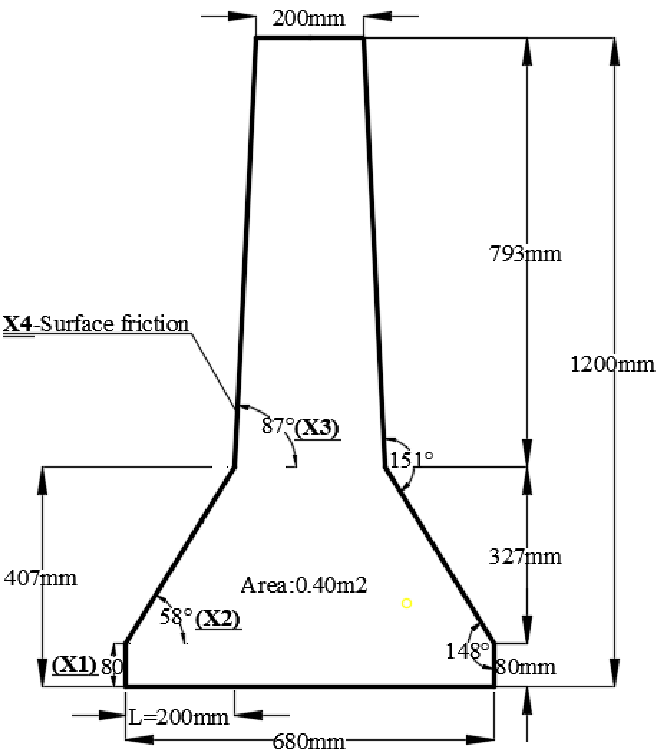

Figure 4.44 : The critical design point on NJ safety-shape barrier.

The standard cross-sectional dimensions of the NJ-type concrete barrier of KIPER Co. Ltd. is shown in Figure 4.44. Based on the standard dimensions of the critical points specified as the variable in the optimization, the limit values of the points are determined. The determined limit values are taken from the combination and limit values where the barrier will not lose its NJ shape and function. These values are set as 0-10 cm for x1, 55-65° for x2, 80-90° for x3 and 0-1.0 for x4. The results obtained from the FEA of these constraint values are given in Table 4.29. When results in the table are observed, it can be seen that x4-friction factor is the most effective factor to consider in design in terms of the effective value of 39.21% on the ASI value, and the factors of corner rounding factor and x3 are the least effective factors with 0.84% effect values. It is understood that among the x1, x2 and x3 factors affecting the geometric design, the x1, and x2 factors are the most effective regions that affect the NJ type concrete barrier shape design in terms of the total impact values of about 25%. These regions are the regions wherein Figure 4.44 the sum of the standard measures of the two factors is given as 407 mm. Although ASI-based optimization, to reduce injury level, is intended in this study, the exit angle-EA and roll angle-RollA are two important parameters in the sense of safety. These two parameter values are given in the table. With the exception of the x4 factor’s 1.00 limit value, the exit angle-EA for all of the other factors appears to remain on the safe side of the constraint value specified for the test evaluation criteria given in Table 4.27. The most significant factor affecting the exit angle-EA is the x4 factor, which indicates the surface friction coefficient between the vehicle and the barrier. However, the exit angle-EA was not affected much by changing the lower and upper limit values of the x1, x2 and x3 shape factors. When the factors regarding the roll angle-RollA safety were examined, it was determined that the high angle of the x2 factor, the low angle of the x3 factor and the high friction value in the x4 factor caused a rollover. The most stable RollA value was obtained with a low angle of the x2 factor.

Based on all of the above-mentioned criteria and determinations, an NJ-type concrete barrier optimization, which gives the minimum ASI value and provides EA and RollA safety criteria, is aimed in our study.

Table 4.29 : Critical design points of NJ concrete barriers and impact factor on ASI.

Variables/Factors	Limit values				Impact factor (%)
Corners	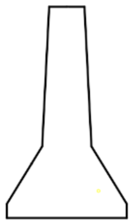	sharp ASI(t) 1.39 EA 12 RollA 10.5	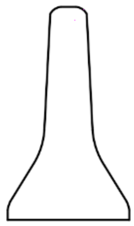	round ASI(t) 1.38 EA 12 RollA 18	0.84
X1	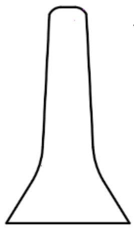	0 cm ASI(t) 1.74 EA 4 RollA 14	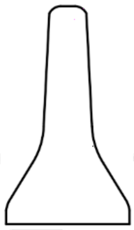	10 cm ASI(t) 1.56 EA 2 RollA 26	11.66
X2	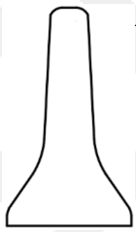	55° ASI(t) 1.70 EA 2 RollA 0	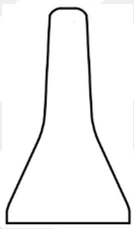	65° ASI(t) 1.50 EA 1 RollA RO*	13.19
X3	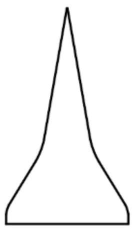	80° ASI(t) 1.57 EA 0 RollA RO*	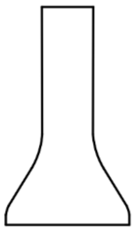	90° ASI(t) 1.58 EA 4 RollA 25	0.84
X4	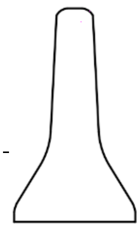	fs=0 ASI(t) 1.38 EA 12 RollA 18	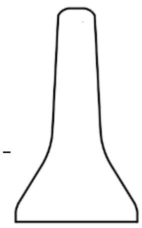	fs=1.0 ASI(t) 1.92 EA 90 RollA RO*	39.21

*Rollover

4.3.3 Input variables and objective functions of MOO

For the optimization of the study, the critical design points in the NJ type concrete barrier design given above are variables and criteria such as ASI, EA and RollA specified in EN1317 are used as objective functions. The limit values of these variables and objective functions are given in Table 4.30. These values are taken as limit values given for x1, x2, and x3 in section 3.2. However, the higher the friction coefficient-x4, the higher the ASI value and the higher the probability of rollover. The smaller the value, the higher the security. Therefore, the x4 factor is not taken into account in the optimization.

Table 4.30 : Constraints for variables and objective functions.

Variables and objective functions	Constraints
x1 (cm)	0-10
x2 (°)	55-65
x3 (°)	80-90
ASI	≤1.42
EA (°)	≤19
RollA (°)	≤20

In this study, the Latin Hypercube Design (LHD) method was employed to generate the initial 11 design points using the design variables given in Table 4.30. The MATLAB `lhsdesign` command was used for this purpose. Derived sampling values and barriers designed with these values are shown in Table 4.31. With modeling the barrier designs in open-coded FE environment, the ASI, EA and RollA objective and constraint functions values corresponding to the samples were obtained and given in the table.

Table 4.31 : Design samples and the FE simulation results of design variables.

Sample no	Variables		Design	Objective functions	
1	x1	5	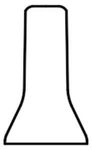	ASI(t)	1.38
	x2	65		EA	9
	x3	89		RollA	8
2	x1	4	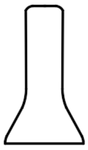	ASI(t)	1.41
	x2	61		EA	4
	x3	90		RollA	4
3	x1	6	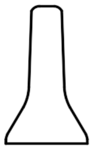	ASI(t)	1.45
	x2	60		EA	3
	x3	88		RollA	5
4	x1	3	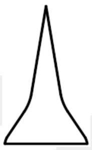	ASI(t)	1.35
	x2	57		EA	8
	x3	81		RollA	28
5	x1	0	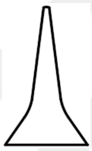	ASI(t)	1.43
	x2	56		EA	5
	x3	83		RollA	11
6	x1	7	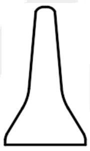	ASI(t)	1.35
	x2	59		EA	4
	x3	85		RollA	13
7	x1	10	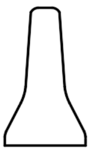	ASI(t)	1.36
	x2	63		EA	9
	x3	86		RollA	19
8	x1	2	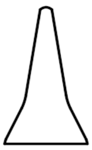	ASI(t)	1.38
	x2	64		EA	4
	x3	81		RollA	8
9	x1	9	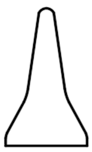	ASI(t)	1.27
	x2	62		EA	2
	x3	82		RollA	13
10	x1	1	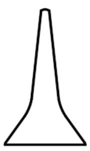	ASI(t)	1.49
	x2	55		EA	5
	x3	84		RollA	6
11*	x1	8	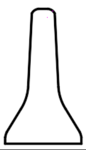	ASI(t)	1.53
	x2	58		EA	3
	x3	87		RollA	35

*Standard dimension

4.3.4 OWPE of RBF-based metamodels construction

RBF surrogate models were constructed by following the path described in Section 3.1 and Section 3.1.1 with the help of variables and objective functions given in Table 4.31. The optimum value of the *c* shape parameter for all functions to be used in the RBF surrogate model was investigated. As shown in Figure 4.45, RMSE values of RBF models were measured by taking *c* parameter values between 0-1. The lowest error value gives the optimum *c* parameter. The error values here are the error rates between the original model and the metamodel. The optimum *c* values are shown in the figure. The important point here is that although the variable and objective functions are the same, the optimum values of *c* are different for all models. In addition, the RMSE error estimation with the lowest value was performed with RBF-LNR for all *c* shape values.

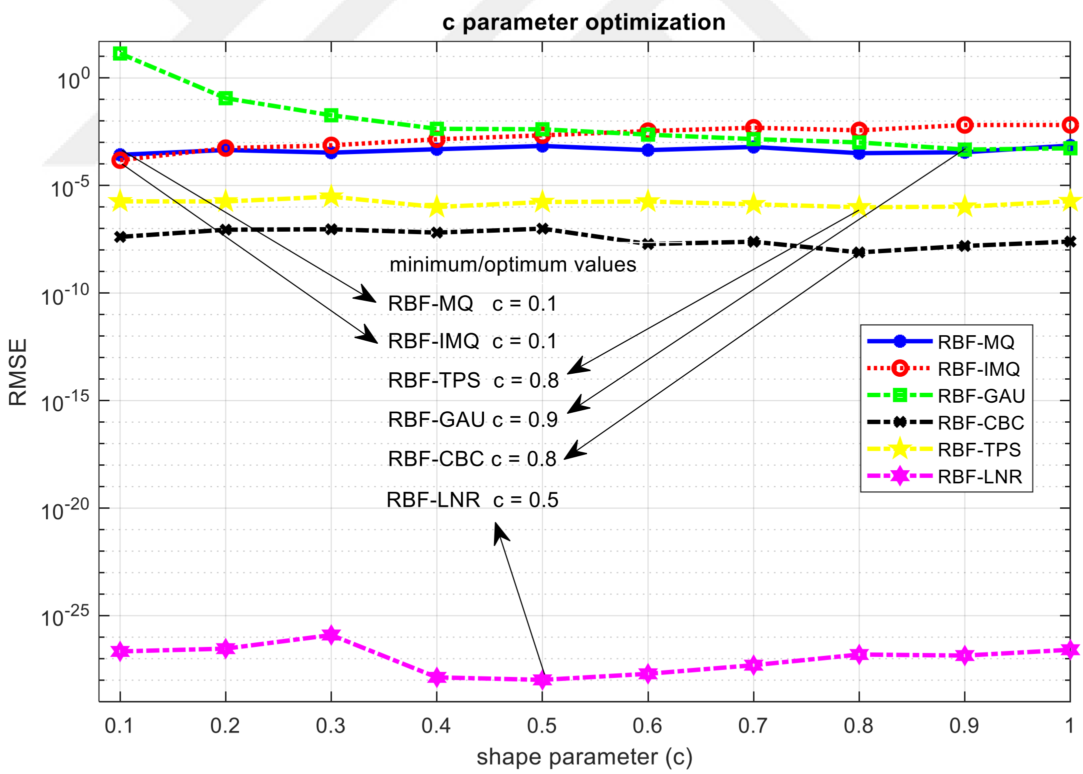

Figure 4.45 : The impact of shape parameter *c* on the behavior and fidelity of the RBF-basis functions.

The accuracy of the metamodels established with the optimum *c* parameters was measured by the GMSE method based on the "*one-out cross-validation*" method. The global error of metamodels was evaluated as a construct metamodel 11 times, each time leaving out one of the training points. Then, the difference between the exact response at the omitted point and that predicted by each variant metamodel was used. The GSME values calculated for each point of the objective functions are given in Figures 4.46-4.48 below. By determining the lowest error points marked in the figures, weight matrices of the sample points in objective functions were obtained as in Equation (4.5). The $W_{ij} = 1$ indicates that the jth RBF model provides more accurate predictions around the ith sample point. The ensemble of RBF models generated by the determined weight matrices and the optimum values of the c are shown in Table 4.32. As can be seen from the table, the OWPE-RBF models for ASI, EA, and RollA objective functions include each of the 6 basis functions. As it is understood from this, each function with different c parameters can be superior in different regions of the design space. In this sense, for multi-objective optimization, preferring ensemble models against individual models provides a higher accuracy estimation.

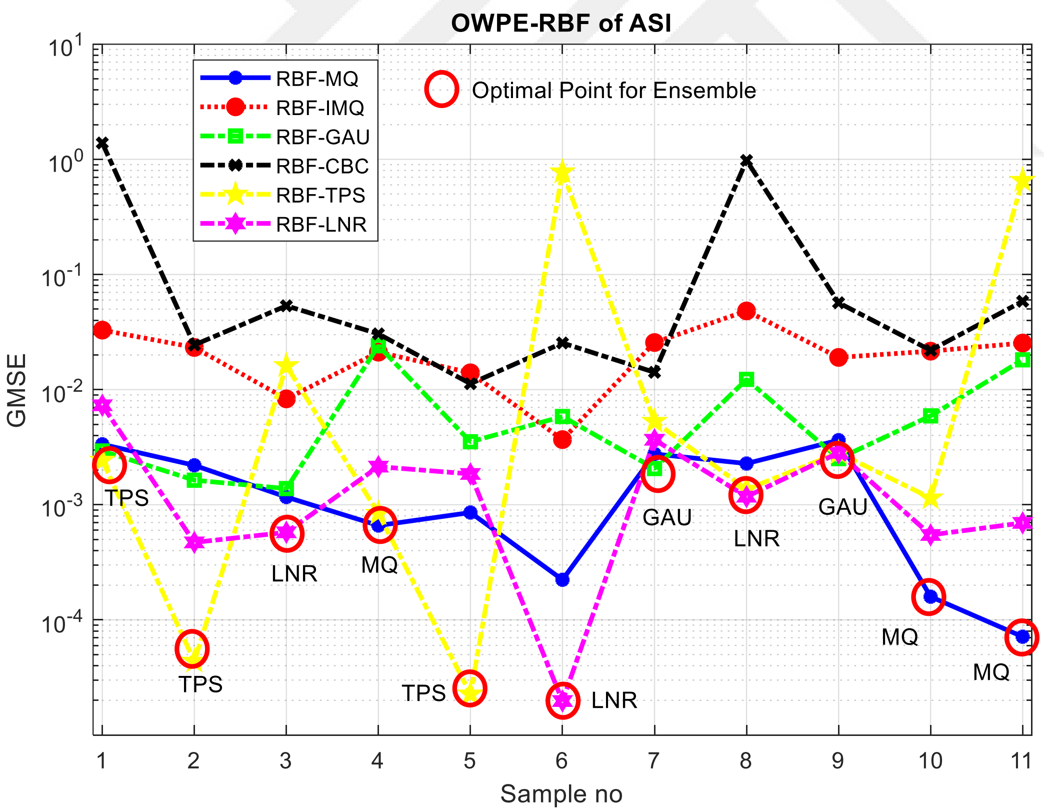

Figure 4.46 : The optimal GMSE point for OWPE-RBF of ASI.

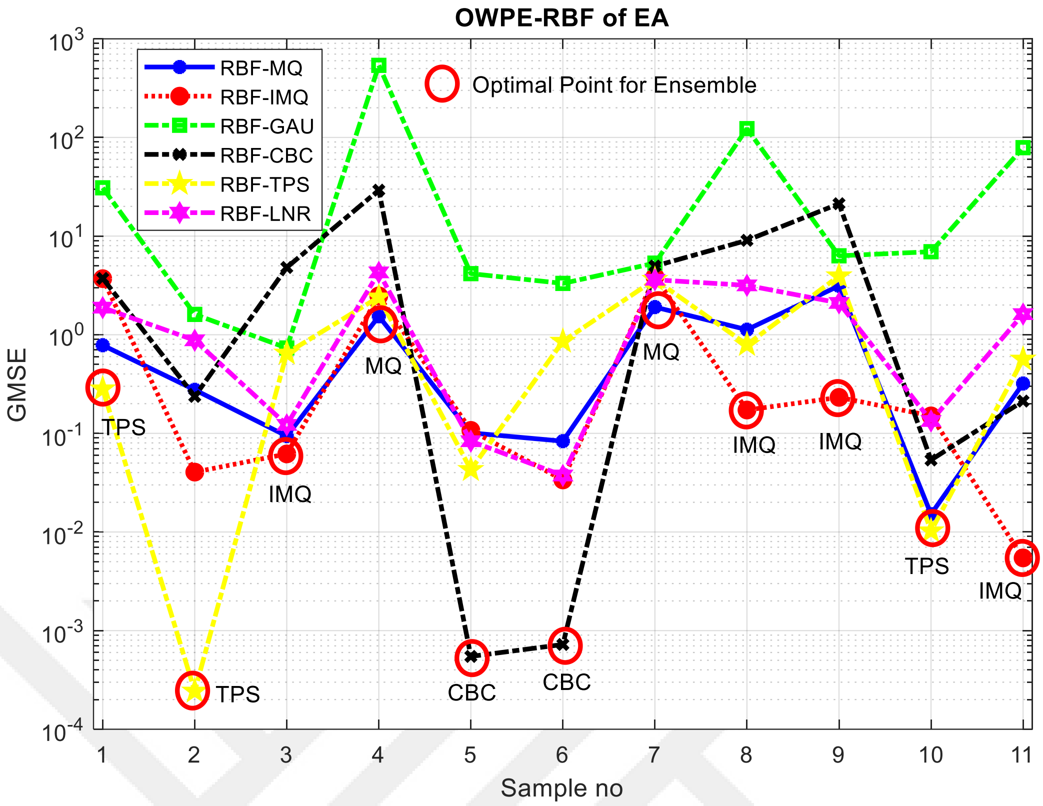

Figure 4.47 : The optimal GMSE point for OWPE-RBF of EA.

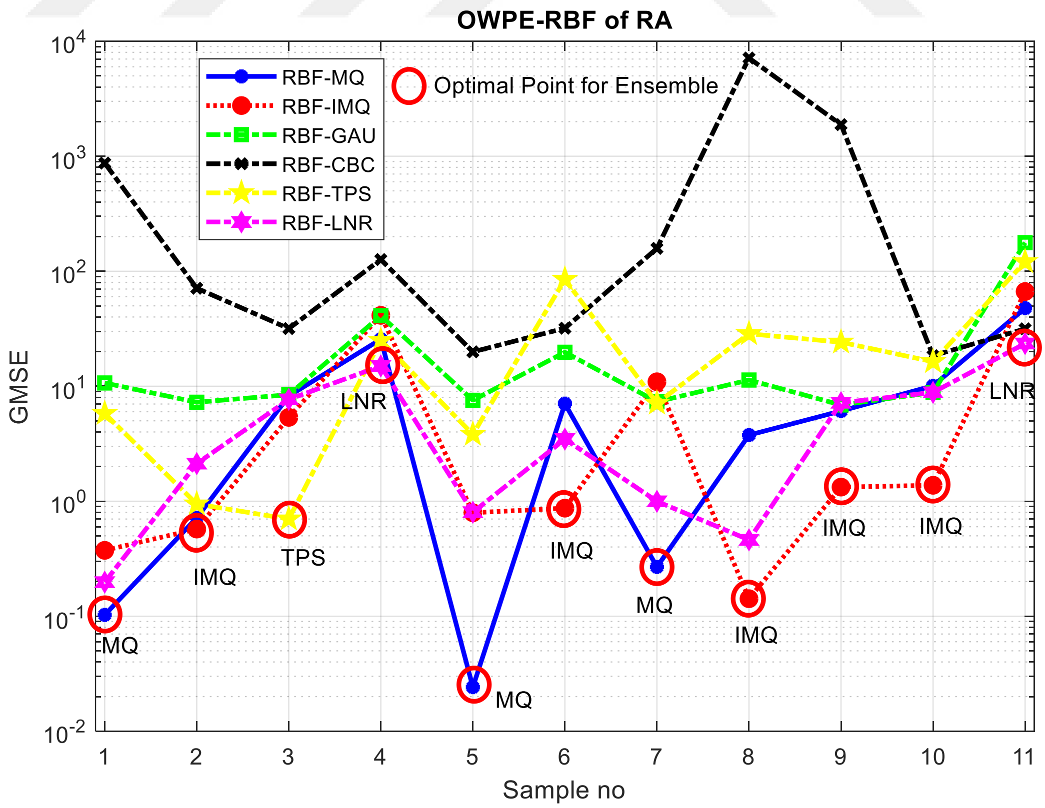

Figure 4.48 : The optimal GMSE point for OWPE-RBF of RollA.

$$W_{ASI,EA,RollA} = [W_{MQ} W_{IMQ} W_{GAU} W_{CBC} W_{TPS} W_{LNR}] = \begin{bmatrix} 0&0&0&0&\mathbf{1}&0 \\ 0&0&0&0&\mathbf{1}&0 \\ 0&0&0&0&0&\mathbf{1} \\ \mathbf{1}&0&0&0&0&0 \\ 0&0&0&0&\mathbf{1}&0 \\ 0&0&0&0&0&\mathbf{1} \\ 0&0&\mathbf{1}&0&0&0 \\ 0&0&0&0&0&\mathbf{1} \\ 0&0&\mathbf{1}&0&0&0 \\ \mathbf{1}&0&0&0&0&0 \\ \mathbf{1}&0&0&0&0&0 \end{bmatrix} = \begin{bmatrix} 0&0&0&0&\mathbf{1}&0 \\ 0&0&0&0&\mathbf{1}&0 \\ 0&\mathbf{1}&0&0&0&0 \\ \mathbf{1}&0&0&0&0&0 \\ 0&0&0&\mathbf{1}&0&0 \\ 0&0&0&\mathbf{1}&0&0 \\ \mathbf{1}&0&0&0&0&0 \\ 0&\mathbf{1}&0&0&0&0 \\ 0&\mathbf{1}&0&0&0&0 \\ 0&0&0&0&\mathbf{1}&0 \\ 0&\mathbf{1}&0&0&0&0 \end{bmatrix} = \begin{bmatrix} \mathbf{1}&0&0&0&0&0 \\ 0&\mathbf{1}&0&0&0&0 \\ 0&0&0&0&\mathbf{1}&0 \\ 0&0&0&0&0&\mathbf{1} \\ \mathbf{1}&0&0&0&0&0 \\ 0&\mathbf{1}&0&0&0&0 \\ \mathbf{1}&0&0&0&0&0 \\ 0&\mathbf{1}&0&0&0&0 \\ 0&\mathbf{1}&0&0&0&0 \\ 0&\mathbf{1}&0&0&0&0 \\ 0&0&0&0&0&\mathbf{1} \end{bmatrix} \tag{4.5}$$

Table 4.32 : Optimal c parameter and basic functions of each point within objective functions for constructing OWPE-RBF.

Sample no	ASI	EA (°)	RollA (°)
1	TPS/c=0.8	TPS/c=0.8	MQ/c=0.1
2	TPS/c=0.8	TPS/c=0.8	IMQ/c=0.1
3	LNR/c=0.5	IMQ/c=0.1	TPS/c=0.8
4	MQ/c=0.1	MQ/c=0.1	LNR/c=0.5
5	TPS/c=0.8	CBC/c=0.8	MQ/c=0.1
6	LNR/c=0.5	CBC/c=0.8	IMQ/c=0.1
7	GAU/c=0.9	MQ/c=0.1	MQ/c=0.1
8	LNR/c=0.5	IMQ/c=0.1	IMQ/c=0.1
9	GAU/c=0.9	IMQ/c=0.1	IMQ/c=0.1
10	MQ/c=0.1	TPS/c=0.8	IMQ/c=0.1
11	MQ/c=0.1	IMQ/c=0.1	LNR/c=0.5

4.3.5 Validation and comparison of individual metamodel and OWPE of the metamodel

Before using the OWPE-RBF metamodel in optimization, the fidelity of surrogate models for NJ type concrete barriers was evaluated by the root mean square k-fold cross-validation error metric, $RMSE_{CV}$. When using existing data by k-fold cross-validation, the prediction accuracy of the metamodel is determined without requiring additional (likely computationally expensive) simulations or analyses. In this approach, we take advantage of the data used to fit the metamodel for validation purposes. In terms of practicality, the k-fold cross-validation strategy provides a reasonable indicator of metamodel fidelity without the use of additional computationally expensive analyses.

To calculate the $RMSE_{CV}$, first, the surrogate model samples were divided five-fold (where 5 is the number of training points), while leaving out one of the training points as the validation data each time. Then, an error value was obtained using Equation (3.11). Prediction errors of objective functions within the RBF metamodels are given in Figure 4.49. As illustrated in the figure, the $RMSE_{CV}$ values of all objective functions within the metamodels are different from each other. Each objective function in an engineering problem defines different behavior of the engineering model. Thus, these behaviors become different. This can be seen from the surface plot of the objective functions in Figure 4.50. Since the objective functions of the metamodel mimic engineering behaviors, each of the 3 objective functions used in this study within the metamodel are expected to have different accuracy.

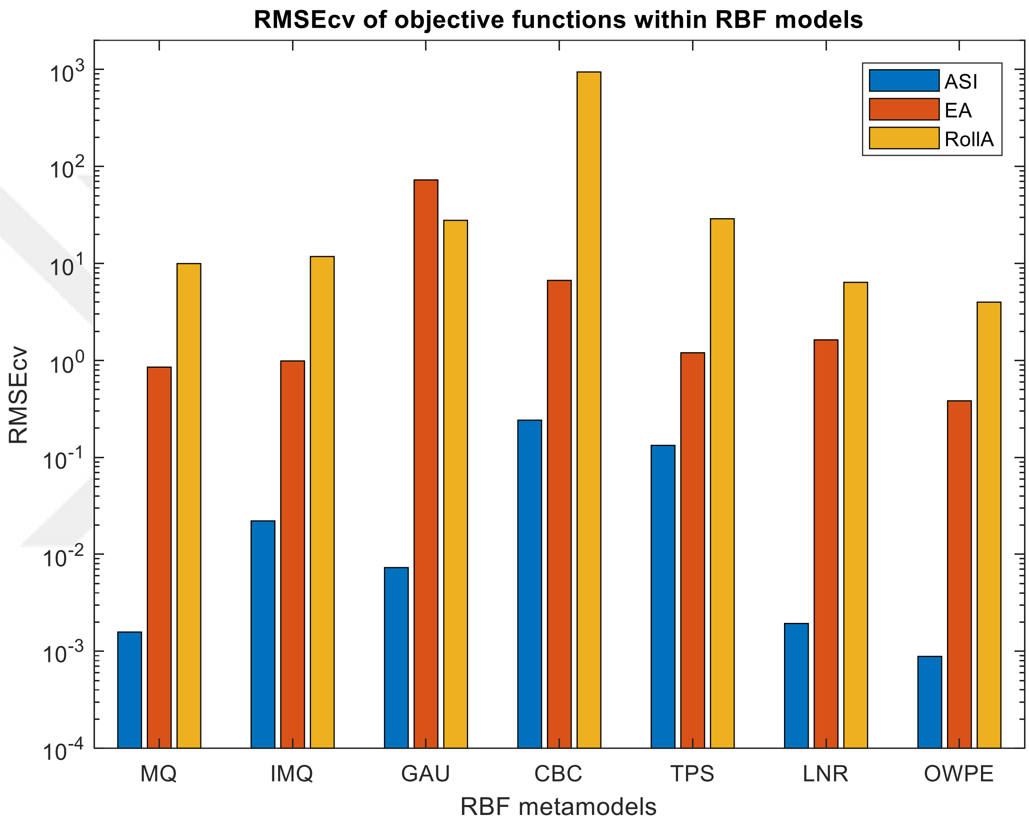

Figure 4.49 : The RMSEcv of objective functions within RBF metamodels.

The $RMSE_{CV}$ values of the objective functions of the RBF models are given in Figure 4.51 as the average $RMSE_{CV}$ of the whole model. As it is understood from here, the error rate is the lowest model, in other words, the prediction accuracy rate is the highest model is the OWPE-RBF metamodel. The OWPE model is followed by LNR, MQ, IMQ, TPS, GAU and CBC models, respectively. It is understood that ensemble RBF metamodels are more accurate than individual metamodels. In particular, the average $RMSE_{CV}$ of the OWPE metamodel can be seen between 0-1.5. An $RMSE_{CV}$ value of 0 indicates a perfect fit. We can say that the $RMSE_{CV}$ trained RBFs result in an almost perfect fit to the engineering design model. As a result of this high accuracy rate obtained for the OWPE of RBF model, the results of the optimization and the engineering design model (FEA) are consistent. All of this provides support that the optimum values obtained in this study are feasible.

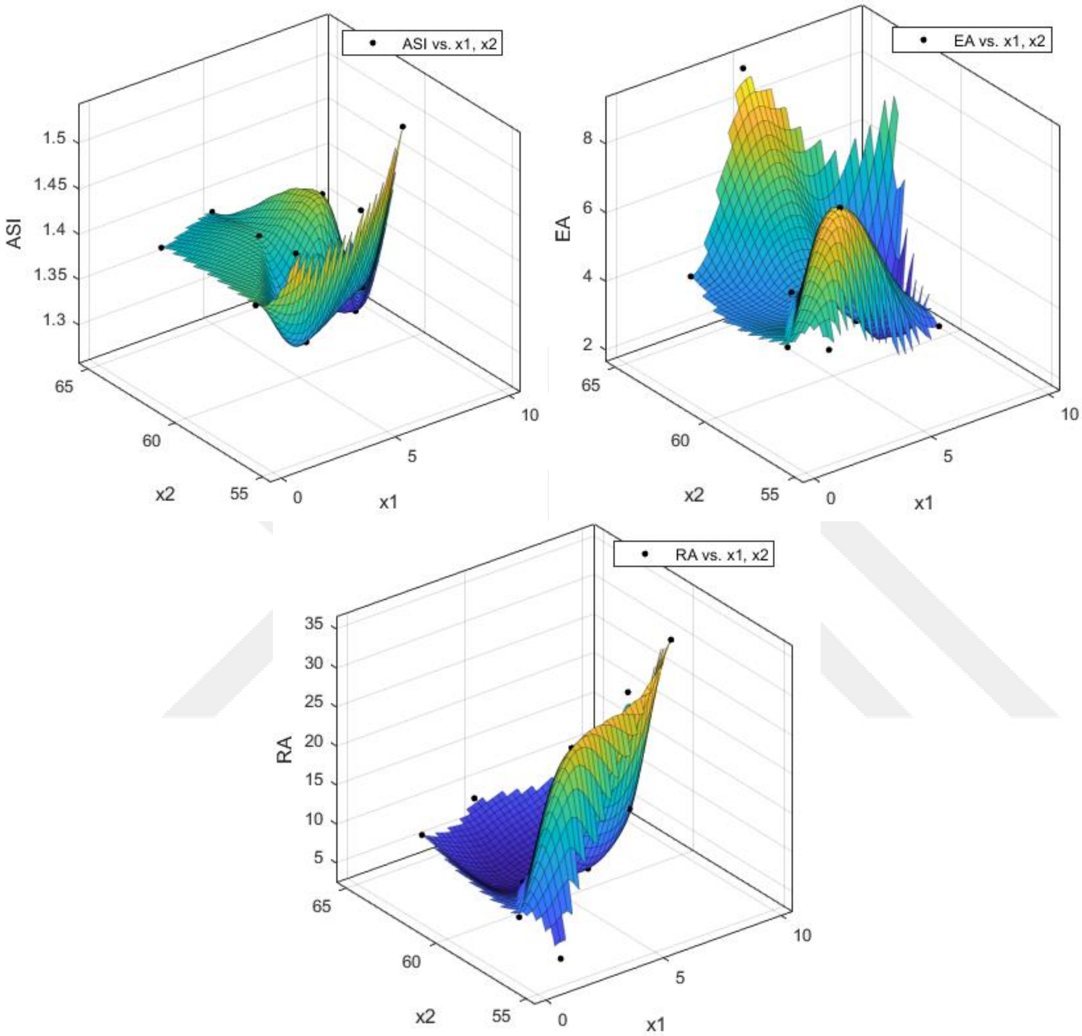

Figure 4.50 : Surface plot of RBF objective functions.

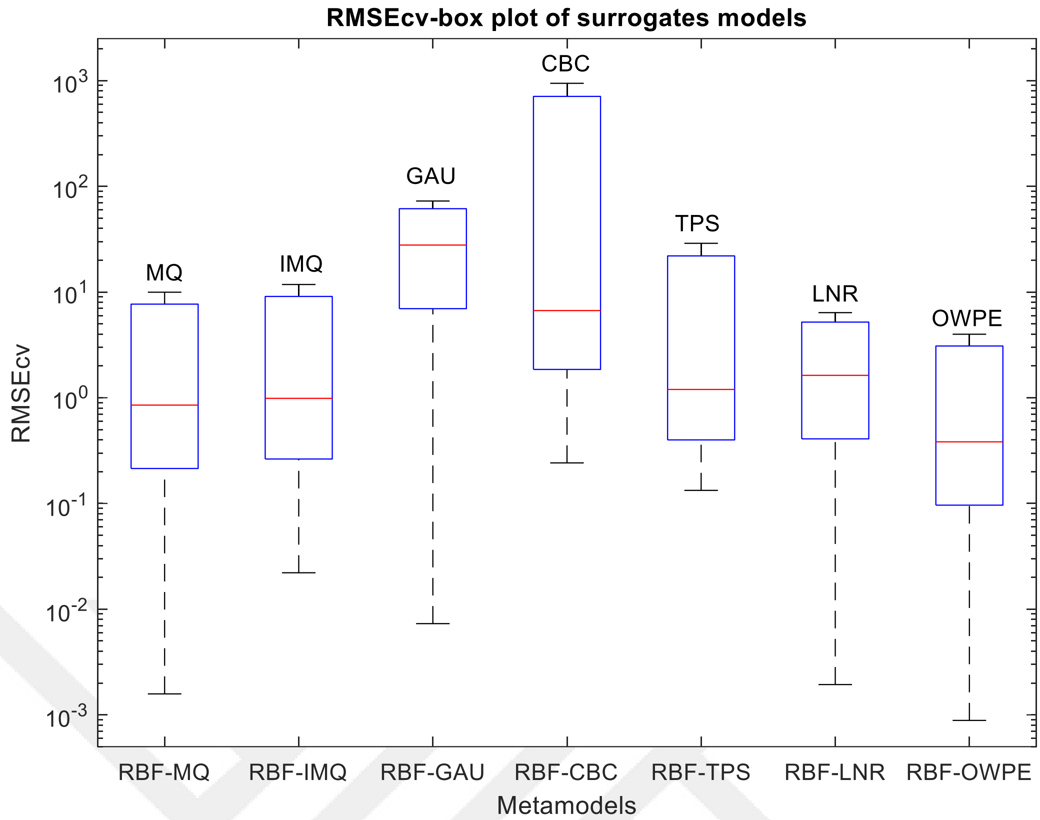

Figure 4.51 : The RMSEcv of RBF metamodels.

4.3.6 The MOO formulation and solution

By using the optimization methodology given in Equation (3.12), the problem of optimizing NJ type concrete barriers to reduce injury levels depending on ASI is formulated as follows:

$$\begin{cases} \text{Min. } [\text{ASI}, \text{EA}, \text{RollA}(x1, x2, x3)] \\ \text{s.t.} \qquad 0 \leq x1 \leq 10 \text{ cm} \\ \qquad 55° \leq x2 \leq 65° \\ \qquad 80° \leq x3 \leq 90° \\ \qquad \text{EA}(x1, x2, x3) \leq 19° \\ \qquad \text{RollA}(x1, x2, x3) \leq 20° \end{cases} \tag{4.6}$$

where ASI, EA, and RollA are objective functions. The ASI is acceleration severity index that defines injury level, EA is exit angle and RollA is the rolling angle that they define safety criteria. As variables of optimization, x1, x2, and x3, which are defined in Section 4.3.2, are the parameters related to the geometric design of the NJ barrier.

The optimization problem was solved with MATLAB code, using the gamultiobj command which is a variant of NSGA-II [103]. The NSGA-II is a well-known, fast sorting and elite multi-objective genetic algorithm. The NSGA-II, in most problems, is able to find a much better spread of solutions and better convergence near the true Pareto-optimal front compared to other elitist MOEAs that pay special attention to creating a diverse Pareto-optimal front [103]. In the NSGA-II, as the search progresses from generation to generation, unusual designs are approaching the real Pareto cluster of the problem. As a result, designs close to Pareto can be produced with NSGA-II without the need for scaling weights to combine different criteria into a single target [103-104, 109]. The NSGA-II was shown to be an effective method [103-104] and was employed in this study to solve the MOO problem given in Equation (4.6).

During the solution of MOO, to investigate the effect of a number of iterations (or generations) on the accuracy of optimization results and convergence, the solutions are obtained at five different iterations, as shown in Figure 4.52. It can be seen from the figure that there is no significant difference among the solutions when the number of iterations is more than 100. Thus, in this study, the maximum number of iterations is set to 200 and used as the convergence criterion for solving the MOO problem.

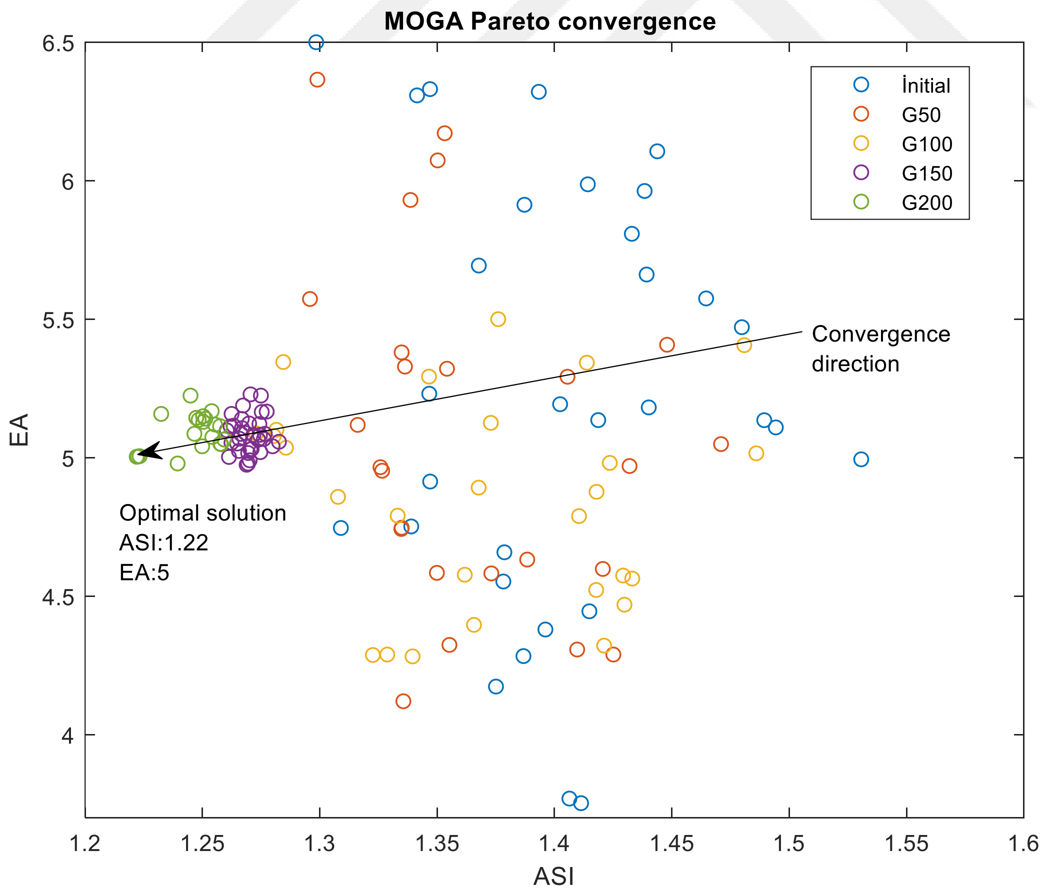

Figure 4.52 : MOGA (NSGA-II) Pareto convergence of NJ barrier optimization.

5. RESULTS AND DISCUSSION

In this thesis, metamodel methods have been successfully applied to road restraint systems and the successful results and discussion that emphasize the research objectives and hypotheses are given below.

5.1 Case 1: Soil Density Depended Optimization of Embedment Depth of C, H and S Post Type

Surrogate models of DC, MC, LC, DH, MH, LH, DS, MS, LS combinations for different posts (C, H, S) and soil types (D, M, L) were created using data obtained from the FE modelling of pendulum impact tests performed on guardrail posts. After validating the accuracy of the surrogate models, optimum PEDs were determined. Acceptability of the optimum PEDs were determined by comparing full scale crash test results of TB11, TB42, TB51 tests as specified in the EN1317 standard. Coherent results support the conclusion that the optimal PEDs determined in this study have the potential to be used in longitudinal barrier designs with confidence. Table 5.1 shows that RBF-based optimization reduce the embedment depth of C post from 950 to 780, 828 and 877 mm in dense, medium and loose soil, respectively. Similarly, embedment depth of S post reduced from 1200 to 759, 915 and 1071 mm in dense, medium and loose soil, respectively. And also embedment depth of H post reduced from 1230 to 700 mm in dense, medium and loose soil. In Turkey, post embedment depth is not allowed below 700 mm, hence 700 mm embedment depth was taken as the lower limit in optimization. Therefore, H post provides a lower limit of embedment depth for all soil types because of it is very strong post.

Table 5.1 : Recommended optimum PEDs vs. standard PEDs in H1 and H2 level longitudinal barriers [50].

Type of Post	Optimum depth/In practice depth		
	Dense Soil	Medium Soil	Loose Soil
H	700 mm/1230 mm	700 mm/1230 mm	700 mm/1230 mm
C	780 mm/950 mm	828 mm/950 mm	877 mm/950 mm
S	759 mm/1200 mm	915 mm/1200 mm	1071 mm/1200 mm

Full scale crash test simulations clearly demonstrate that optimum PEDs for longitudinal barriers incorporating C, H, and S posts will vary depending on soil properties. The economic advantages of using optimum PEDs in H1 and H2 barriers are given in Table 5.2. In Table 5.2, savings/%reduction are expressed as the ratio of difference between the in practice PED and the optimum PED over in practice PED. The table shows that range of savings/%reduction is between 17.89-43.09%, 12.84-43.09% and 7.68-43.09% for dense, medium and loose soil, respectively. This table is of importance since it shows the potential for significant savings when thousands of kilometres of guardrails are considered, even in a small decrease in the height and, accordingly in weight of the guardrails. Note that serious economic savings are possible, particularly for H type posts and dense soil condition.

Table 5.2 : Economic savings (% reduction) according to optimum PEDs [50].

Type of Post	Dense Soil	Medium Soil	Loose Soil
C	17.89%	12.84%	7.68%
S	36.75%	23.75%	10.75%
H	43.09%	43.09%	43.09%

5.2 Case 2: S235JR, S275JR and S355JR Material-Based Cross-sectional Optimization of H1W4 and H2W4 Performance Level Guardrails

Table 5.3 presents the optimum design variables (x_1, x_2) and their values in practice. When the table is examined, it is clear that the optimum values recommended within the scope of the study are considerably lower than the in-practice values. This finding suggests that the standard dimensions of guardrail systems remain on the safe side. In the table percentages concerning cost savings that can be achieved with optimum values are also given. There seems to be significant savings for different material selections of both guardrail systems. The percentages are calculated as the ratio of difference between the original values and the optimal values over the original value. The percentages in the table are of importance since they show the potential for larger savings when thousands of kilometers of guardrails are considered, even in a small decrease in the size and, accordingly in weight, of the guardrail components.

Table 5.3 : Comparison of optimal and original variables and cost saving [49].

System type	Material	Optimum/Original		Cost saving		
		x_1 (mm)	x_2 (mm)	x_1 (%)	x_2 (%)	Σ
H1W4	S235JR	105/120	2.8/3.0	12.50%	6.67%	19.17%
	S235JR/275JR*	103/120	2.8/3.0	14.17%	6.67%	20.83%
	S275JR	101/120	2.6/3.0	15.83%	13.33%	29.17%
	S275JR/355JR**	100/120	2.5/3.0	16.67%	16.67%	33.33%
	S355JR	100/120	2.5/2.5	16.67%	0.00%	16.67%
H2W4	S235JR	100/120	2.5/3.0	16.67%	16.67%	33.33%
	S235JR/275JR*	100/120	2.5/3.0	16.67%	16.67%	33.33%
	S275JR	100/120	2.5/3.0	16.67%	16.67%	33.33%
	S275JR/355JR**	100/120	2.5/3.0	16.67%	16.67%	33.33%
	S355JR	100/120	2.5/2.5	16.67%	0.00%	16.67%

*Rail's material is S235JR and post's material is S275JR
**Rail's material is S275JR and post's material is S355JR

5.3 Case 3: ASI-Based Safety Enhanced of NJ Concrete Barrier

5.3.1 Optimal values

From the optimization, the optimum variable and objective functions obtained by NSGA-II convergent Pareto solution are given in Table 5.4. When compared with the original design ASI, the optimal design ASI value is reduced by 14.1%. This means that the level of injury associated with ASI is reduced at the same level. The original design and optimum safe design are given in Figure 5.1. The cross-sectional area of the original design is 0.40 m^2 and the cross-sectional area of the optimal safe design is 0.42 m^2. It can be seen that the cross-sectional area of the optimum design is approximately the same as the original. This means that a safer design is achieved with the same cost by optimal design.

Table 5.4 : Responses of original and optimal designs.

Design type	x1 (cm)	x2 (°)	x3 (°)	ASI	EA (°)	RollA (°)
Original design	8	58	87	1,42	12,5	10
Optimal design	10	65	80	1,22	5	19

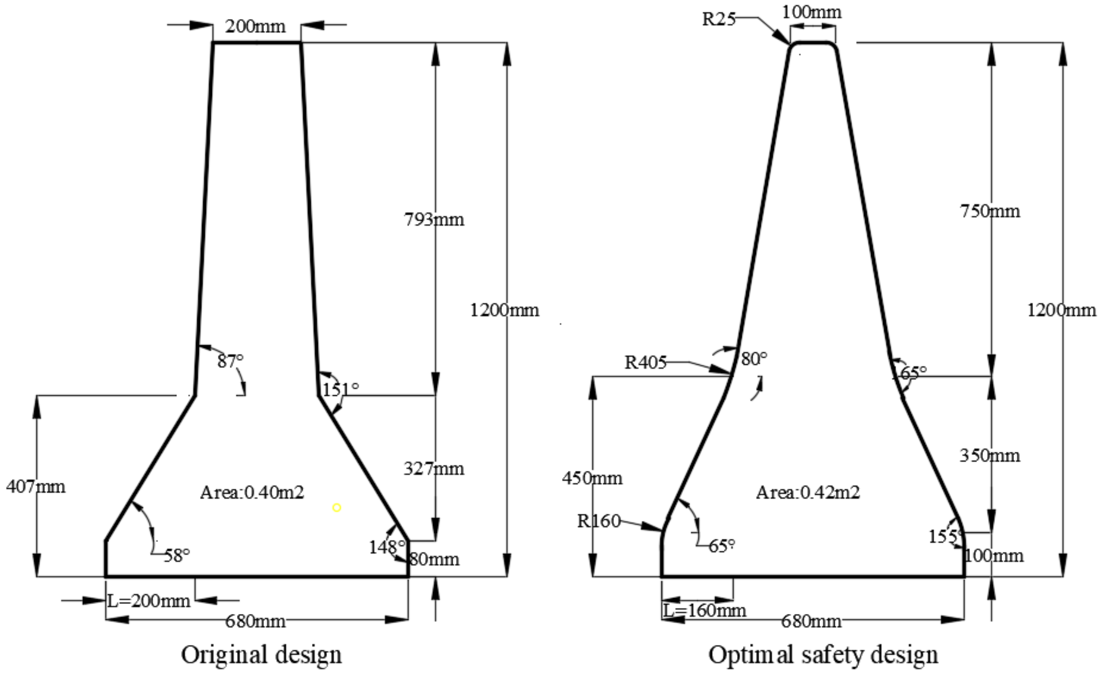

Figure 5.1 : Cross-sections of the original and optimal designs.

In the original design, the barrier is fixed to the floor by anchors, and an optimal safe design has been developed assuming the barrier with 0 displacements. However, it is clear that if the barrier is allowed to displace, the energy of the vehicle will be more absorbed and, hence, the ASI value will decrease. The working width of the KIPER Co. Ltd. barrier has been tested as W2 ($W_N \leq 0.8$m in EN1317/2) [107]. Since the bottom width of the barrier is 0.68 m, it is possible to displace 12 cm in a way that does not exceed the W2 limit [3]. The 12 cm displacement permits were given to the optimum safe barrier to observe the changing ASI value depending on displacement, the result is given in Table 5.5. As a result of displacement permitting the optimal safe design such that it remains within the working width of W2, a 9.4% reduction in the ASI value was observed. It is understood that the displacement/working width is an important factor in the impact energy absorption. When considering the effect on ASI, the displacement-based barrier design can be considered for subsequent studies.

Table 5.5 : Quantitative comparison of fixed and displacement allowed optimal design.

Design type	Constraint	x1 (cm)	x2 (°)	x3 (°)	ASI	EA (°)	RollA (°)
Optimal design	Fixed	10	65	80	1,22	5	19
Optimal design	Displacement allowed	10	65	80	1,11	3	10

ASI comparison of the original design, optimum safe design and the displacement allowed optimum safe design is given in Figure 5.2. As can be seen from the figure, with the help of the analytical method followed in this study, the ASI value of the optimum model was reduced by 22-23% when compared to the original model. From this, it can be said that the risk of ASI-related injury is reduced by about a quarter with regard to the original barrier.

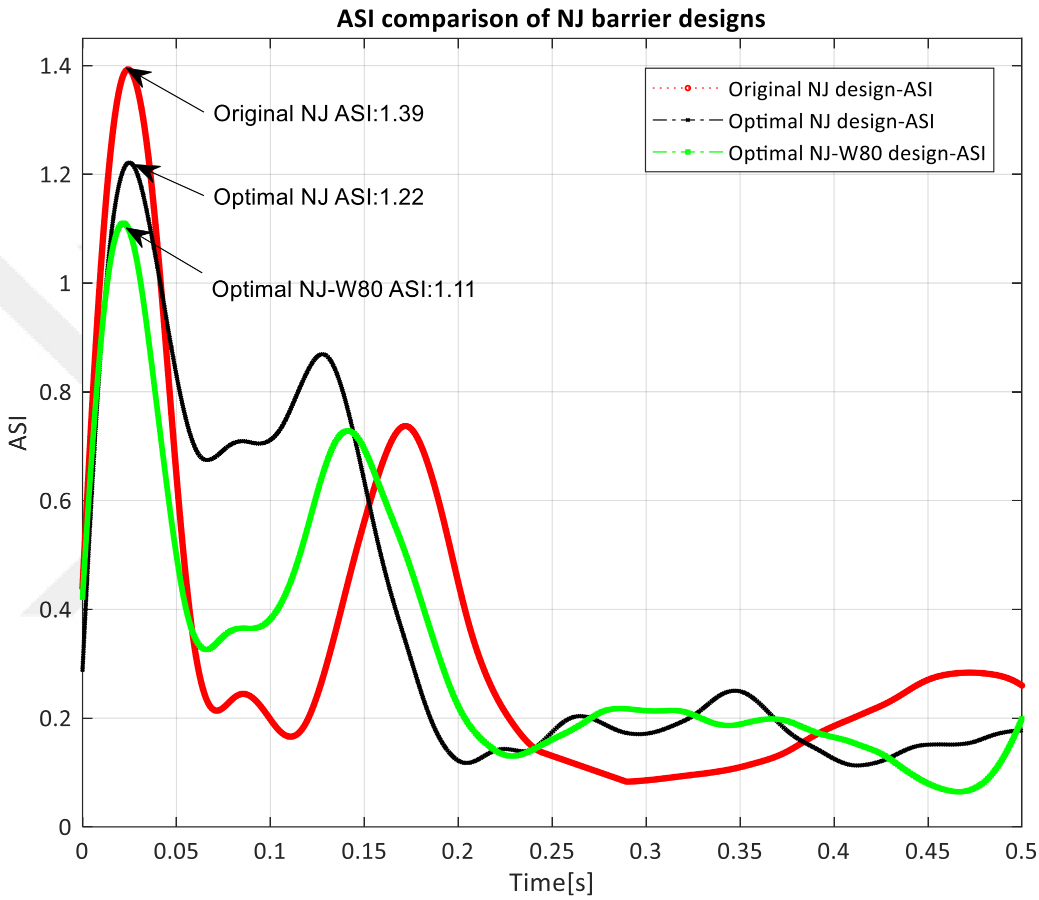

Figure 5.2 : Comparison of ASI graph of NJ barrier designs.

5.3.2 Comparison of original and optimal design

The qualitative and quantitative comparison of the original model with the optimum safe model is given below. The ASI, EA, and RollA of the optimum safe model obtained with OWPE-RBF metamodel and ASI, EA and RollA obtained from the FE model of optimum variables are given in Table 5.6. The RAE has less than 4.5% based on the result given in the table. Figure 5.3 illustrates the qualitative comparison of the original design and the optimal safe design for TB11 test. It has been observed that it meets the requirements of EA and RollA specified in the EN1317 standard. The important factor affecting the difference in ASI values between the original model and the optimal model is that the optimal model absorbs the impact energy of the vehicle by climbing the barrier more easily and allowing it to fly higher and more. The difference can easily be seen at 0.30 and 0.65 s. Since the optimal design is in the H4b class, it must meet the criteria specified in the EN1317 for the TB81 test. Figure 5.4 compares the optimal design with the original design. The figure shows that the test is successful for EA and RollA safety criteria.

Table 5.6 : Quantitative comparison for FEA of optimum variables and OWPE-RBF optimum.

Analysis type	ASI	EA (°)	RollA(°)
OWPE-RBF metamodelling optimum	1.2211	5.14	19.86
FEA of optimum variables	1.2200	5.00	19.00
RAE (%)	0.09	2.72	4.33

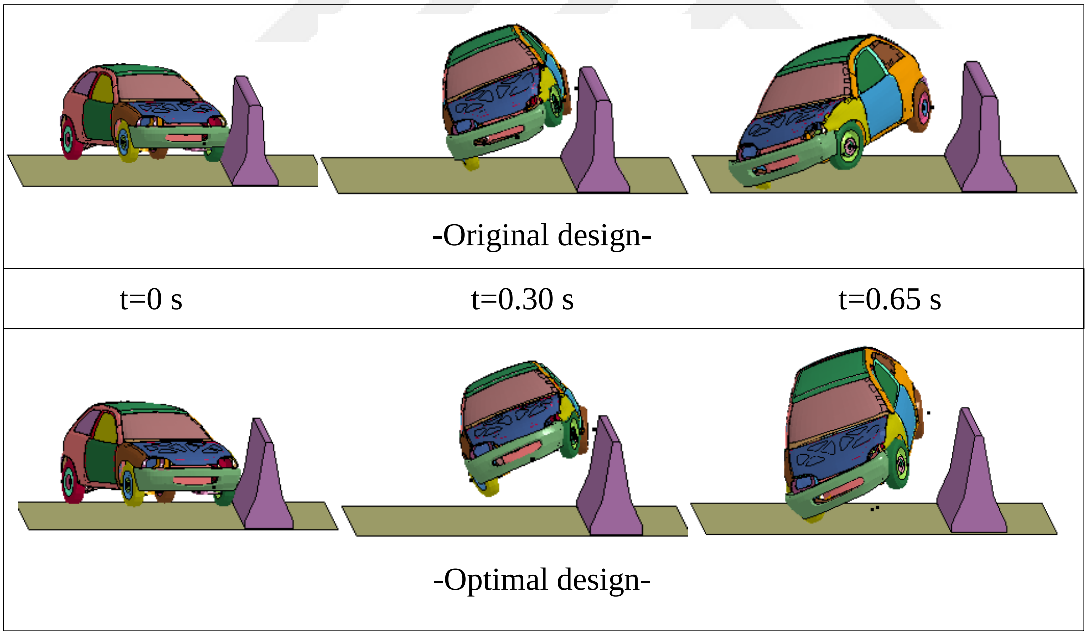

Figure 5.3 : Qualitative comparison for FE model of TB11 test of original and optimal designs.

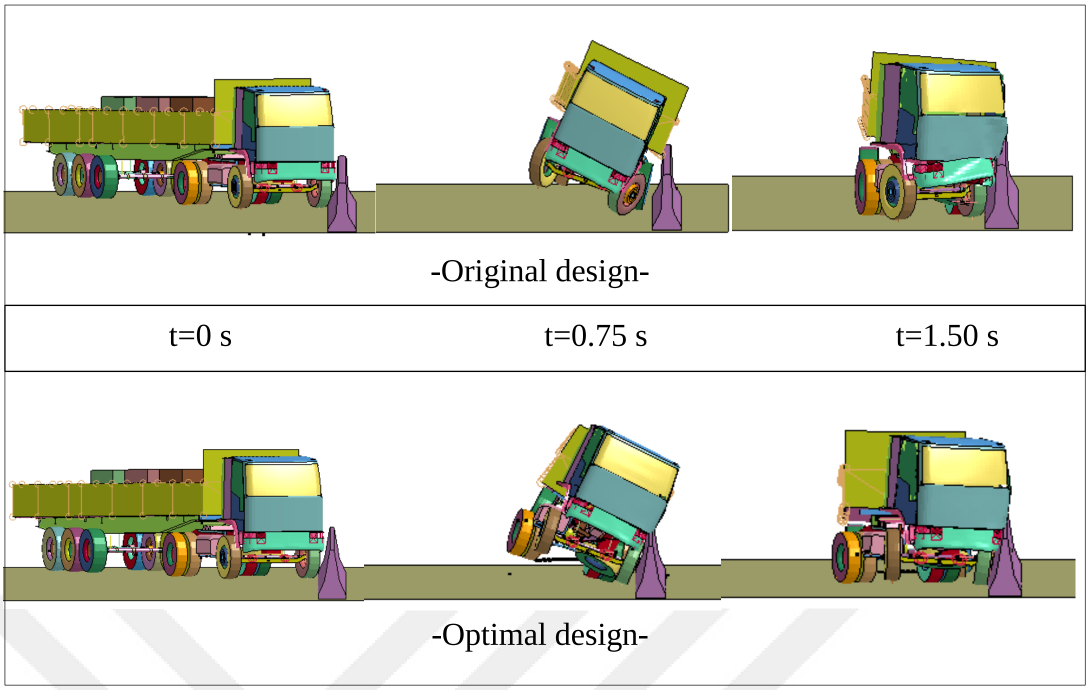

Figure 5.4 : Qualitative comparison for FE model of TB81 test of original and optimal designs.

6. CONCLUSIONS AND RECOMMENDATIONS

For this dissertation, I successfully implemented RBF-based metamodel in three case of road restraint systems. The conclusions and recommendations for the studies conducted in the light of the hypotheses and the objectives of the thesis are summarized below.

6.1 Case 1: Soil Density Depended Optimization of Embedment Depth of C, H and S Post Type

In this case a series of experimental impact tests, corresponding FE simulations, and detailed RBF-based design optimization studies were performed to determine the optimum PED in H1 and H2 level longitudinal barriers used in Turkey. To reduce the computational cost of optimization that required a large number of simulations, an RBF-based metamodeling methodology was employed to create surrogate models that are used to replace expensive 3D FE models. The metamodel was constructed with the help of FFD, FEA, and RBF methods. MOO of the RBF-based metamodels was accomplished by writing a code by using the MOGA options in MATLAB. From the results obtained, the following observations were made:

- RBF surrogate modeling–based optimization reduced the embedment depth of the C post from 950 mm to 780 (17.89% reduction), 828 (12.84% reduction) and 877 mm (7.68% reduction) for dense, medium and loose soil, respectively.
- RBF surrogate modeling–based optimization reduced the embedment depth of the S post from 1200 mm to 759 (36.75% reduction), 915 (23.75% reduction) and 1071 mm (10.75% reduction) for dense, medium and loose soil, respectively.
- RBF surrogate modeling–based optimization reduced the embedment depth of the H post from 1230 to 700 mm (43.09% reduction) for dense, medium and loose soil.
- The validity of the crash simulations was verified using available full scale crash test results. Results clearly indicated that the optimal PEDs determined

in this study have the potential to be used in longitudinal barrier designs with confidence. In addition, longitudinal barriers with optimum PEDs will provide significant cost effectiveness compared to existing designs.

Finally, this study showed that the variation of soil density significantly affects the PED and the impact performance of the guardrail posts embedded in soil. In performance-based guardrail design standards, the effect of the ground is mostly ignored. In this sense, it is expected that this study will contribute to the state-of-the-art for this research. Based on the research findings it can be concluded that the RBF-based design optimization method shows promise and can be used in future road restraint system design studies with confidence.

6.2 Case 2: S235JR, S275JR and S355JR Material-Based Cross-sectional Optimization of H1W4 and H2W4 Performance Level Guardrails

In this case, safety and economical optimization of the widely used H1W4 and H2W4 barrier systems in Turkey have been studied. The optimization was performed based on the safety criteria of the EN1317 standard. For optimization, the crash tests specified for H1 and H2 levels described in the EN1317 standard are modeled using FE. Since running numerous full scale FE simulations is a time-consuming task, a RBF-based metamodel is utilized to reduce the amount of FE analysis cases. For optimization of H1 and H2 guardrail systems post and rail geometries were chosen as design variables and, the guardrail's working width (w), and the vehicle's exit angle (α) were used as objective and constraint functions.

As a result of optimization using MOGA (NSGA-II), the optimum variables were achieved for post and rail as parts of H1W4 and H2W4 systems manufactured from S235JR, S275JR and S355JR grade steel materials and their combination. Then the validity of the optimum variables was validated by simulating in LS-DYNA. The FE models of optimum variables were compared with real crash test results and it was found that they met the necessary safety criteria in EN1317. The optimum variables indicate that the standard guardrail cross-sections used in actual designs are determined to be on the safe side. When compared to existing guardrail designs, the designs, which are obtained by using metamodel-based optimization, provide the economic advantage up to 33.33% in terms of construction cost. The optimization results also show that the metamodel based optimization method is effective and efficient in the design process of guardrails. Consequently, RBF-based metamodel shows potential as a valid and applicable method for the design and optimization of roadside safety systems.

6.3 Case 3: ASI-Based Safety Enhanced of NJ Concrete Barrier

This study investigates the validity of metamodel-based optimization as an analytical method to minimize the level of ASI-related injury in an NJ barrier design. As an analytical method, the solution of OWPE-RBF-based metamodel optimization with MOGA (NSGA-II) has been proposed. The proposed method is one of the most successful methods in the solution of multi-objective engineering optimization problems in existing individual and ensemble metamodels. The $RMSE_{CV}$ of OWPE-RBF based metamodel established in the study is between 0-1.5 and it is important for the consistency of the results. Before starting the optimization in the NJ barrier design, critical points that affect the ASI and injury level were investigated and optimization was completed in light of determined critical points. The critical design points of NJ type barriers, important determinations regarding the OWPE-RBF model, and the reduction of the ASI/injury level achieved in this study are concluded as follows:

- The higher the friction coefficient-x4, the higher the ASI value and the higher the probability of a roll-over for a vehicle; the smaller the value, the better.
- It is understood that among the x1, x2 and x3 factors affecting the geometric design, the x1, and x2 factors are the most effective regions affecting the NJ type concrete barrier shape design in terms of total impact values of about 25%. These regions are the regions, wherein Figure 4.44 the sum of the standard measures of the two factors is given as 407 mm.
- The most significant factor affecting the exit angle-EA is the x4 factor, which indicates the surface friction coefficient between the vehicle and the barrier. However, the exit angle-EA was not affected much by changing the lower and upper limit values of the x1, x2 and x3 shape factors.
- When the factors regarding the roll angle-RollA safety were examined, it was determined that the high angle of the x2 factor, the low angle of the x3 factor and the high friction value in the x4 factor caused a rollover. The most stable RollA value was obtained with a low angle of the x2 factor.

- The optimum values of the c shape parameter are different for each basis function.
- The metamodel construction with the lowest RMSE prediction for all c constant values was made by the RBF-LNR.
- For multi-objective optimization, preferring ensemble models against individual models provides a higher accuracy estimation.
- When comparing with the original design ASI, the optimal design ASI value is reduced by 14.1%. This means that the level of injury associated with ASI is reduced at the same level.
- The cross-sectional area of the optimal design is approximately the same as the original. This means that a safer design is achieved with the same cost by optimal design.
- As a result of displacement permitting the optimal safe design such that it remains within the working width of W2, a 9.4% reduction in the ASI value was observed.
- With the help of the analytical method followed in this study, an ASI value of the optimum model was reduced by 22-23% when compared to the original model. From this, it can be said that the risk of ASI-related injury is reduced by about a quarter for the original barrier.
- The important factor affecting the difference of ASI value between the original model and the optimal model is that the optimal model absorbs the impact energy of the vehicle by climbing the barrier more easily and allowing it to fly higher and more.
- The displacement or working width has been found to be an important factor on impact energy absorption. In this sense, it is suggested to investigate in subsequent studies barrier designs with safer ASI/injury levels due to displacement/working width.
- In concrete barrier design, safer designs can be obtained with metamodel-based design optimization methods instead of expensive full-size crash tests and excessive FE simulation numbers that cause a computational burden.
- In this case, only barrier-related factors were investigated as effective factors in barrier design. However, we know that the chassis, bumper geometry, and center of gravity of the vehicles used in the crash test are factors that affect the

safety criteria. It can also be discussed how well the vehicles used for the crash test represent the vehicles used in traffic. In future studies, it is thought that by investigating all these factors, crash physics and dynamics will be better understood, and thus more comprehensive and safe roadside security elements will be designed.

REFERENCES

[1] **Ray, M. H. and Patzner, G. S.** (1997). Finite-element model of modified eccentric loader terminal MELT, Transportation Research Record 1599, Transportation Research Board, Washington, DC, 11–21.

[2] **AASHTO MASH-1.** (2009). Manual for assessing safety hardware (MASH). 1st ed. Washington (DC): American Association of State Highway Transportation Officials, Washington, USA

[3] **CEN**. (2014). European Committee for Standardization. European Standard EN1317, Testing and Evaluation of Road Restraint Systems, Brussels.

[4] **Anh-Tuan, N., Reiter, S., and Rigo, P.** (2014). A review on simulation-based optimization methods applied to building performance analysis. *Applied Energy* ***113***:1043–1058.

[5] **Yolanda, C., and Maria, A.** (1997). Simulation optimization: methods and applications. Proceedings of the 29th conference on winter simulation. IEEE Computer Society.

[6] **Konak, A., Coit, D. W., and Smith, A. E.** (2006). Multi-objective optimization using genetic algorithms: A tutorial. *Reliability Engineering and System Safety,* ***91*** (2006) 992–1007.

[7] **Mannering F. L., and Bhat, C. R.** (2014). Analytic methods in accident research: Methodological frontier and future directions. *Analytic Methods in Accident Research,* ***1***, 1–22.

[8] **Holdridge, J., Shankar, V., Ulfarsson. G.** (2005). The crash severity impacts of fixed roadside objects. *Journal of Safety Research*, ***36(2)***, 139-147.

[9] **Sicking, D. L.** (1995). Applications of simulation in design and analysis of roadside safety features. Transportation Research Circular 435, TRB, National Research Council, Washington DC, USA.

[10**] LSTC.** (2014). A general purpose dynamic finite element analysis program, LS-DYNA version 971 user's manual. Livermore Software Technology Corporation, Livermore, California, USA.

[11] **Committee on Guardrails and Guide Posts.** (1962). Proposed full-scale testing procedures for guardrails. Highway research correlation service circular 482. Washington (DC): Highway Research Board, USA.

[12] **Reid, J. D., Sicking, D. L., Faller, R. K. et al.** (1997). Development of a new guardrail system. *Transp Res Rec.*, ***1599***(1):72–80.

[13] **Ray, M., Engstrand, K., Plaxico C. et al**. (2001). Improvements to the weak-post W-beam guardrail. *Transp Res Rec.*, ***1743***(1):88–96.

[14] **Sicking, D. L, Reid, J. D., and Rohde, J. R.** (2002). Development of the mid-west guardrail system. *Transp Res Rec.*, ***1797***:44–52.

[15] **Consolazio, G. R., Chung, J. H., and Gurley, K. R.** (2002). Impact simulation and full scale crash testing of a low profile concrete work zone barrier. *Comput Struct.,* ***81***:1359–74.

[16] **Atahan, A. O.** (2002). Finite element simulation of a strong-post W-beam guardrail system. *Simulation,* ***78*** (10):587–99.

[17] **Atahan, A. O.** (2003). Impact behaviour of G2 steel weak-post W-beam guardrail on nonlevel terrain. *Int J Heavy Veh Syst.,* ***10(3)***:209–23.

[18] **Faller, R. K., Polivka, K. A., Kuipers, B. D. et al.** (2004). Midwest guardrail system for standard and special applications. *Transp Res Rec.,* ***1890(1)***:19–33.

[19] **Atahan, A. O., and Cansiz, O. F.** (2005). Impact analysis of a vertical flared back bridge rail-to-guardrail transition structure using simulation. *Finite Elem Anal Des.,* ***41***:371–96.

[20] **Atahan, A. O., and Cansiz, O. F.** (2005). Improvements to G4 (RW) strong-post round-wood, W beam guardrail system. *J Transp Eng;* ***131(1)***:63–73.

[21] **Ren, Z., and Vesenjak, M.** (2005). Computational and experimental crash analysis of the road safety barrier. *Eng Fail Anal.,* ***12***:963–73.

[22] **Cansiz, O. F., and Atahan, A. O.** (2006). Crash test simulation of a modified thrie-beam high containment level guardrail under NCHRP report 350 TL 4-12 conditions. *Int J Heavy Veh Syst.,* ***13***:2–18.

[23] **Buth, C. E., Bullard, D. L., and Menges, W. L.** (2006). NCHRP report 350 test 3-11 of the long-span guardrail with 5.7 m clear span and nested W-beams over 11.4 m. Report 405160-1-1, Texas: Texas Transportation Institute, USA.

[24] **Plaxico, C. A., Kennedy, J. C., and Miele, C. R.** (2006). Development of an NCHRP report 350 TL-3 New Jersey shape 50-inch portable concrete barrier. Final report FHWA/OH- 2006/16, Ohio Department of Transportation, Ohio, USA.

[25] **Davids, W. G., Botting, J. K., and Peterson, M.** (2006). Development and structural testing of a composite-reinforced timber highway guardrail. Constr Build Mater., 20:733–43.

[26] **Faller, R., Sicking, D., Bielenberg, R. et al.** (2007). Performance of steel-post, W-beam guardrail systems. *Transp Res Rec.,* ***2025***:18–33.

[27] **Faller, R. K., Reid, J. D., Kretschmann, D. et al.** (2009). Midwest guardrail system with round timber posts. *Transp Res Rec;* ***2120***:47–59.

[28] **Atahan, A. O., and Arslan, T.** (2012). Collision behaviour of double W-beam transition. *Int J Heavy Veh Syst.,* ***19(1)***:76–91.

[29] **Soltani, M., Moghaddam, T. B., Karim, M. R. et al.** (2013). The safety performance of guardrail systems: review and analysis of crash tests data. *Int J Crashworthiness,* ***18***:530–43.

[30] **Atahan, A. O., Yucel, A. O., and Erdem, M. M.** (2014). Crash testing and evaluation of a new generation L1 containment level guardrail. *Eng Fail Ana.,* ***38***:25–37.

[31] **Fang, H,, Wang, Q,, and Weggel, D, C.** (2015). Crash analysis and evaluation of cable median barriers on sloped medians using an efficient finite element model. *Adv Eng Softw.,* ***82***:1–13.

[32] **Atahan, A. O., and Erdem, M. M.** (2016). Evaluation of 12 m Long Turned Down Guardrail End Terminal Using Full-Scale Crash Testing and Simulation. Latin American Journal of Solids and Structures, *Vol.* ***13***, No. 16, 11/2016, p. 3107-3125, ISSN: 1679-7825.

[33] **Fang, H., Rais-Rohani, M., Liu, Z. et al.** (2005). A comparative study of metamodeling methods for multi-objective crashworthiness optimization. *Comput Struct.,* ***83***:2121–36.

[34] **Xiang, Y., Wang, Q., Fan, Z. et al.** (2006). Optimal crashworthiness design of a spotwelded thin-walled hat section. *Finite Elem Anal Des.,* ***42(10)***:846–55.

[35] **Hou, S., Li, Q., Long, S. et al.** (2007). Design optimization of regular hexagonal thin-walled columns with crashworthiness criteria. *Finite Elem Anal Des.,* ***43***:555–65.

[36] **Hou, S., Li, Q., Long, S. et al.** (2008). Multiobjective optimization of multi-cell sections for the crashworthiness design. *Int J Impact Eng.,* ***35*** (11):1355–67.

[37] **Liao, X., Li, Q., Yang, X. et al.** (2008). Multiobjective optimization for crash safety design of vehicles using stepwise regression model. *Struct Multidiscip Optim.,* ***35(6)***:561–9.

[38] **Hou, S., Li, Q., Long, S. et al.** (2009). Crashworthiness design for foam filled thin-walled structures. *Mater Des.,* ***30(6)***:2024–32.

[39] **Horstemeyer, M. F., Ren, X., Fang, H. et al.** (2009). A comparative study of design optimization methodologies for side-impact crashworthiness using injury-based versus energy-based criterion. *Int J Crashworthiness,* ***14 (2)***:125–38.

[40] **Bi, J., Fang, H., Wang, Q. et al.** (2010). Modelling and optimization of foam-filled thinwalled columns for crashworthiness designs. *Finite Elem Anal Des.,* ***46 (9)***:698–709.

[41] **Yin, H., Wen, G., Hou, S. et al.** (2011). Crushing analysis and multiobjective crashworthiness optimization of honeycomb-filled single and bitubular polygonal tubes. *Mater Des.,* ***32***:4449–60.

[42] **Hou, S. J., Liu, T. Y., Dong, D. et al.** (2014). Factor screening and multivariable crashworthiness optimization for vehicle side impact by factorial design. *Struct Multidiscip Optim.,* ***49***:147–167.

[43] **Ayancik, F., Acar, E., Celebioglu, K. et al.** (2016). Simulation-based design and optimization of Francis turbine runners by using multiple types of metamodels. *Proc IMechE Part C: J Mechanical Engineering Science,* ***0(0)*** 1–18. DOI: 10.1177/0954406216658078.

[44] **Acar, E., Tüten, N., and Güler, M. A.** (2018). Design optimization of an automobile torque arm using global and successive surrogate modeling approaches. *Proc IMechE, Part D: J Automobile Engineering,* ***1–13***. DOI: 10.1177/0954407018772739.

[45] **Yin, H., Fang, H., Wang, Q. et al.** (2016). Design optimization of a MASH TL-3 concrete barrier using RBF-based metamodels and nonlinear finite element simulations. *Eng Struct.*, ***0141***–0296.

[46] **Yin, H., Xiao, Y., Wen, G., et al.** (2017). Design optimization of a new W-beam guardrail for enhanced highway safety performance. *Adv Eng Softw.*, ***112***; 154-164.

[47] **Hou, S., Zheng, Y., Xie, J. et al.** (2014). Optimization design of NJ shaped guardrail based on collision safety consideration. *Int J Comput Methods*, ***11***:1350083-1–1350083-20.

[48] **Hou, S., Tan, W., Zheng, Y. et al.** (2014). Optimization design of corrugated beam guardrail based on RBF-MQ surrogate model and collision safety consideration. *Adv Eng Softw.*, ***78***:28–40.

[49] **Ozcanan, S., and Atahan A. O.** (2019). RBF surrogate model and EN1317 collision safety-based optimization of two guardrails. *Struct Multidisc Optim*., Epub ahead of print 23 January 2019. DOI: 10.1007/s00158-019-02203-z.

[50] **Ozcanan, S., and Atahan, A. O.** (2019). Radial basis function surrogate model-based optimization of guardrail post embedment depth in different soil conditions. *Proc IMechE, Part D: J Automobile Engineering.*, Epub ahead of print 20 May 2019. DOI: 10.1177/0954407019848548.

[51] **Hussain, M. F., Barton, R. B., and Joshi, S. B.** (2002). Metamodeling: radial basis functions, versus polynomials. *Eur J Oper Res.*, ***138***:142-154.

[52] **Elsayed, K., Vucinic, D., d'Ippoliro, R., et al.** (2012). Comparison between RBF and kriging surrogates in design optimization of high dimensional problems. 3rd International Conference on Engineering Optimization, 1-5 July, Rio de Janeiro, Brazil.

[53] **Mullur, A. A., and Messac, A.** (2005). Extended Radial Basis Functions: More Flexible and Effective Metamodeling. *AIAA Journal*, ***43(6)***; 1306-1315.

[54] **Acar, E**. (2014). Simultaneous optimization of shape parameters and weight factors in ensemble of radial basis functions. *Struct Multidiscip Optim.*, ***49(6)***:969–978.

[55] **Queipo, N. V., Haftka, R. T., Shyy, W., Goel, T., Vaidyanathan, R., and Tucker, P. K.** (2005). Surrogate-Based Analysis and Optimization. *Prog. Aerosp. Sci.*, ***41(1)***, pp. 1–28.

[56] **Forrester, A. I. J., Sobester, A., and Keane, A. J.** (2007). Multi-Fidelity Optimization Via Surrogate Modeling. *Proc. R. Soc. London A.*, ***463(2088)***, pp. 3251–3269.

[57] **Gorissen, D., Couckuyt, I., Demeester, P., Dhaene, T., and Crombecq, K.** (2010). A Surrogate Modeling and Adaptive Sampling Toolbox for Computer Based Design. *J. Mach. Learn. Res.*, ***11(1)***, pp. 2051–2055.

[58] **Song, X., Sun, G., Li, G., Gao, W., and Li, Q.** (2013). Crashworthiness Optimization of Foam-Filled Tapered Thin-Walled Structure Using Multiple Surrogate Models. *Struct. Multidiscipli. Optim.*, ***47(2)***, pp. 221–231.

[59] **Peri, D., and Campana, E. F.** (2005). High-Fidelity Models and Multiobjective Global Optimization Algorithms in Simulation-Based Design. *J. Ship Res.*, ***49(3)***, pp. 159–175.

[60] **Yang, J., Zhan, Z., Zheng, K., Hu, J., and Zheng, L.** (2016). Enhanced Similarity-Based Metamodel Updating Strategy for Reliability-Based Design Optimization. *Eng. Optim.*, ***48(12)***, pp. 2026–2045.

[61] **Ong, Y. S., Nair, P. B., Keane, A. J., and Wong, K. W.** (2005). Surrogate Assisted Evolutionary Optimization Frameworks for High-Fidelity Engineering Design Problems. Knowledge Incorporation in Evolutionary Computation, Springer, Berlin, pp. 307–331.

[62] **Draper, N. R., and Smith, H.** (2014). Applied Regression Analysis. 3rd ed., Wiley, New York, USA.

[63] **Matheron, G.** (1963). Principles of Geostatistics. Econ. Geol., 58(8), pp. 1246–1266.

[64] **Sacks, J., Schiller, S. B., and Welch, W. J.** (1989). Designs for Computer Experiments. *Technometrics,* ***31(1)***, pp. 41–47.

[65] **Sacks, J, Welch, WJ, Mitchell, TJ, and Wynn, H. P.** (1989). Design and Analysis of Computer Experiments. *Stat. Sci.*, ***4(4)***, pp. 409–423.

[66] **Fang, H., and Horstemeyer, M. F.** (2006). Global Response Approximation With Radial Basis Functions. *Eng. Optim.*, ***38(4)***, pp. 407–424.

[67] **Acar, E.** (2010). Optimizing the Shape Parameters of Radial Basis Functions: An Application to Automobile Crashworthiness. *Proceedings of the Institution of Mechanical Engineers, Part D: Journal of Automobile Engineering*, ***Vol. 224***, No. 12, pp. 1541–1553. doi:10.1243/09544070JAUTO1560.

[68] **Acar, E.** (2014). Simultaneous Optimization of Shape Parameters and Weight Factors in Ensemble of Radial Basis Functions. *Struct Multidisc Optim.*, ***Vol. 49***, No. 6, pp. 969–978. doi:10.1007/s00158-013-1028-0.

[69] **Vapnik, V. N.** (1998). Statistical Learning Theory. Wiley, New York, USA.

[70] **Girosi, F.** (1998). An Equivalence Between Sparse Approximation and Support Vector Machines. *Neural Comput.*, ***10(6)***, pp. 1455–1480.

[71] **Zhou, X. J., and Jiang, T.** (2016). Metamodel Selection Based on Stepwise Regression. *Struct. Multidiscip. Optim.*, ***54(3)***, pp. 641–657.

[72] **Goel, T., Haftka, R. T., Shyy, W., and Queipo, N. V.** (2007). Ensemble of Surrogates. *Struct. Multidiscip. Optim.*, ***33(3)***, pp. 199–216.

[73] **Simpson, T. W., Mauery, T. M., Korte, J. J., and Mistree, F.** (2001). Kriging Models for Global Approximation in Simulation-Based Multidisciplinary Design Optimization. *AIAA J.*, ***39(12)***, pp. 2233–2241.

[74] **Wang, G. G., and Shan, S.** (2007). Review of Metamodeling Techniques in Support of Engineering Design Optimization. *ASME J. Mech. Des.*, ***129(4)***, pp. 370–380.

[75] **Clarke, S. M., Griebsch, J. H., and Simpson, T. W.** (2005). Analysis of Support Vector Regression for Approximation of Complex Engineering Analyses. *ASME J. Mech. Des.*, ***127(6)***, pp. 1077–1087.

[76] **Jin, R., Chen, W., and Simpson, T. W.** (2001). Comparative Studies of Metamodelling Techniques Under Multiple Modelling Criteria. *Struct. Multidiscip. Optim.*, ***23(1)***, pp. 1–13.

[77] **Fang, H., Rais-Rohani, M., Liu, Z., and Horstemeyer, M. F.** (2005). A Comparative Study of Metamodeling Methods for Multiobjective Crashworthiness Optimization. *Comput. Struct.*, ***83(25–26)***, pp. 2121–2136.

[78] **Zerpa, L. E., Queipo, N. V., Pintos, S., and Salager, J. L.** (2005). An Optimization Methodology of Alkaline–Surfactant–Polymer Flooding Processes Using Field Scale Numerical Simulation and Multiple Surrogates. *J. Pet. Sci. Eng.*, ***47(3–4)***, pp. 197–208.

[79] **Acar, E., and Rais-Rohani, M.** (2009). Ensemble of Metamodels With Optimized Weight Factors. *Struct. Multidiscip. Optim.*, ***37(3)***, pp. 279–294.

[80] **Viana, F. A. C., Haftka, R. T, and Steffen, V. Jr.** (2009). Multiple Surrogates: How Cross-Validation Errors Can Help Us to Obtain the Best Predictor. *Struct. Multidiscip. Optim.*, ***39(4)***, pp. 439–457.

[81] **Ferreira, W. G., and Serpa, A. L.** (2016). Ensemble of Metamodels: The Augmented Least Squares Approach. *Struct. Multidiscip. Optim.*, ***53(5)***, pp. 1019–1046.

[82] **Acar, E.** (2010). Various Approaches for Constructing an Ensemble of Metamodels Using Local Measures. *Struct. Multidiscip. Optim.*, ***42(6)***, pp. 879–896.

[83] **Zhang, J., Chowdhury, S., and Messac, A.** (2012). An Adaptive Hybrid Surrogate Model. *Struct. Multidiscip. Optim.*, ***46(2)***, pp. 223–238.

[84] **Liu, H., Xu, S., Wang, X., Meng, J., and Yang, S.** (2016). Optimal Weighted Pointwise Ensemble of Radial Basis Functions With Different Basis Functions. *AIAA J.*, ***54(10)***, pp. 3117–3133.

[85] **Lee Y, and Choi D.** (2014). Pointwise Ensemble of Meta-Models Using t Nearest Points Cross-Validation. *Struct. Multidiscip. Optim.*, ***50(3)***, pp. 383–394.

[86] **Buhmann, M.D.** (2003). Radial Basis Functions: Theory and Implementations, Cambridge University Press, New York, NY, USA.

[87] **Benki, A., Habbal, A., and Mathis, G**. (2017). A metamodel-based multicriteria shape optimization process for an aerosol can. *Alexandria Eng J.* http://dx.doi.org/10.1016/j.aej.2017.03.036.

[88] **Gutmann, H. M**. (2001). A Radial basis function method for global optimization. *Journal of Global Optimization* ***19***: 201–227.

[89] **McDonald, D. B., Grantham, W. J., Tabor, W. L., Murphy, M. J**. (2007). Global and local optimization using radial basis function response surface models. *Applied Mathematical Modelling,* ***31***:2095–2110.

[90] **Rudholm, J., and Wojciechowski, A**. (2007). A method for simulation based optimization using radial basis functions. Master's Thesis, Göteborg University, Göteborg, Sweden.

[91] **Sui, Y. K., Li, S. P., Guo, Y. Q**. (2008). An efficient global optimization algorithm based on augmented radial basis function. *Int J Simul Multidisci Des Optim.*, ***2***:49–55.

[92] **Forrester, A. I. J., Keane, A. J.** (2009.) Recent advances in surrogate-based optimization. *Progress in Aerospace Sciences* ***Volume 45***, Issues 1–3 January–April, Pages 50-79.

[93] **Cao, L., Jiang, P., Chen, Z., Zhou, Q., and Zhou, H.** (2015). Metamodel assisted robust optimization under interval uncertainly based on reverse model. *IFAC-Papers Online* ***48***-28:1178–1183.

[94] **Ky, V. K., D'Ambrosio, C., Hamadi, Y., and Liberti, L.** (2016). Surrogate-based methods for black-box optimization. *International Transactions in Operational Research*, ***24(3)***:393-424. https://doi.org/10.1111/itor.12292.

[95] **Meckesheimer, M., Booker, A. J, Barton, R. R., et al.** (2002). Computationally inexpensive metamodel assessment strategies. *AIAA J.*, ***40(10)***:2053–2060.

[96] **Kim, I. Y., and De Weck, O. L.** (2006). Adaptive weighted sum method for multiobjective optimization: a new method for Pareto front generation. *Struct Multidisc Optim.*, ***31(2)***:105–16.

[97] **Atahan, A. O., Ornek, M., Buyuk, M., et al.** (2016). Investigation of effect of soil properties on embedded guardrail post performance using in-situ tests and numerical analysis. 213M516, The Scientific and Technological Research Council of Turkey, Ankara, Turkey.

[98] **Wu, W., and Thomson, R.** (2007). A study of the interaction between a guardrail post and soil during quasi-static and dynamic loading. International *Journal of Impact Engineering*, ***34***, 883-98.

[99] **Atahan, A. O.** (2003). Impact behavior of G2 steel weak-post W-beam guardrail on non-level terrain, Heavy Vehicle Systems. A series of the *International Journal of Vehicle Design*, ***10(3)***, 209-23.

[100] **Brinkgreve, R. B. J., Broere, W., and Waterman, D.** (2004). Plaxis finite element code for soil and rock analysis, 2D –Version 8.6.

[101] **MATLAB.** (2017). Matlab and Statistics Toolbox Release (2017b), The MathWorks, Inc., Natick, Massachusetts, USA.

[102] **Hardy, R. L.** (1971). Multiquadric equations of topography and other irregular surfaces. *J Geophys Res.*, ***76***, 1905–1915.

[103] **Deb, K., Pratap, A., Agarwal, S., et al.** (2002). A fast and elitist multiobjective genetic algorithm: NSGA-II. *IEEE Trans on Evolutionary Comput.*, ***6(2)***:182-197.

[104] **Holland, J. H.** (1975). Adaptation in natural and artificial systems, 2nd ed. Cambridge, MA: MIT Press, USA.

[105] **FEMA**. (2002). Finite Element Model Archive, FHWA/NHTSA National Crash Analysis Center, http://www.ncac.gwu.edu/vml/models.html, Virginia, USA.

[106] **CSI-SPA**. (2017). Crash testing of H1 and H2 guardrails systems. 0021\ME\HRB\17, Bollate, Italy.

[107] **CSI-SPA.** TB11 crash testing of KİPER-H4b-DS6.0 barrier systems. 0089\ME\HRB/18, and Bollate, Italy, 2018.

[108] **CSI-SPA.** TB81 crash testing of KİPER-H4b-DS6.0 barrier systems. 0090\ME\HRB/18, and Bollate, Italy, 2018.

[109] **Liao, X., Li, Q., Yang, X., et al.** (2008). Multiobjective optimization for crash safety design of vehicles using stepwise regression model. *Struct Multidiscip Optim.*, ***35(6)***:561–9.

APPENDICES

APPENDIX A: Comparison of FE simulations and real crash tests

APPENDIX A: Comparison of FE simulations and real crash tests

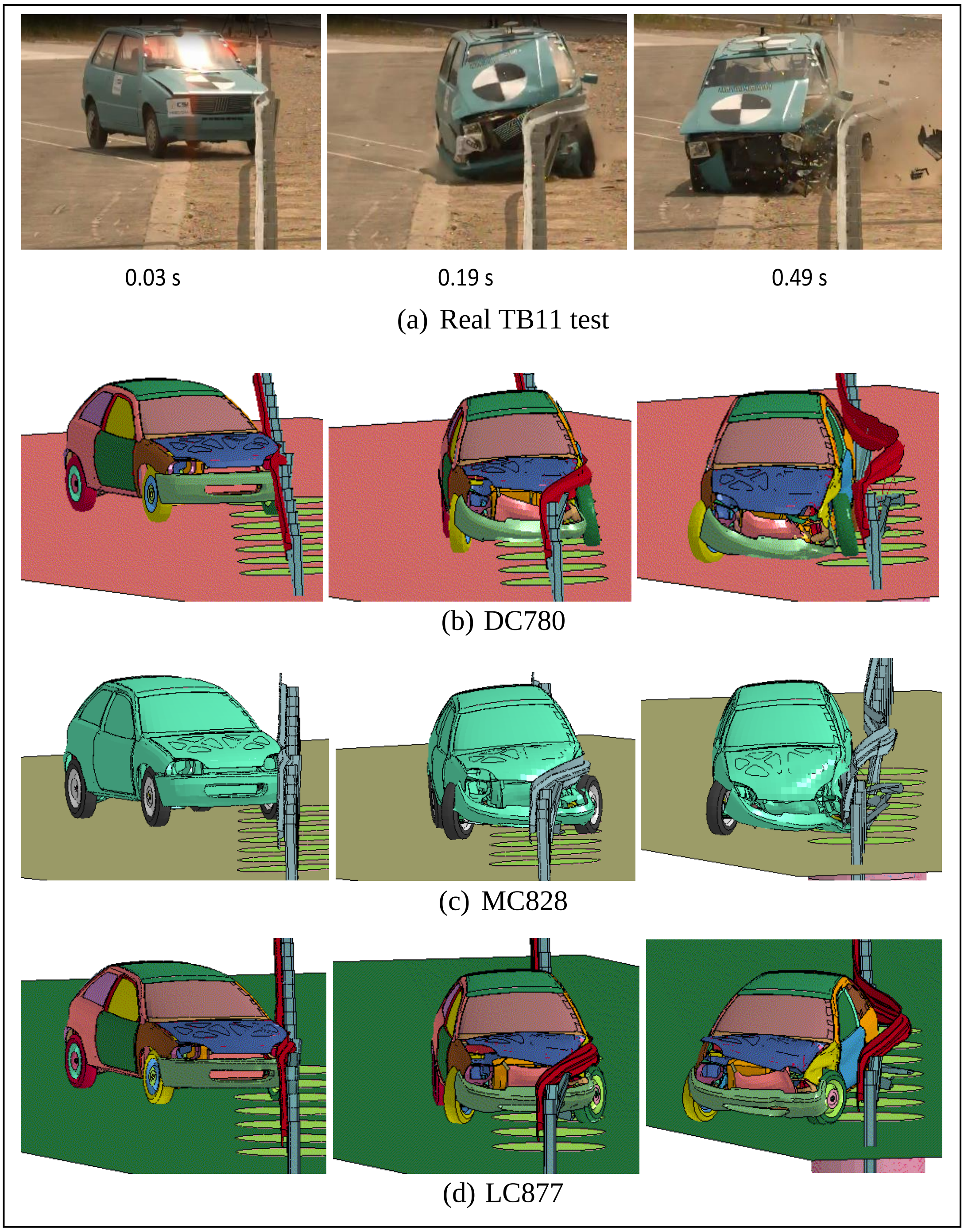

Figure A.1 : Comparison of FEA results and real crash test (a) of TB11 for C post in Dense (b), Medium dense (c) and Loose (d) soil [50].

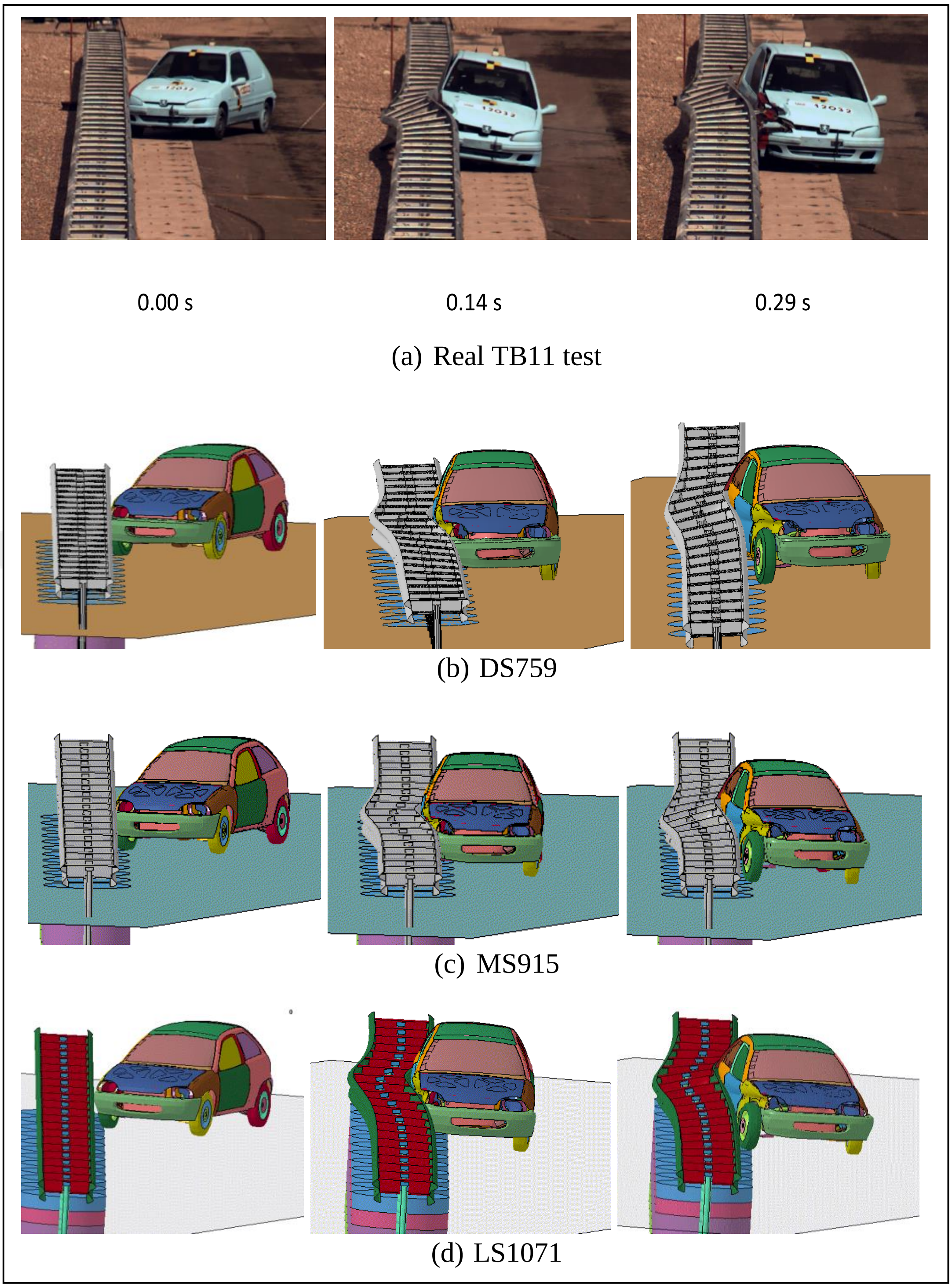

Figure A.2 : Comparison of FEA results and real crash test (a) of TB11 for S post in Dense (b), Medium dense (c) and Loose (d) soil [50].

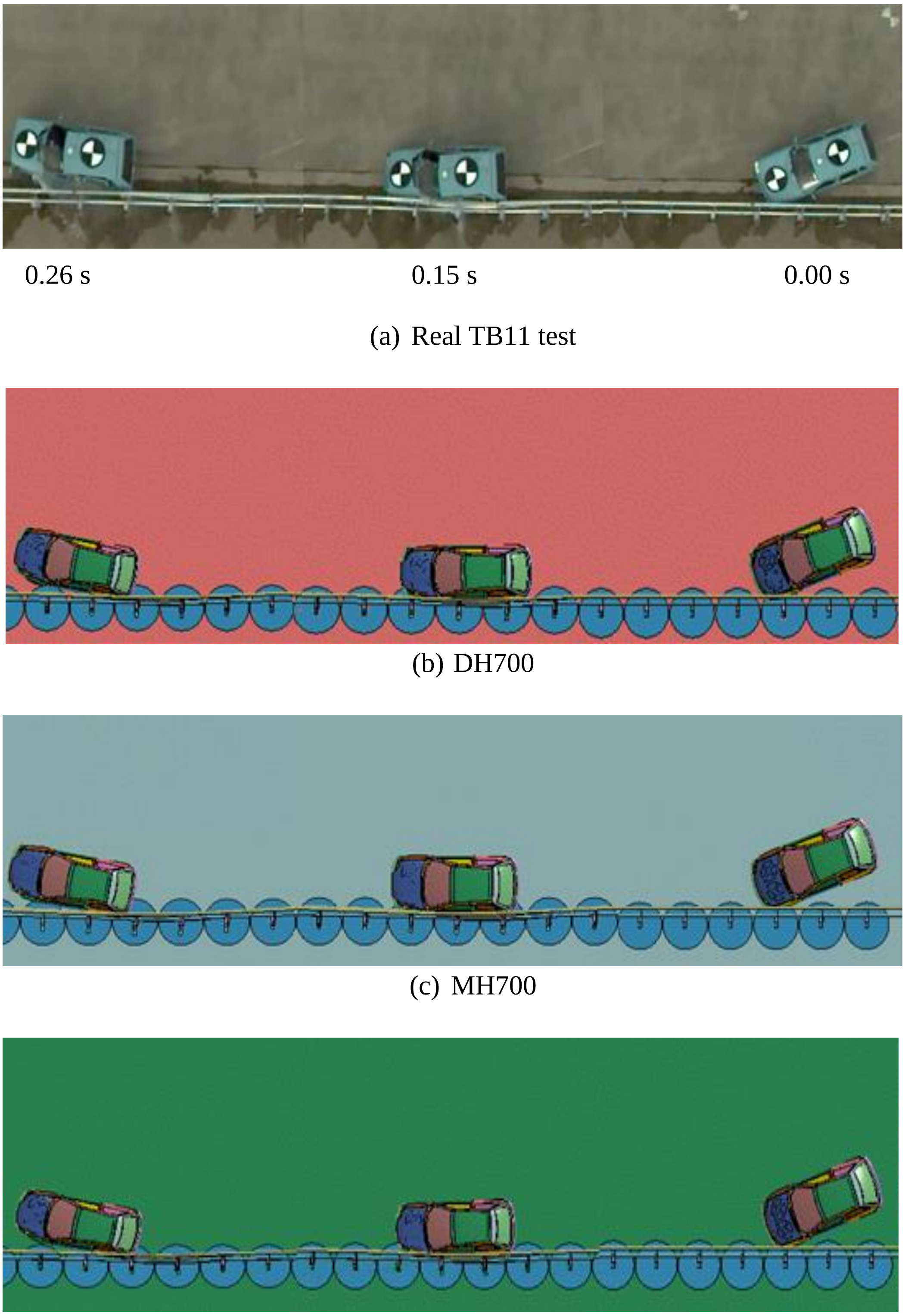

Figure A.3 : Comparison of FEA results and real crash test (a) of TB11 for H post in Dense (b), Medium dense (c) and Loose (d) soil [50].

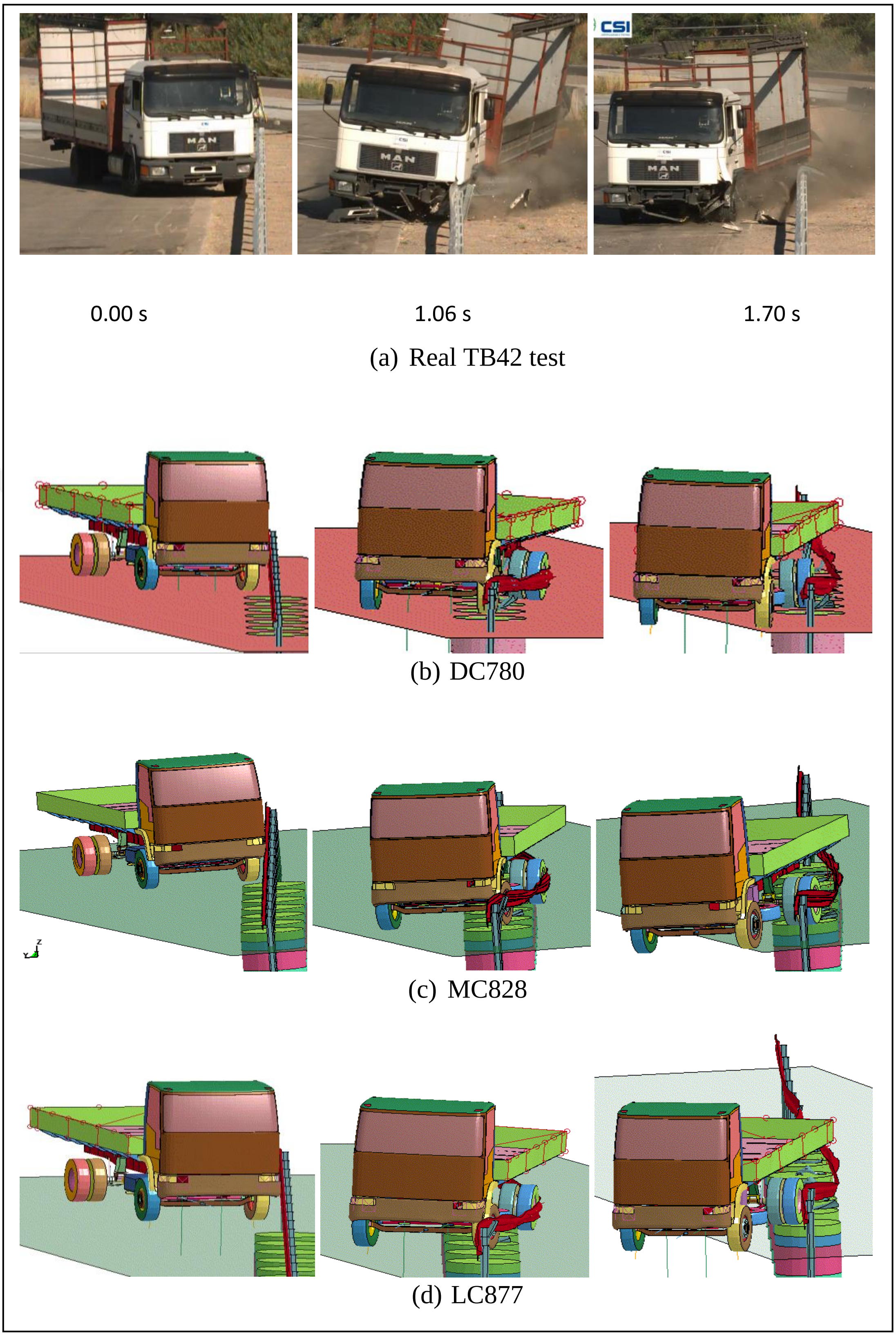

Figure A.4 : Comparison of FEA results and real crash test (a) of TB42 for C post in Dense (b), Medium dense (c) and Loose (d) soil [50].

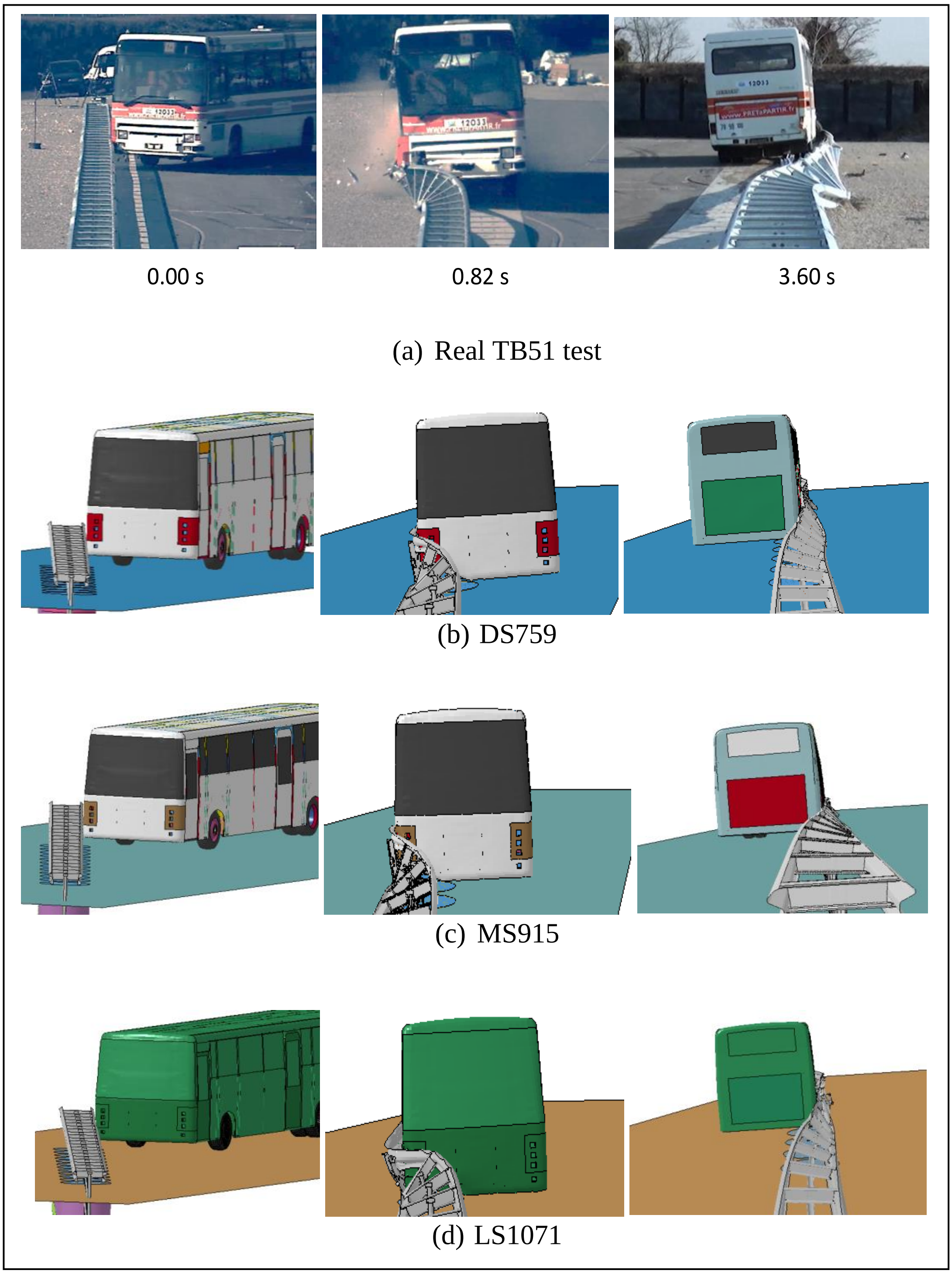

Figure A.5 : Comparison of FEA results and real crash test (a) of TB51 for S post in Dense (b), Medium dense (c) and Loose (d) soil [50].

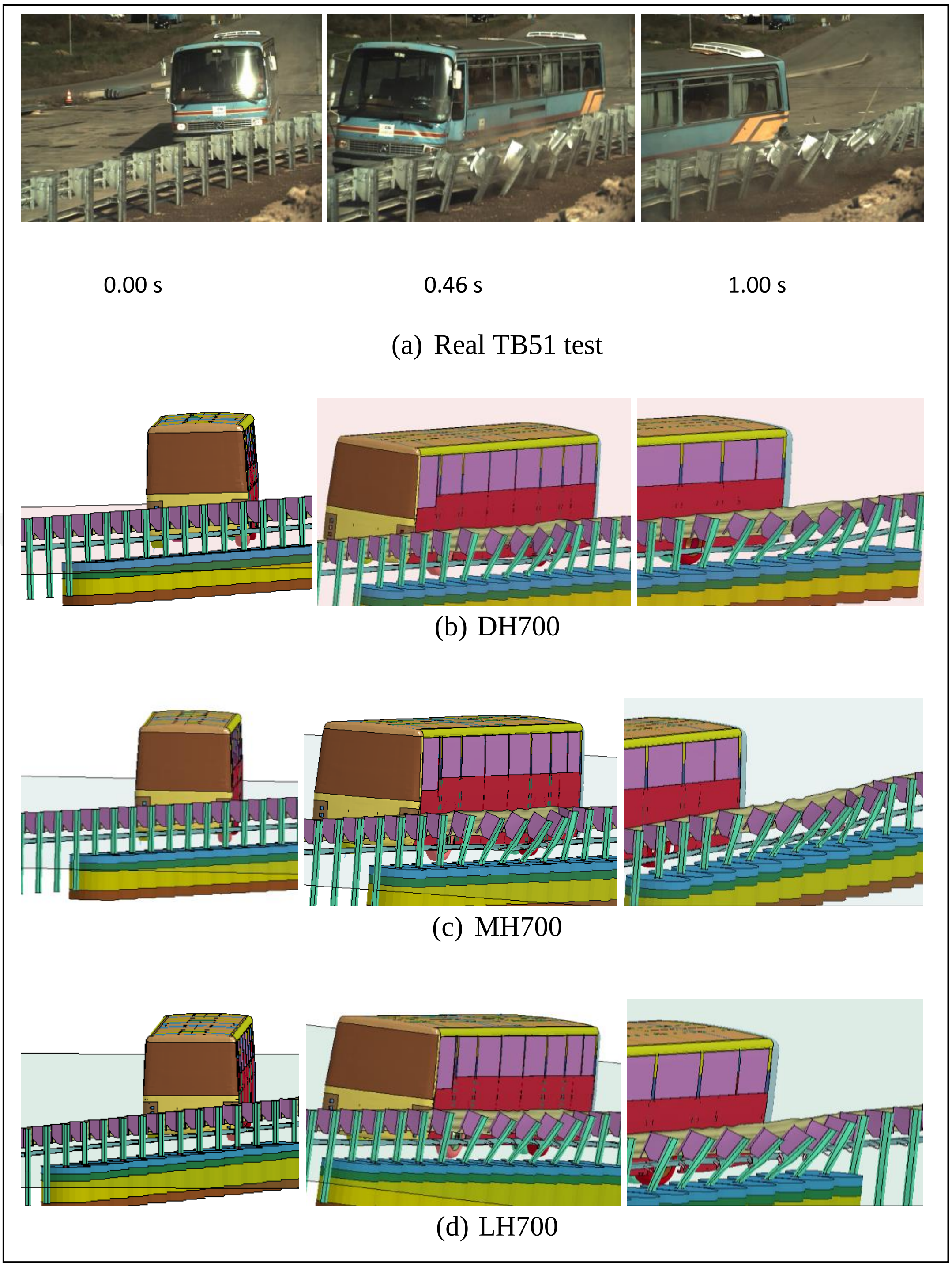

Figure A.6 : Comparison of FEA results and real crash test (a) of TB51 for H post in Dense (b), Medium dense (c) and Loose (d) soil [50].

CURRICULUM VITAE

Name Surname **:** Sedat OZCANAN

Place and Date of Birth **:** Yuksekova 14/06/1984

E-Mail **:** sedat.divali@gmail.com

EDUCATION **:**

- **B.Sc.** **:** 2007, Sakarya University, Technical Education Faculty, Construction
- **B.Sc.** **:** 2015, Istanbul Technical University, Civil Engineering Faculty, Civil Engineering
- **M.Sc.** **:** 2011, Karadeniz Technical University, Graduate School Of Science Engineering And Technology, Civil Engineering

PROFESSIONAL EXPERIENCE AND REWARDS:

- 2012-2013 Research Assistant, Sirnak University, SIRNAK.
- 2013-2019 Research Assistant, Istanbul Technical University, ISTANBUL.

PUBLICATIONS, PRESENTATIONS AND PATENTS ON THE THESIS:

- **Ozcanan S.,** and Atahan A. O. 2019. RBF surrogate model and EN1317 collision safety-based optimization of two guardrails. *Struct Multidisc Optim.*, Epub ahead of print 23 January 2019. DOI: 10.1007/s00158-019-02203-z.
- **Ozcanan S.,** and Atahan A. O. 2019. Radial basis function surrogate model-based optimization of guardrail post embedment depth in different soil conditions. *Proc IMechE, Part D: J Automobile Engineering.*, Epub ahead of print 20 May 2019. DOI: 10.1177/0954407019848548.

- **Ozcanan S.,** and Atahan A. O**.** 2019. Minimization of accident severity index in concrete barrier designs using metamodel-based optimization. *Optimization and Engineering*. (Under review)

OTHER PUBLICATIONS, PRESENTATIONS AND PATENTS:

- **S. Özcanan**, M. V. Akpınar, "Esnek Üstyapılarda Kritik Tekerlek ve Aks Konfigürasyonların Mekanistik Analizlere Göre Tespit Edilmesi", *IMO Teknik Dergi*, Ocak 2014.
- M.V. Akpınar, **S. Özcanan**, Y. Zandi, O. Karpuz, B. Mahdizadeh, Y.Z, Akpınar,"Accelerated Pavement Testing Pit Dimension Effects on Pavement Stress Analysis, 9th International Congress on Advances in Civil Engineering Pg. 27-30 September 2010, Karadeniz Technical University, Trabzon, Turkey.
- Ali Atahan, Gozde Bakioglu, Muhammet Balcilar, Mehmet Ali Silgu, **Sedat Ozcanan**, Murat Buyuk, Ilgın Gokasar, Hilmi Berk Celikoglu, "Incident Detection Algorithms: A Literature Review" IRF 1st Europe and Central Asia Regional Congress 15-18 September, 2015, Istanbul, Turkey.
- Günay Tümen, **Sedat Ozcanan**, Ali Osman Atahan, "Zemine Çakılı Otokorkulukların Darbe Davranışının Sonlu Elemanlar Analiziyle İncelenmesi" IRF 1st Europe and Central Asia Regional Congress 15-18 September, 2015, Istanbul, Turkey.
- M.V. Akpınar, Ü.Y. Bal, **S. Özcanan**, "Beton Yolların Mekanistik Tasarımlarının ve Performanslarının Sonlu Elemanlar Yöntemi ve Hızlandırılmış Yol Testleriyle Belirlenmesi", Hazır Beton Fuarı. 21-23 Şubat 2013, CNR Expo, İstanbul, Türkiye.
- **Özcanan, S.**, Akpınar, M.V. "Temel Tabakası Rijitliğine Bağlı Olarak Kaplama Kalınlığının Mekanistik Analizle Tayini", 6.Ulusal Asfalt Sempozyumu ve Sergisi, 27-28 Kasım 2013, Sheraton Otel, Ankara, Türkiye.